DEVELOPMENT AND CHARACTERIZATION OF FUNCTIONALIZED SUPERPARAMAGNETIC NANOPARTICLES FOR INTERSTITIAL APPLICATIONS

By

Samuel James Kuhn

Dissertation

Submitted to the Faculty of the

Graduate School of Vanderbilt University

in partial fulfillment of the requirements

for the degree of

DOCTOR OF PHILOSOPHY

in

Biomedical Engineering

December 2005

Nashville, Tennessee

Approved:

Todd D. Giorgio

Dennis E. Hallahan

Frederick R. Haselton

Vito Quaranta

Franz J. Baudenbacher

ACKNOWLEDGEMENTS

My family provided me the drive and support to see my journey through to the completion of my doctorate. Thank you Danielle, Hans, Martha, Hannah, Bill, Anthony, Nancy, Gene, Kurt, Craig, Adrienne, Tom, Olga, and Loren.

Undergraduate students Jordan Bush, Michelle Schrenk, Alex Li, and Albert Attia spent countless hours developing various portions of this project. Stephanie Finch was instrumental in generating sufficient data to publish the work described in Chapter III. Their willingness to engage this research project with was greatly appreciated.

The Giorgio lab members provided moral support and scientific troubleshooting. Likewise, members of the Haselton laboratory shared their lab space and science acumen during my doctoral studies. Thank you to Chinmay Soman, Daniel Dorset, Shelby Wyatt, Adam Smith, Ashley Weiner, Greg Stone, Ash Jayagopal, Tricia Russ, Todd Monroe, and Mark McQuain, Ning Li, and Ian Tomlinson. The Hallahan laboratory members Jeff Brousal, Allie Fu, Ling Geng, and Kate Osusky assisted me in a variety of imaging studies and the *in vivo* portion of this effort.

Thank you to those instructors who nurtured my scientific interest during my years of study. Deb Reynolds engaged me in my first independent research project as a high school student. Louis Kuo provided my first opportunity to publish in a scientific journal. Janis Lochner and Bethe Scalettar engaged me in a productive and useful research project during my undergraduate study. Deborah Lycan encouraged me to be rigorous in my writing and scientific approach.

My doctoral advisor, Todd Giorgio, offered scientific mentoring throughout my long trek to the doctorate. His encouragement to investigate interesting and innovative areas of study allowed us to develop this unique project. Dennis Hallahan assisted in my growth as a scientist by helping me appreciate the clinical implications of my work. The other members of my doctoral committee, Vito Quaranta, Rick Haselton, and Franz Baudenbacher also graciously gave their time to mentor me as I progressed toward the doctorate.

A number of other faculty and students freely gave their time and energy in support of this project. Haakil Lee, Ron Price, Ed Donnelly, Ken Lewis, Todd Peterson, and Jeff Clanton assisted in a trial imaging efforts using MRI, radio emitters, CT, and planar x-ray. Prasad Shastri allowed me free use of his fluorescent plate reader, greatly reducing the experimental workload. Finally, Tim Rice, Steve Uhlhorn and Richard Chen provided useful scientific and social diversion on the long road to the PhD.

No project can succeed without financial support. Todd Giorgio and Dennis Hallahan graciously provided the majority of my support from NIH and DOD grants. Vanderbilt's Institute for Nanoscale Science and Engineering, an NIH training grant in Quantitative and Integrative Physiology, and the Vanderbilt Graduate School also provided additional financial support for my salary and travel.

TABLE OF CONTENTS

LIST OF TABLES

LIST OF FIGURES

Figure Page

CHAPTER I

CHAPTER II

CHAPTER III

CHAPTER IV

APPENDIX A

APPENDIX B

CHAPTER I

INTRODUCTION TO SUPERPARAMAGNETIC NANOPARTICLES FOR INTERSTITAL APPLICATIONS

Rationale

A persistent limitation to clinical application of macromolecular therapeutic agents is an inability to deliver high levels of therapeutic agent throughout a specific tissue volume without impacting surrounding tissues. Viral vectors for gene therapy of both genetic defects and anticancer therapy have demonstrated substantial toxicity, and even death in some cases due to non-target delivery both by intravascular delivery and interstitial injection (1-4). Liposomes and other micro and nano-encapsulation strategies that attempt to concentrate molecular therapeutics such as doxorubicin within a solid tissue volume have minimal penetration into the interstitium following either intravascular or interstitial delivery (5-9).

Multifunctional nanoscale constructs that encompass therapeutic agents, imaging moieties and targeting ligands have the potential to radically change the treatment and morbidity profile of cancer and other significant human pathogens by synergistically combining enhanced targeting, reporting, and treatment of specific sites in the body. Application of these emerging multifunctional nanoscale constructs will be limited until strategies for comprehensive solid tissue access are developed.

Solid tissue transport is governed by fluid forces, such as diffusion and convection, geometric factors, such as steric hindrance, and by molecular interactions, including nonspecific adsorption. Fluid transport in the interstitial space has been

characterized both for molecular, and nanoscale therapeutics. Molecular interactions between therapeutic constructs and biological surfaces have been addressed through the development of biocompatible coatings (*e.g.* polyethylene glycol). Strategies for overcoming geometric barriers to macromolecular therapeutic delivery are only now emerging (10, 11). Within this dissertation, strategies for overcoming these steric barriers will be addressed.

The most effective route of administration for a therapeutic agent is determined by the physiology of target tissue(s) and the characteristics of the therapeutic agent. Some administration routes provide higher drug concentrations in specific physiological compartments (*e.g.* intramuscular/intratissue injection, nasal/mucosal, ocular) and other routes are characteristic of rapid access to multiple tissues (*e.g.* oral/gastrointestinal, intravascular injection). The administration of therapeutic agents that are larger than small molecules must consider the exceptionally limited mobility of large molecules within solid tissues. Pharmacokinetic distributions are significantly modulated by the physical, chemical and biological characteristics of the therapeutic agent. The biodistribution for large therapeutic agents is generally poor, even within sites that allow administration by multiple interstitial injections.

The rate of therapeutic agent transport is controlled by the relative strengths of mechanisms that enable motion and corresponding resistances modulated by proportionality factors controlled by physical characteristics. Mobility can be increased by appropriate change in any of these three transport aspects. The work described here leverages the improvement in biotransport that may be achieved through addition of a mechanism to enable motion and an approach to reduce the local resistance to motion.

Specifically, the simultaneous application of a magnetic force on the therapeutic construct and the use of proteolysis to reduce tissue resistance to improve the biodistribution of nanoscale agents are explored in this study.

Early efforts to develop magnetic nanoparticles for therapeutic applications demonstrated the potential to apply a substantial force to superparamagnetic structures in the vasculature (12, 13). Studies have demonstrated that lytic enzymes such as collagenase or hyluronidase can have a substantial impact on the passive mobility of macromolecules in the interstitial space (10, 11). Based on this evidence, I propose to enhance the distribution of macromolecular therapies and nanostructures such as some chemotherapy agents, radiotherapy seeds, or gene therapy vectors within a tissue volume by utilizing a proteolytic superparamagnetic nanoparticle carrier.

Specific Aims

I propose to explore magnetic nanoparticle carriers for interstitial dispersion over the course of three specifics aims:

Aim I – Characterize interstitial transport of SPM NPs in *in vitro* tissue models and murine subjects.

I propose to provide an integrated, calculation-based characterization of interstitial SPM NP mobility. I will computationally estimate the forces that influence the motion of SPM NPs in tumor interstitium. Computational findings will be tested in *in vitro* tissue models. Based on the calculation and *in vitro* experimental findings, I will image interstitial transport of SPM NPs in a murine solid tumor. SPM NP mobility will

be modulated by an external magnetic field and will be quantitatively imaged using two-dimensional x-ray imaging.

Aim II – Investigate NP-linked enzyme degradation of steric barriers to interstitial NP mobility.

I propose to develop a mobile construct capable of local modification of the interstitial space. To enhance NP mobility by interstitial remodeling, I will develop a collagenase-SPM NP construct. I will quantify NP-collagenase proteolytic activity and NP-collagenase construct stability in an *in vitro* system. Based on the *in vitro* evidence, I will quantitatively assess NP-collagenase particle mobility in *ex vivo* tumor sections by high-resolution, semiquantitative CT imaging and quantitative fluorescent imaging.

Aim III – Develop a multivalent enzyme-nanoparticle synthesis strategy.

I propose to demonstrate a multifunctional nanoparticle that has efficacy against two or more classes of biological substrates, including carbohydrates (α-glucosidase) and proteins (collagenase). To facilitate future multifunctional nanoparticle development, I will examine the cross reactivity of the target enzymes in each enzyme activity assay system. I will leverage synthetic strategies developed in Aim II to provide a straightforward, inexpensive synthetic strategy.

Significance

This body of work makes several contributions to the development of macromolecular and nanoparticle-based therapeutic agents for interstitial applications. The *in vitro* interstitial model system detailed in Manuscripts 1 and 2 is a simple and

flexible assay system that provides quantitative data suitable for mathematical description of nanoparticle interactions with the extracellular matrix. Creation of proteolytic enzyme-nanoparticle conjugates will allow study of individual enzymatic elements during invasive cellular processes such as metastasis or neuronal development (Manuscripts 2 and 3). Clinical development of proteolytic enzyme-nanoparticle conjugates will allow minimally invasive and enhanced dispersion of otherwise immobile macromolecular and nanoscale therapies in solid tissue. Demonstration of multivalent enzyme-nanoparticle conjugates provides a foundation for generalized multifunctional biomolecule-nanoparticles that incorporate enzymatic activity, receptors or ligands, imaging agents, and radio- or thermotherapeutic elements in a single nanoparticle structure (Manuscript 3).

Background

Despite the prominence of cancer in terms of both academic study and financial expenditure, more than 1.2 million people in the United States were diagnosed with this disease in 1999. Over 500,000 people died of cancer in 1999 (14). The continued prevalence of cancer diagnosis and death necessitate new efforts to develop novel therapies for treatment.

Treatment Strategies Are Limited by Tumor Physiology

Tumor physiology and structure limit therapeutic approaches. Diffusion-driven mobility is insufficient to disperse some therapeutic agents (TAs) throughout a modest tumor volume (15, 16). A high interstitial pressure gradient generated by leaky

vasculature drives molecular TAs out of the tumor volume via convection. Therapeutic agents larger than ten nanometers have high retention rates within tumor tissue due to their negligible intrinsic mobility (17). Vascular delivery of TAs to tumor is complicated by nonspecific delivery and retention in cardiovascular filtration systems (18). The anatomy and physiology of the tumor cause irregular deposition of therapeutic agents that leads to incomplete treatment of the tumor volume (19). Macromolecular therapies (*e.g.* antibodies or NPs) face additional steric restrictions to interstitial motion from the interstitial collagen network (20). Current intravascular and interstitial delivery and dispersion strategies for NP-based therapeutic strategies are limited in their application due to a lack of precise intravascular delivery and effective, long-term interstitial dispersion.

Better Biodistribution and Enhanced Specific Delivery Towards Improved Treatment

Enhanced distribution of TAs within the tumor can be achieved by increasing the retention time of the TA within the tumor and by increasing therapy mobility within the tumor. Enzyme-linked SPM NPs minimize undirected passive motion while maximizing targeted motion with the tumor volume. Enzymatic degradation of the interstitial network allows use of otherwise inadequately mobile SPM NPs as therapeutic agents.

Prior Evidence of Magnetic Targeting of TAs

Qualitative evidence of enhanced retention and deposition of intravascularly delivered SPM NP therapy carriers in specific tumors has been reported. Retention of magnetic particles on the order of 1 μm diameter in specific regions of an animal

following intravascular administration has been documented by Gruttner *et al* (21). Gruttner *et al*.'s work, however, found only a 25-30% increase in retention of the magnetic particles in the presence of a 0.4 T magnet field. The remainder of the particles was found in the liver of the animals. This level of liver delivery is indicative of first-pass capture by filtering processes and highlights the need for a long-circulating magnetic particle. Gruttner *et al.* dismisses NPs less than 100 nm in diameter for use *in vivo* due to their poor magnetic mobility in contradiction with other existing work (22, 23). Minimizing NP size is desirable due to a corresponding reduction in NP elimination by filtration (18).

Publications by other scientists affiliated with FeRx Incorporated (San Diego, CA) suggest that ferromagnetic particles on the order of 1 μm may be suitable for site-specific intravascular or intravesical delivery. Rudge *et al.* found that particle retention could exceed 90% for a 1 μm iron particle (FeRx MTCs) in an *in vitro* model vascular system consisting of a 35% glycerol solution flowing at 0.2 cm/s through a hollow fiber cartridge in a 0.01 T field (24). However, no negative control data was presented, leaving significant concerns regarding the passive trapping of particles by the hollow fibers in the cartridge. During *in vivo* studies, FeRx scientists demonstrated the local intravascular delivery of doxorubicin on a magnetically targeted carrier particle (MTC) to the liver under the exposure of an external magnetic field (25). The level of retention in the liver tissue was not documented quantitatively nor was the retention rate of particles not under the influence of an external magnetic field measured. Intravesical injection of doxorubicin loaded MTCs into porcine bladder and subsequent magnetic guidance into

the bladder wall demonstrated enhanced site-specific delivery of doxorubicin over free doxorubicin treatment (26).

Goodwin *et al.* documented success specifically targeting FeRx particles to lung or liver lobes following injection in the upstream blood supply of the target organ after a period of 60 minutes (27). The remainder of the MTCs was found distributed in the bladder, salivary glands and thyroid in both targeted organ studies. Early literature reports of interstitial application of magnetic NPs were restricted to incidental findings in intravascular delivery studies (28). More recently, FeRx Corporation has investigated delivery of MTCs to the bladder wall interstitial space from the bladder lumen (26). Additionally, Hooligan et al. reported limited mobility of SPM NPs in an *in vitro* model of the vitreous of the eye (29). Interest in the application of SPM NPs to biological systems is evident in the annual biological/medical applications special issue of the *Journal of Magnetism and Magnetic Materials*.

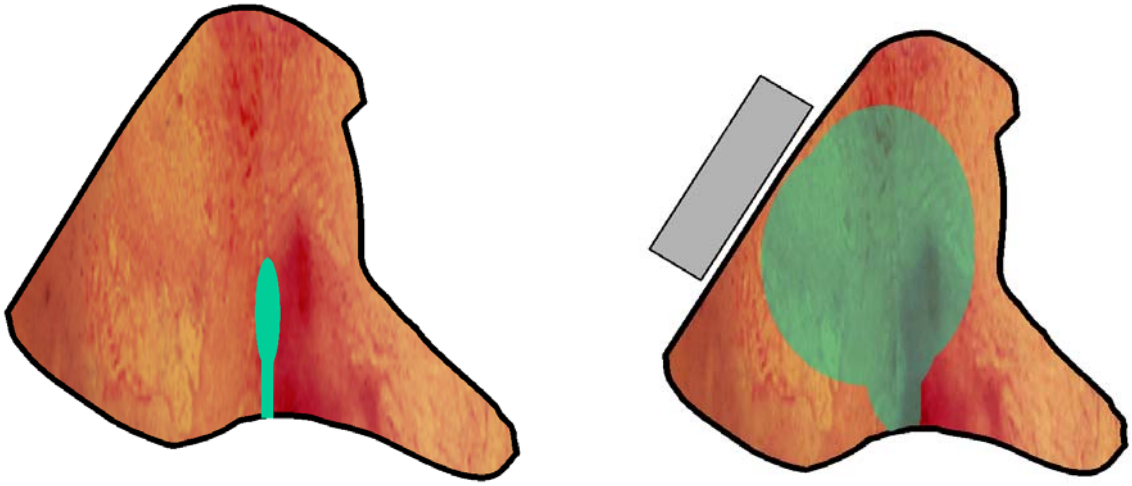

Figure 1. Illustration of desired goal of enhancing SPM NP with an external magnetic field. NPs (green) injected into a tumor without an external force (panel A) remain in the needle track or in the initial injection volume. SPM NPs injected into a tumor in the presence of an external magnetic field source (gray box) spread throughout the tumor volume due to their greatly enhanced mobility (panel B).

NP Toxicity

The complex nature of SPM NP-TA constructs requires examination of the chemical nature of the NP for toxicity as well as the possible immunogenic structures contained on the surface of the NP. Hafeli *et al.* examined the toxicity of iron oxide and iron NPs and determined that the coating of the NP generally is a strong indicator of the toxicity profile of the NPs *in vivo* (30). Unfortunately, a large fraction of Hafeli *et al.*'s data was not statistically significant, limiting the interpretation of their work. Long term, the degradation of the particles may result in liberation of the core materials of the particle. Liberation of iron from particles is unlikely to be a significant concern, as the level of free iron known to be toxic to humans is on the order of 260 mg per kilogram, well above any potential levels found in any iron-particle therapeutic strategy (31). Iron-containing SPM NPs have been safely utilized for contrast enhanced MRI imaging in human subjects (32).

Quantitative imaging of interstitial transport of SPM NPs

The iron content of SPM NPs allows quantitative spatial and temporal x-ray and CT imaging of NP localization, concentration, and mobility within a tumor volume or tissue sample (33). High-resolution electron microscopy imaging of the particle interaction with interstitial structures is also possible due to the iron content of the SPM NPs (34, 35). The wide variety of commercially available surface treatments for NP also allows fluorescence quantification of NP mobility and position (micromod, Spherotech, Pierce, *etc.*). SPM NP transport may be compared with previous *in vivo* studies of macromolecular therapy constructs by quantitative imaging (36-40).

Prior evidence of NP motion in interstitium

Jain and Yuan, among others, have studied interstitial microstructures extensively through the use of a variety of *in vitro* and *in vivo* techniques (41-46). While the tumor vasculature has been found to allow passive extravasation of NPs as large as 700 nanometers, *in vitro* experiments have shown the interstitial space to sharply limit passive motion of macromolecules larger than 10-15 nanometers in diameter (46, 47). Computational work by Yuan *et al.* has also suggested a diameter limit of approximately 10 nanometers for unimpeded diffusion or convection-driven motion of macromolecules in the interstitium (17).

NP motion through the interstitial space is retarded by the presence of the network of extracellular proteins and carbohydrates. The network of proteins in the interstitium forms channels and pores, creating a barrier to NP motion through the tissue. Netti *et al.* have identified the collagen fiber network as the most significant barrier to passive NP motion in the interstitium (10). The collagen fiber network has been estimated to have gaps ranging from 20-42 nanometers in "dense" tumors to 75-130 nanometers in "soft" tumors (48). These narrow gaps in the collagen network form a physical barrier to passive NP motion. Hyaluronic acid has been implicated as a barrier biomolecule in the center of a tumor (48).

ECM protein network resistance

Due, in part, to the historic difficulties in precision manufacturing of useful nanoscale therapy carriers, the body of evidence available regarding quantitative measurement of interstitial NP transport is limited. The paucity of published reports is an

opportunity to lay the groundwork for interstitial NP applications through computational models and quantitative imaging studies of interstitial NP dynamics.

Some evidence of nanoscale structural behavior can presumably be extrapolated from studies of antibody mobility in the interstitium (20). Pluen *et al.* identified the collagen content, rather than the glycosaminoglycan concentration, of a tumor as the primary source of decreased antibody mobility. Treatment of the tumor with collagenase for 24 hours was shown to increase antibody diffusion by 100% (10).

Invasive bacteria and viruses, ranging in size from 100 nm to 2000 nm, are nanoscale structures with enhanced interstitial mobility. The microorganisms utilize surface bound and secreted enzymes to increase their access to distant tissues. Invasion into the interstitial space relies on proteases such as collagenase as well as other nonspecific proteolytic enzymes (49-51). Nonspecific degradation of the extracellular and cellular space serves to cause inflammation and fluid retention, easing the passive convective or active transport of the organism to distant sites (52-54).

Calculation of interstitial forces acting on SPM NPs

Physical properties of the SPM NPs and known, or estimated, characteristics of the tumor obtained from literature may be used to estimate the net force acting on the SPM NPs. The net force acting on the SPM NPs is a function of the drag force, buoyant force, and magnetic force, in addition to contributions from diffusion and convection. Based on the work of Zbrowski, Hooligan *et al.* developed a mathematical model that describes the mobility of nanoparticles in the interstitial space (29, 55). The model developed by Hooligan provides a predictive measure for estimating the fluid-phase

interstitial velocity of SPM NPs based on magnetic and fluid parameters. These estimations of mobility may be utilized to narrow the investigation of candidate SPM NPs for interstitial applications.

In vitro tissue models, previous findings

Diffusive mobility is sufficient to saturate a 200 micron diameter tumor in approximately six hours with a small chemical agent (15, 16). While molecular therapies may have sufficient diffusion or convection driven mobility within the tumor volume, the motion of those agents is driven by concentration/pressure gradients not applicable to therapeutic goals. Agents of sizes larger than five nanometers (*e.g.* viruses, nonviral gene therapy constructs, NP carriers) remain largely within the initial injection volume as is shown in Figure 2. A variety of mechanisms presumably contribute to this low mobility behavior, including nonspecific adsorption of the virus to the surrounding biological environment and limited initial tissue penetration by the injection volume (3, 19, 56).

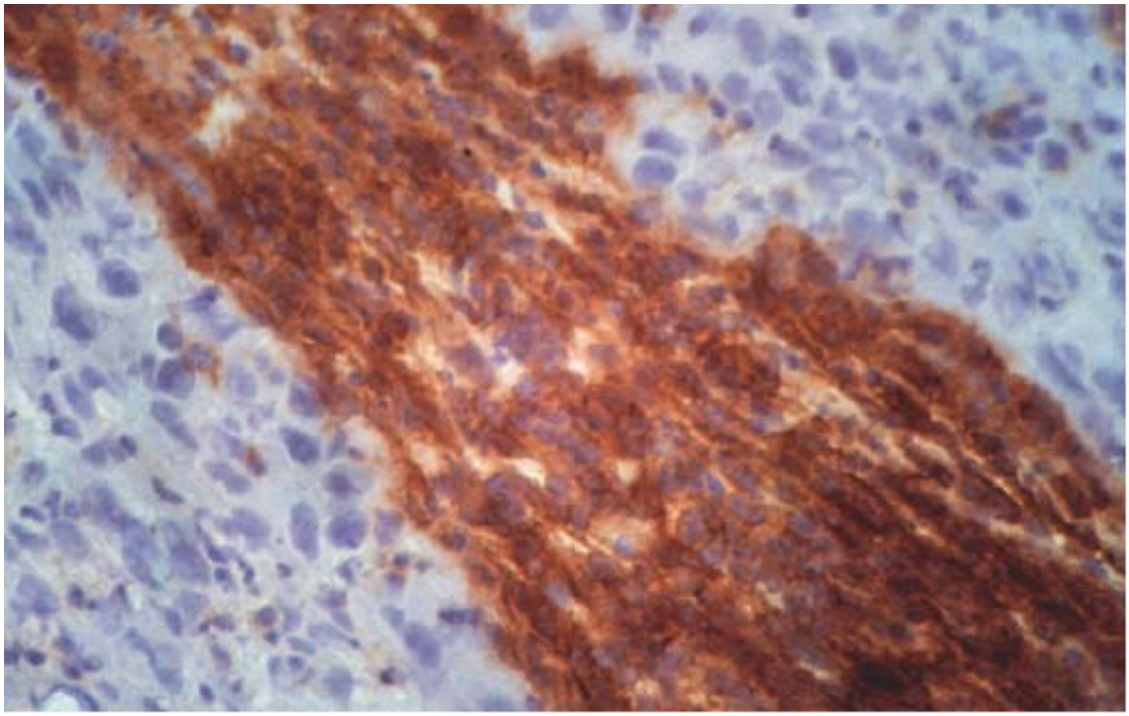

Figure 2. Anti-tumor necrosis factor (TNF) staining of cells by viral gene therapy vector (brown) along the needle injection track. Tissue is counterstained (blue) (Hallahan, unpublished).

The role of proteolytic activity in biological processes

Collagenase, and other related MMP have been an exceptionally active area of research due to their involvement in tissue rearrangement during development and cancer metastasis (57-59). MMP and MMP inhibitor involvement in wound healing, both as a therapeutic agents and as native processes, have been well characterized (60-62). Proteases that degrade the structural components of the extracellular matrix are also found on invasive microorganisms in the genera *Bacteroides*, *Clostridium,* and *Peptostreptococcus* (54), enabling alteration of the local structural environment to allow active mobility to distant sites in the host organism.

Strategies to link functional enzymes to the NP surface

Sophisticated strategies for linking biomolecules to NPs based on methods of modern immunology are available. The synthetic approach developed by Duncan *et al.* incorporates simple covalent modification reagents *N*-succinimidyl-S-acetylthiopropionate (SATP) and sulfosuccinimidyl 4-[*N*-maleimidomethyl]cyclohexane-1-carboxylate (sulfo-SMCC) (63). SATP is a well-characterized reagent that modifies primary amines to sulfhydryl groups. Sulfo-SMCC is a heterobifunctional crosslinker that converts primary amines to maleimide reactive groups. Together, these two reactive chemicals form a covalent thioether linkage between structures suitable for NP-therapeutic agent conjugation.

Quantification of NP-bound enzyme activity

Due to the SPM nature of the NPs in this proposal, magnetic purification of the NP-enzyme construct is possible. Quantification strategies for total enzyme binding and enzymatic function have both been developed into commercially available kits (Pierce, Invitrogen). Total protein activity may be assessed by simple spectroscopic detection of fluorogenic amino acids (*i.e.* tryptophan), or through traditional histological staining techniques. Quantification of NP-bound enzyme activity can be assessed through zymography, dye-quenched fluorogenic substrates, or colorimetric substrates (64). The tools required for quantitative assessment of enzyme activity, even for proteins conjugated to the NP surface, are available.

Summary

Specific Aim I builds upon magnetic targeting evidence and low iron-based nanoparticle toxicity previous reported in the literature by Goodwin and others to develop an *in vitro* and calculational means to characterize and quantify NP mobility in the interstitial space. A proteolytic enzyme-nanoparticle construct is proposed in Specific Aim II based on previous biomolecule conjugation strategies to overcome the specific protein barriers, such as collagen I fibers, which form a steric barrier to NP interstitial motion. Finally, the collagenase-nanoparticle enzyme from Specific Aim II is extended to create multifunctional nanoparticles that are modeled after existing lytic sets of proteins in invasive cells in Specific Aim III.

References

1. Lozier, J.N., et al., *Toxicity of a first-generation adenoviral vector in rhesus macaques.* Hum Gene Ther, 2002. **13**(1): p. 113-24.

2. Marshall, E., *Gene therapy death prompts review of adenovirus vector.* Science, 1999. **286**(5448): p. 2244-5.

3. Zhang, R., F.H. Straus, and L.J. DeGroot, *Effective genetic therapy of established medullary thyroid carcinomas with murine interleukin-2: dissemination and cytotoxicity studies in a rat tumor model.* Endocrinology, 1999. **140**(5): p. 2152-8.

4. Paielli, D.L., et al., *Evaluation of the biodistribution, persistence, toxicity, and potential of germ-line transmission of a replication-competent human adenovirus following intraprostatic administration in the mouse.* Mol Ther, 2000. **1**(3): p. 263-74.

5. Yuan, F., et al., *Microvascular permeability and interstitial penetration of sterically stabilized (stealth) liposomes in a human tumor xenograft.* Cancer Res, 1994. **54**(13): p. 3352-6.

6. Zhou, R., R. Mazurchuk, and R.M. Straubinger, *Antivasculature effects of doxorubicin-containing liposomes in an intracranial rat brain tumor model.* Cancer Res, 2002. **62**(9): p. 2561-6.

7. Trubetskoy, V.S., et al., *Massage-induced release of subcutaneously injected liposome-encapsulated drugs to the blood.* J Control Release, 1998. **50**(1-3): p. 13-9.

8. Kostarelos, K., et al., *Binding and interstitial penetration of liposomes within avascular tumor spheroids.* Int J Cancer, 2004. **112**(4): p. 713-21.

9. Kostarelos, K., et al., *Engineering lipid vesicles of enhanced intratumoral transport capabilities: correlating liposome characteristics with penetration into human prostate tumor spheroids.* J Liposome Res, 2005. **15**(1-2): p. 15-27.

10. Netti, P.A., et al., *Role of extracellular matrix assembly in interstitial transport in solid tumors.* Cancer Research, 2000. **60**(9): p. 2497-503.

11. Alexandrakis, G., et al., *Two-photon fluorescence correlation microscopy reveals the two-phase nature of transport in tumors.* Nat Med, 2004. **10**(2): p. 203-7.

12. Pulfer, S.K. and J.M. Gallo, *Enhanced brain tumor selectivity of cationic magnetic polysaccharide microspheres.* Journal of Drug Targeting, 1998. **6**(3): p. 215-27.

13. Goodwin, S.C., et al., *Single-dose toxicity study of hepatic intra-arterial infusion of doxorubicin coupled to a novel magnetically targeted drug carrier.* Toxicological Sciences, 2001. **60**(1): p. 177-83.

14. Group, U.S.C.S.W., *United States Cancer Statistics: 1999 Incidence*. 2002, Department of Health and Human Services,Centers for Disease Control and Prevention and National Cancer Institute: Atlanta, GA.

15. Raghavarao, K.S., M. Dueser, and P. Todd, *Multistage magnetic and electrophoretic extraction of cells, particles and macromolecules.* Advances in Biochemical Engineering-Biotechnology, 2000. **68**: p. 139-90.

16. Au, J.L., et al., *Determinants of drug delivery and transport to solid tumors.* Journal of Controlled Release, 2001. **74**(1-3): p. 31-46.

17. Yuan, F., A. Krol, and S. Tong, *Available space and extracellular transport of macromolecules: effects of pore size and connectedness.* Annals of Biomedical Engineering, 2001. **29**(12): p. 1150-8.

18. Sugibayashi, K.a.M., Y., *Biomedical Applications of Magnetic Drug Carriers in Cancer Chemotherapy*, in *Polymeric Nanospheres and Microparticles*. 1986, CRC Press: Boca Raton, FL. p. 95-133.

19. Wang, Y., et al., *Systemic dissemination of viral vectors during intratumoral injection.* Mol Cancer Ther, 2003. **2**(11): p. 1233-42.

20. Pluen, A., et al., *Role of tumor-host interactions in interstitial diffusion of macromolecules: cranial vs. subcutaneous tumors.* Proc Natl Acad Sci U S A, 2001. **98**(8): p. 4628-33.

21. Gruttner, C., Teller, J, Schutt, W, Westphal, F., Chumichen, C., Paulke, B.R., *Prepartation and Characterization of Magnetic Nanospheres For In Vivo Application*, in *Scientific and Clinical Applications of Magnetic Carriers*, U. Hafeli, Schutt, W., Teller, J., Zborowski, M., Editor. 1997, Plenum Press: New York, New York. p. 53-67.

22. Miltenyi, S., et al., *High gradient magnetic cell separation with MACS.* Cytometry, 1990. **11**(2): p. 231-8.

23. Prestvik, W.S., Berge, A., Mork, P.C., Stenstad, P.M., Ugelstad, J., *Preparation and Application of Monosize Magnetic Particles in Selective Cell Separation*, in *Scientific and Clinical Applications of Magnetic Carriers*, U. Hafeli, Schutt, W., Teller, J., Zborowski, M., Editor. 1997, Plenum Press: New York, New York. p. 11-33.

24. Rudge, S.R., et al., *Preparation, characterization, and performance of magnetic iron-carbon composite microparticles for chemotherapy.* Biomaterials, 2000. **21**(14): p. 1411-20.

25. Rudge, S., et al., *Adsorption and desorption of chemotherapeutic drugs from a magnetically targeted carrier (MTC).* Journal of Controlled Release, 2001. **74**(1-3): p. 335-40.

26. Leakakos, T., et al., *Intravesical administration of doxorubicin to swine bladder using magnetically targeted carriers.* Cancer Chemother Pharmacol, 2003. **51**(6): p. 445-50.

27. Goodwin, S.C., et al., *Targeting and retention of magnetic targeted carriers (MTCs) enhancing intra-arterial chemotherapy.* Journal of Magnetism and Magnetic Materials, 1999. **194**: p. 132-139.

28. Lubbe, A.S., et al., *Clinical experiences with magnetic drug targeting: a phase I study with 4'-epidoxorubicin in 14 patients with advanced solid tumors.* Cancer Research, 1996. **56**(20): p. 4686-93.

29. Holligan, D.L., G.T. Gillies, and J.P. Dailey, *Magnetic guidance of ferrofluidic nanoparticles in an in vitro model of intraocular retinal repair.* Nanotechnology, 2003. **14**(6): p. 661-666.

30. Hafeli, U. and G.J. Pauer, *In vitro and in vio toxicity of magnetic microspheres.* Journal of Magnetism and Magnetic Materials, 1999. **194**(01): p. 76-82.

31. *ACS Material Safety Data Sheet: "Iron (III) Chloride Hexahydrate - Ferric Chloride"*. 1998.

32. Torchia, M.G., et al., *Interstitial MR lymphangiography for the detection of sentinel lymph nodes.* Journal of Surgical Oncology, 2001. **78**(3): p. 151-6; discussion 157.

33. Gneveckow, U., et al., *Description and characterization of the novel hyperthermia- and thermoablation-system MFH 300F for clinical magnetic fluid hyperthermia.* Med Phys, 2004. **31**(6): p. 1444-51.

34. Jendelova, P., et al., *Magnetic resonance tracking of transplanted bone marrow and embryonic stem cells labeled by iron oxide nanoparticles in rat brain and spinal cord.* J Neurosci Res, 2004. **76**(2): p. 232-43.

35. Jendelova, P., et al., *Imaging the fate of implanted bone marrow stromal cells labeled with superparamagnetic nanoparticles.* Magn Reson Med, 2003. **50**(4): p. 767-76.

36. Peira, E., et al., *In vitro and in vivo study of solid lipid nanoparticles loaded with superparamagnetic iron oxide.* Journal of Drug Targeting, 2003. **11**(1): p. 19-24.

37. Brown, E., et al., *Dynamic imaging of collagen and its modulation in tumors in vivo using second-harmonic generation.* Nat Med, 2003. **9**(6): p. 796-800.

38. Davies Cde, L., et al., *Comparison of IgG diffusion and extracellular matrix composition in rhabdomyosarcomas grown in mice versus in vitro as spheroids reveals the role of host stromal cells.* Br J Cancer, 2002. **86**(10): p. 1639-44.

39. Illum, L., et al., *Development of systems for targeting the regional lymph nodes for diagnostic imaging: in vivo behaviour of colloidal PEG-coated magnetite nanospheres in the rat following interstitial administration.* Pharmaceutical Research, 2001. **18**(5): p. 640-5.

40. Weissig, V., J.W. Babich, and V.P. Torchilin, *Long-circulating gadolinium-loaded liposomes: potential use for magnetic resonance imaging of the blood pool.* Colloids and Surfaces B: Biointerfaces, 2000. **18**: p. 293-299.

41. Leunig, M., et al., *Angiogenesis, microvascular architecture, microhemodynamics, and interstitial fluid pressure during early growth of human adenocarcinoma LS174T in SCID mice.* Cancer Research, 1992. **52**(23): p. 6553-60.

42. Yuan, F., et al., *Microvascular permeability of albumin, vascular surface area, and vascular volume measured in human adenocarcinoma LS174T using dorsal chamber in SCID mice.* Microvascular Research, 1993. **45**(3): p. 269-89.

43. Yuan, F., et al., *Vascular permeability and microcirculation of gliomas and mammary carcinomas transplanted in rat and mouse cranial windows.* Cancer Research, 1994. **54**(17): p. 4564-8.

44. Lichtenbeld, H.C., et al., *Perfusion of single tumor microvessels: application to vascular permeability measurement.* Microcirculation, 1996. **3**(4): p. 349-57.

45. Monsky, W.L., et al., *Regulation of transport pathways in tumor vessels: role of tumor type and microenvironment.* Proceedings of the National Academy of Sciences of the United States of America, 1998. **95**(8): p. 4607-12.

46. Monsky, W.L., et al., *Augmentation of transvascular transport of macromolecules and nanoparticles in tumors using vascular endothelial growth factor.* Cancer Research, 1999. **59**(16): p. 4129-35.

47. McGuire, S. and F. Yuan, *Quantitative analysis of intratumoral infusion of color molecules.* American Journal of Physiology - Heart & Circulatory Physiology, 2001. **281**(2): p. H715-21.

48. Pluen, A., et al., *Role of tumor-host interactions in interstitial diffusion of macromolecules: cranial vs. subcutaneous tumors.* Proceedings of the National Academy of Sciences of the United States of America, 2001. **98**(8): p. 4628-33.

49. Tamura, F., et al., *Proapoptotic effect of proteolytic activation of matrix metalloproteinases by Streptococcus pyogenes thiol proteinase (Streptococcus pyrogenic exotoxin B).* Infect Immun, 2004. **72**(8): p. 4836-47.

50. Avidano, M.A., et al., *Analysis of protease activity in human otitis media.* Otolaryngol Head Neck Surg, 1998. **119**(4): p. 346-51.

51. Smola-Hess, S., et al., *Expression of membrane type 1 matrix metalloproteinase in papillomavirus-positive cells: role of the human papillomavirus (HPV) 16 and HPV8 E7 gene products.* J Gen Virol, 2005. **86**(Pt 5): p. 1291-6.

52. Buczko, W., et al., *Biological effects of degradation products of collagen by bacterial collagenase.* British Journal of Pharmacology. Aug;69(4):551-4, 1980.

53. Sela, M.N., et al., *Enzymatic degradation of collagen-guided tissue regeneration membranes by periodontal bacteria.* Clinical Oral Implants Research. Jun;14(3):263-8, 2003.

54. Steffen, E.K. and D.J. Hentges, *Hydrolytic enzymes of anaerobic bacteria isolated from human infections.* Journal of Clinical Microbiology. Aug;14(2):153-6, 1981.

55. Zborowski, M., et al., *Analytical magnetapheresis of ferritin-labeled lymphocytes.* Anal Chem, 1995. **67**(20): p. 3702-12.

56. Bledsoe, A.W., G.Y. Gillespie, and C.D. Morrow, *Targeted foreign gene expression in spinal cord neurons using poliovirus replicons.* J Neurovirol, 2000. **6**(2): p. 95-105.

57. Hendrix, M.J., et al., *Remodeling of the microenvironment by aggressive melanoma tumor cells.* Ann N Y Acad Sci, 2003. **995**: p. 151-61.

58. Vaillant, C., et al., *MMP-9 deficiency affects axonal outgrowth, migration, and apoptosis in the developing cerebellum.* Mol Cell Neurosci, 2003. **24**(2): p. 395-408.

59. Friedl, P. and K. Wolf, *Proteolytic and non-proteolytic migration of tumour cells and leucocytes*, in *Proteases and the Regulation of Biological Processes*. 2003. p. 277-285.

60. Aldemir, M., et al., *Effectiveness of collagenase in the treatment of sacrococcygeal pilonidal sinus disease.* Surgery Today.;33(2):106-9, 2003.

61. Mekkes, J.R., et al., *In vitro tissue-digesting properties of krill enzymes compared with fibrinolysin/DNAse, papain and placebo.* Int J Biochem Cell Biol, 1997. **29**(4): p. 703-6.

62. Moorhead, L.C. and N. Radtke, *Enzyme-assisted vitrectomy with bacterial collagenase. Pilot human studies.* Retina. Spring-Summer;5(2):98-100, 1985.

63. Duncan, R.J., P.D. Weston, and R. Wrigglesworth, *A new reagent which may be used to introduce sulfhydryl groups into proteins, and its use in the preparation of conjugates for immunoassay.* Anal Biochem, 1983. **132**(1): p. 68-73.

64. McIntyre, J.O., et al., *Development of a novel fluorogenic proteolytic beacon for in vivo detection and imaging of tumour-associated matrix metalloproteinase-7 activity.* Biochem J, 2004. **377**(Pt 3): p. 617-28.

CHAPTER II

MANUSCRIPT 1: CHARACTERIZATION OF SUPERPARAMAGNETIC NANOPARTICLE INTERACTIONS WITH EXTRACELLULAR MATRIX IN AN *IN VITRO* SYSTEM

Sam J Kuhn[1]

Dennis E Hallahan[1,2,3]

Todd D Giorgio[1]

[1]Department of Biomedical Engineering

Vanderbilt University

Nashville, TN

[2]Department of Radiation Oncology

Vanderbilt University School of Medicine

Nashville, TN

[3]Department of Cancer Biology

Vanderbilt-Ingram Cancer Center

Vanderbilt University School of Medicine

Nashville, TN

(This manuscript is in press in *Annals of Biomedical Engineering*)

Abstract

Controlled dispersion of therapeutic agents within liquid and gel filled cavities represents a barrier to treatment of some cancers and other pathological states. Interstitial delivery is compromised by the poor mobility of macromolecules and larger nanoscale structures. We developed an *in vitro* system to quantify the suitability of superparamagnetic nanoparticles (SPM NPs) as a site-specific therapeutic vehicle for delivery through fluid and gel based systems. SPM NP motion was induced by an external magnetic field. NP migration was modulated by NP concentration and surface coating. 135 nm radius PEGylated NPs moved through the extracellular matrix with an average velocity of 1.5 mm hr^{-1}, suitable for some clinical applications. Increasing the SPM NP radius to 400 nm while maintaining the same per NP magnetic susceptibility resulted in a greater than 1000 fold reduction in magnetic mobility, to less than 0.01 mm hr^{-1}. The critical influence of NP size on gel permeation was also observed in silica coated 135 nm SPM NPs that aggregated under the experimental conditions. Aggregation played a critical role in determining the behavior of the nanoparticles. SPM NPs allow significant free-solution mobility to specific sites within a cavity and generate sufficient force to penetrate common *in vivo* gels.

Introduction

Superparamagnetic nanoparticle (SPM NP) therapeutic carriers hold the promise of site-specific delivery in a cavity, even in the presence of common biological barriers. Treatment of specific lesions or target tissues in a biological cavity has historically been

achieved by cavity lavage, or direct injection of a therapeutic agent at the target location. Lavage results in nonspecific delivery of the therapeutic agent to all surfaces within a cavity (1). Therapeutic agent penetration at the target site is limited by surface coatings such as biogels or membranes that block free agent mobility by adhesion or steric hindrance (2, 3). Direct injection is limited in its utility to sites that are accessible by a needle and to strategies that utilize small therapeutic molecules.

Biodistribution of therapeutic agents is controlled by the physics of mass transport. Diffusion is controlled by the molecular diameter, concentration, and the physical properties of the surrounding medium. Small molecules diffuse within a gel or fluid volume over the course of several hours (4). For therapies larger than small molecules, such as viral vectors, diffusion is negligible on the time scale appropriate for therapeutic action (5).

Despite velocities on the order of 5 cm s^{-1} in some cavities, convective therapeutic agent delivery has limited utility due to nonspecific delivery of therapeutic agents (6, 7). Convective delivery is further limited by the significant barrier of mucus and other proteinaceous gels characteristic of many cavities. These gels resist convective mobility and substantially reduce the diffusive mobility of introduced agents (3). Nanoparticle therapeutic carrier mobility can be additionally hindered by molecular interactions at the surface of target tissue, such as charge-charge attraction or nonspecific adhesion.

Direct injection into target tissue delivers therapy only to the needle track and to the immediately surrounding tumor tissue (4, 8, 9). This restricted biodistribution limits the therapeutic effect of injected agents. Interstitial convective mass transport depends on the presence of a fluid velocity gradient. In tumor tissue, the pressure difference and

corresponding fluid velocity gradient points radially outward from the necrotic core, discharging the therapy from the tumor. Convective fluid motion is capable of transporting macromolecules (*e.g.* antibodies) within tumor tissue only over a submillimeter distance during a therapeutic time window (10).

Interstitial NP motion is retarded by the presence of the network of extracellular proteins and carbohydrates. Netti et al. have identified the collagen fiber network as the most significant barrier to passive NP motion in the interstitium (11). The collagen fiber network in the ECM has been estimated to have gaps ranging from 20-42 nm in "dense" tumors to 75-130 nm in "soft" tumors (12). These gaps in the collagen network form a physical barrier to passive NP motion. Hyaluronic acid has been implicated as a barrier protein in the center of the tumors (12). In addition to the physical barriers formed by protein and carbohydrate networks within the tumor interstitium, NP interactions with surrounding tissue, soluble proteins, carbohydrates, and other NPs also reduce interstitial transit of NPs. These interactions may lead to adhesion of the NPs to fixed structures or may result in the formation of NP agglomerates consisting of NPs and the biomolecules that strongly interact with them.

Jain and Yuan, among others, have studied interstitial microstructure extensively through the use of a variety of *in vitro* and *in vivo* techniques (13-18). While the tumor vasculature has been found to allow passive extravasation of NPs as large as 700 nm, *in vitro* experiments have shown the interstitial space to sharply limit passive motion of macromolecules larger than 10-15 nm in diameter (4, 18). Computational work by Yuan et al. has also suggested a diameter limit of approximately 10 nm for unimpeded diffusion or convection-driven motion of macromolecules in the interstitium (19).

The same biophysical characteristics that limit the application of traditional therapies can be exploited to improve biodistribution using a novel approach based on SPM NP therapy delivery. SPM NPs can be specifically localized within a fluid filled cavity to the site of a lesion or target tissue by an external magnetic field. Protein and carbohydrate-based biogels can be displaced or penetrated by the SPM NPs, allowing direct NP-target interaction. Aggregation of SPM NPs does not pose a barrier for localization in a fluid or gel filled space; larger aggregate size presumably generates a proportionally larger magnetic force necessary to overcome gel-based barriers to mobility.

Comparison of the magnetic force experienced by a 145 nm SPM NP to reported values of particle mobility in tissue in (20) suggests that a magnetic force on the order of 100 fN per NP may be sufficient to overcome the barriers that inhibit NP transport (20). Gel and fluid can be deformed by force on the order of hundreds of pN or less (21). The net motive force of a SPM NP is governed by electromagnetic theory and Newton's Law and is determined by the sum of forces acting on the NP including diffusion, convection, and an external magnetic force. Calculation of the total force impinging on a single NP allows estimation of velocity and direction in a viscous medium (22). The diffusive force is orders of magnitude smaller than the magnetic forces that can be generated with SPM NPs (23).

Ferrous oxide (Fe_3O_4) is among the most suitable magnetic material for use in biological applications due to its well-characterized behavior, low toxicity, and history of use in clinical applications such as MRI contrast agents (24, 25). SPM materials respond to an external magnetic field as a single-domain crystal and travel along the field

gradient. In the absence of an external field, a SPM material has a negligible remnant field. SPM materials are ideal for use in submicron magnetic carriers because they are magnetically responsive to an external field but lack the capacity for autonomous magnetic behavior such as attraction between individual NPs.

We hypothesize that a magnetic force applied to a SPM NP by an external magnet field gradient can be utilized to overcome the mechanisms that limit the transport and uniform distribution of antitumor therapies delivered within a gel/fluid filled cavity. Specifically, we seek an integrated study in which *in vitro* experiments are conducted under conditions informed by the theory of mass transport modulated by a magnetic force.

Methodology

NP Characteristics

SPM NPs were obtained from micromod Partikeltechnologie GmbH (Germany) with silica surface coating (135 nm radius) and 300 MW PEG surface coating (145 and 400 nm radius). The manufacturer reported CV of 0.42, 0.47, and 0.72, for these samples. The NPs had a smooth surface as observed by transmission electron microscopy. The micromod NP is a Fe_3O_4-dextran-silica composite that consists of an inner region of continuous phase dextran containing Fe_3O_4 crystals, with an dextran-silica composite shell. Fe_3O_4 mass per NP was uniform; percentage Fe_3O_4 mass composition was 75% for the 135 nm and 145 nm NPs and 7% for the 400 nm NPs. The NP volumetric magnetic susceptibility (χ_V) was 0.2105 for 135 nm and 145 nm NPs and 0.0081 for 400nm NP

under saturating conditions ($H > 7.96 \times 10^5$ A m^{-1}). NPs with the native characteristics of a silica shell on the NP surface and NPs with a surface coating of 300 MW PEG were utilized.

All NPs were maintained in a pH 7.6 phosphate buffered saline (PBS) solution consisting of: 1.9 mM NaH_2PO_4, 8.1mM Na_2HPO_4, 5.4 mM KCl, and 154 mM NaCl.

Three Dimensional Mapping Of The Magnetic Field

A 2.54 cm cube of grade 40 NdFeB magnet (National Imports) was utilized for *in vitro* measurement of nanoparticle behavior. An equipolar xy plane on a nonpole face of the magnet was utilized for *in vitro* experiments. The magnetic field was measured by a Lakeshore 421 Gaussmeter with a MMA-2502-VH Hall probe. A three dimensional optical tracking system (Optotrack) was utilized to measure the position of the gaussmeter probe (Lakeshore) over time. The gaussmeter probe was rigidly affixed to an Optotrack probe mount. The Optotrack system reported the probe's position in space (X,Y,Z) and the yaw, roll and pitch of the probe. Position and orientation measurements were collected every 50 ms for 10,500 samples. Measurements relative to the Optotrack were registered to the physical surface of the magnet by measuring the corners of the measured face in both physical space and in Optotrack space. The transformation from the measured position of the Optotrack probe and the rigidly attached gaussmeter probe was calculated and applied to position data produced by the Optotrack system. The magnetic field was not measured within two millimeters of the surface due to the gaussmeter probe design.

9,400 measurements of the magnetic field were retained after values collected when the probe was at an angle greater than five degrees off perpendicular were discarded. Data within the equipolar region of the magnet surface utilized during *in vitro* experiments were averaged and characterized by field strength as a function of distance from the magnet surface.

Extracellular Matrix Viscosity Measurement

Extracellular matrix purified from Engelbreth-Holm-Swarm murine sarcoma was purchased from Sigma-Aldrich. Anton Paar was contracted to provide rheological characterization of the ECM gel undiluted and at 1:1 dilution with Dulbecco's Modified Medium. Briefly, samples were held at 37° C for 40 minutes following introduction into the cone and plate measurement chamber. ECM gel response was measured over a shear ramp from 10^{-4} to 10^{-1} Hz (n=3). Viscosity was determined to be $1.1 \times 10^{6} \pm 1.5 \times 10^{5}$ cP for the undiluted sample and $4.0 \times 10^{5} \pm 6.4 \times 10^{4}$ cP for the 1:1 diluted sample.

In Vitro Visualization System

ECM was thawed overnight at 4° C from -70° C storage. 100 μL of extracellular matrix was deposited into a glass vial measuring 3.5 mm inner diameter by 3 cm height at 4° C. The vial was stored for 12 hours at 4° C to allow release of trapped air from the ECM, and then incubated for 40 minutes at 37° C to induce polymerization of the ECM gel. Nanoparticle solutions were created at 1 mg mL^{-1}, 0.250 mg mL^{-1} and 0.083 mg mL^{-1} utilizing each nanoparticle cohort: 135 nm radius, PEG coated; 145 nm radius, silica coated; and 400 nm radius, PEG coated. 50 μL of 37° C NP solution in PBS was

sonicated for 5 s, and then introduced onto the surface of the gel. Evaporation was prevented by sealing the vial with wax film. The vial was placed on the surface of the magnet inside a vertical support frame. Mean maximum ECM gel height above the magnet was 9.5 mm, 7.8 mm, 7.0 mm for the 400 nm radius, PEG coated; 135 nm radius, PEG coated; and 145 nm radius, silica coated NP cohorts, respectively.

Digital images of the NP location were captured using a 3 megapixel digital camera (Canon) equipped with a macro lens at 37° C. Camera settings, timing, and data capture were remotely controlled via a personal computer and Cam4you software (Hans-David Alkenius). NP behavior was imaged over 24 hours. The digital images had a resolution of 2020 μm^2 per square pixel.

Computational Data Analysis

NP position in the ECM gel was determined by contrast measurement of leading edge of the NP motion in the gel. Conversion from pixels to microns was based on measurement of fixed elements within the digital images. NP velocity was calculated in triplicate by linear regression over a two-hour time interval spanning the median position measurement ($d_{½}$)($r^2 > 0.97$). NP position relative to the magnet surface was normalized within each radius/surface coating cohort. This single velocity value comparison was selected to provide uniform magnetic field characteristics for all samples and to minimize the potential influence of end effects on SPM NP mobility.

Electron Microscopic Imaging of SPM NPs

The SPM NPs were imaged with a Philips CM-12, 120 keV transmission electron microscope. NP samples were suspended in a negative staining solution (NanoW) and dried on a copper grid. The samples were then visualized under 31,000x and 300,000x magnification at 80 KeV. Images were captured with a digital imaging camera (AMT Digital).

Theoretical Estimation of SPM NP mobility

The primary forces influencing magnetic NP mobility in a biological system are the drag force (F_D) and the external magnetic force (F_M). Colloidal NPs are prone to aggregation, particularly in a complex biological environment. In a gel system, aggregate behavior may be modeled by assuming a solid sphere geometry of the aggregate radius and by adjusting the magnetic composition of the aggregate to accommodate the packing structure of the NPs in the aggregate (26).

Holligan et al. have described a system of equations for calculating the velocity of SPM NPs in a tissue phantom based on the work of Zborowski (22, 27) . The magnitude and direction of the force F_M on an SPM NP aggregate is a function of the NP volumetric magnetic susceptibility (χ_V), the volume of SPM material (V_m, m^3), the gradient of the magnetic field (∇B, T m^{-1}), and the magnetic field strength (B, T).

The maximum magnitude of the magnetic force can be calculated, when NP magnetic moments are aligned and the magnetic domains are saturated by the following equation:

$$F_M = \frac{\chi_V V_m \nabla B^2}{2\mu_0} \quad (1)$$

where μ_0 is the permeability of free space, is $4\pi \times 10^{-7}$ (T m A^{-1}).

The drag force on the aggregate at terminal velocity, F_D, can be calculated as:

$$F_D = 6\pi r\eta v \quad (2)$$

where r is the radius of the aggregate (m), η is the viscosity the surrounding fluid (N s m^{-2}), and v is the aggregate velocity (m s^{-1}). The NPs reach their terminal velocity when magnetic force, F_M and the drag force, F_D are equal. This terminal velocity can be calculated from (eq. 1) and (eq. 2):

$$v = \frac{\chi_V V_m \nabla B^2}{12\pi\mu_0 r\eta} \quad (3)$$

Aggregates below 500 μm in diameter can be assumed to instantaneously reach their terminal velocity in a viscous fluid (*e.g.* a 500 μm diameter aggregate of density 2.5 g cm^3 achieves terminal velocity in 35 ns in a 1×10^6 cP fluid) (28).

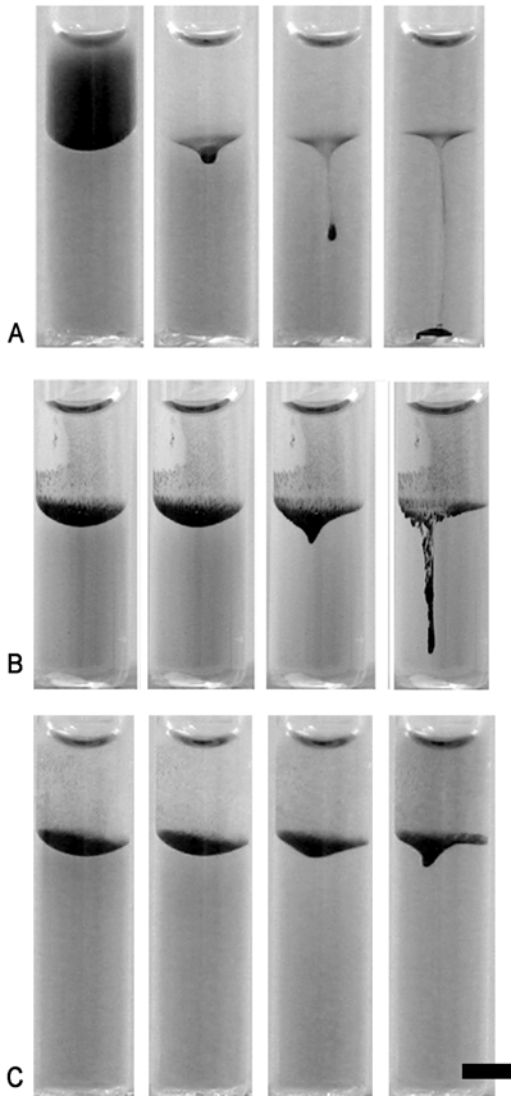

Figure 1. Qualitative velocity changes were observed during time lapse series images of NP migration in *in vitro* ECM gel system. Each panel contains 4 frames: 0, 1, 4.8, 22 hours (left to right). Panel A. 135 nm radius PEG surface coated particles ($\chi = 0.2104$) B. 145 nm radius silica-coated surface particles ($\chi = 0.2104$) C. 400 nm radius PEG surface coated particles ($\chi = 0.081$). 2 mm scale bar.

Results

SPM NPs were mobile in a purified extracellular matrix under guidance of an external magnetic field (Figure 1). NP velocity through the gel was visually distinct between NP cohorts of surface coating and solution concentration. NP surface coating and NP solution concentration made a qualitative difference in NP-gel interactions and NP mobility. Velocity of NPs with PEG surface coating was increased compared to the velocity of NPs with a silica coating. In the absence of a magnetic field, NPs showed slight accumulation at the aqueous-gel interface over 24 hours; NPs did not enter the gel in the absence of a magnetic field.

145 nm radius PEG coated NPs achieved a $d_{½}$ velocity of 1.5 ± 0.71 mm hr^{-1} (mean ± SD), seven times greater than the $d_{½}$ velocity of 135 nm radius silica coated NPs of equivalent magnetic response (0.21 ± 0.07 mm hr^{-1}) (Figure 2). The larger 400 nm radius PEG-coated NPs had a velocity of less than 0.01 mm hr^{-1} and never achieved the $d_{½}$ position. The three surface coating / size NP cohorts had statistically significant difference between their mean velocities.

SPM NP velocity increased as a function of NP solution concentration. NP solution concentrations of 1000 μg mL^{-1}, 250 μg mL^{-1}, 83 μg mL^{-1} migrated through the ECM gel at 1.5 ± 0.71 mm hr^{-1}, 0.27 ± 0.15 mm hr^{-1}, 0.087 mm hr^{-1} ± 3.5 x 10^{-4} mm hr^{-1}, respectively (Figure 3). NP mobility increased with concentration over the range from 83.33 μg mL^{-1} to 1000 μg mL^{-1}.

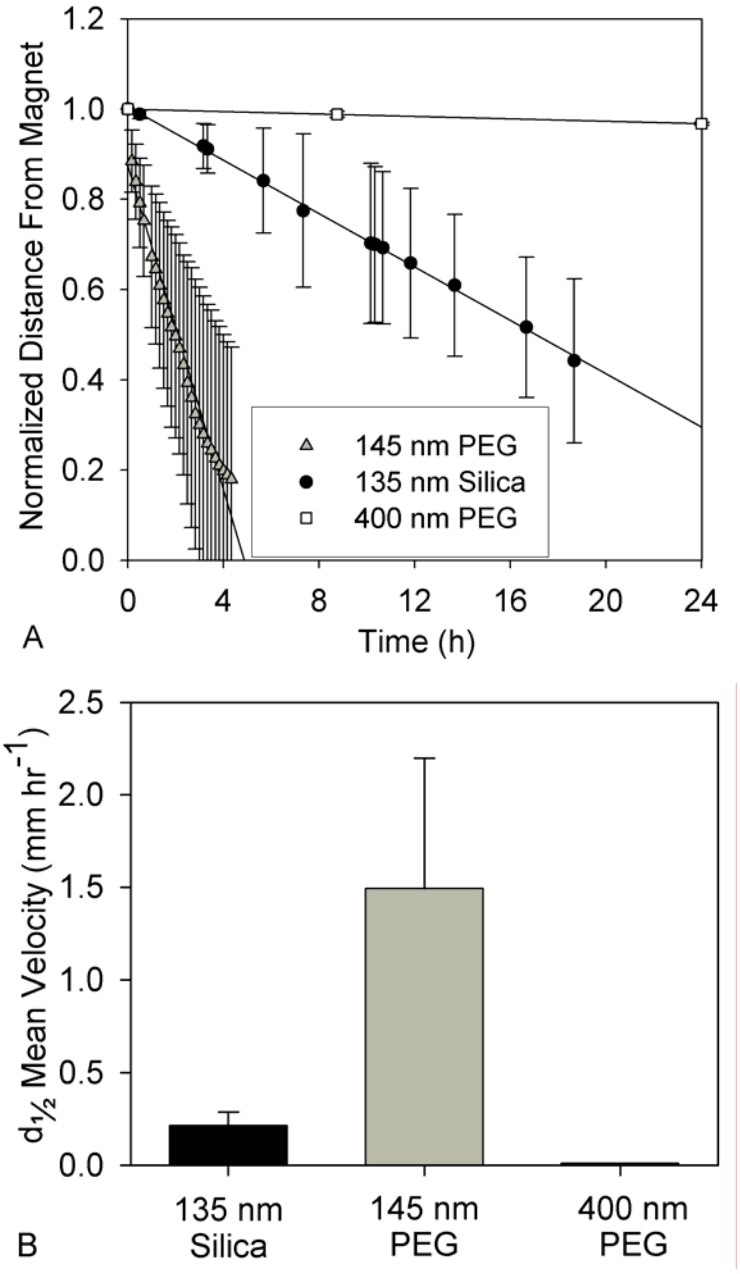

Figure 2. Increased NP velocity at smaller radii and with PEG coating. Panel A. NP aggregate leading edge position as a function of time based on normalized distance. 50 μL of 1 mg mL^{-1} 135 nm silica, 145 nm PEG coated and 400 nm PEG coated NP solution mobilities are plotted with linear regression underlay (n=3). Panel B. Mean velocity measurement for each NP cohort over two-hour time interval spanning the median position measurement ($d_{½}$)(n=3). Error bars represent standard deviation. P=0.004 for all comparisons by Kruskal-Wallis One Way ANOVA on Ranks.

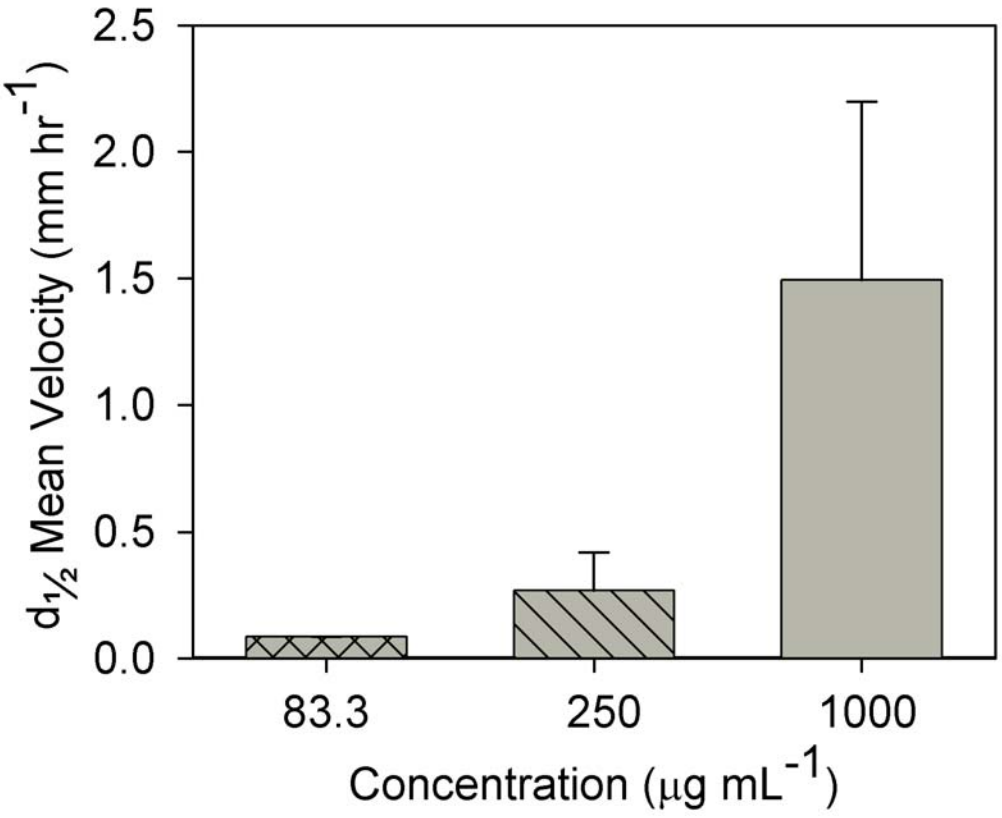

Figure 3. Increasing concentration of NPs resulted in increased mean aggregate velocity. Bulk mobility of 145 nm PEG coated SPM NPs increased with initial concentration. Mean velocity for each cohort over the two-hour time interval spanning the median position measurement ($d_{½}$) is shown as a function of initial NP concentration (n=3). Error bars represent standard deviation. P=0.001 for all comparisons by Kruskal-Wallis One Way ANOVA on Ranks.

NP mobility estimated from theory (eq. 3) correlated well with the movement of 145 nm radius PEG-coated NP through the extracellular matrix. Plotting aggregate velocity (eq. 3) over the range of experimentally observed aggregation diameters and literature-supported fractal aggregate packing densities (ϕ_m), the velocity range (0 - 2.8 mm hr^{-1}) matches the observed velocity of 145 nm radius PEG-coated NPs (1.5 ± 0.75 mm hr^{-1}) accurately (Figure 4). The upper limit of packing density ($\phi_m = 0.15$), was set by previous reports of fractal aggregate formation from NPs in solution (29). The 145 nm radius PEG-coated NP aggregate was determined to generate a force of approximately 750 μN (eq. 1).

The magnetic field was uniform over the xy plane of NP mobility analysis. The permanent magnetic utilized in this study generated a magnetic field between 100 mT and 500 mT over the height of the ECM gel contained in the glass vial. The magnetic field gradient in this range was 45 T m^{-1} (Figure 5).

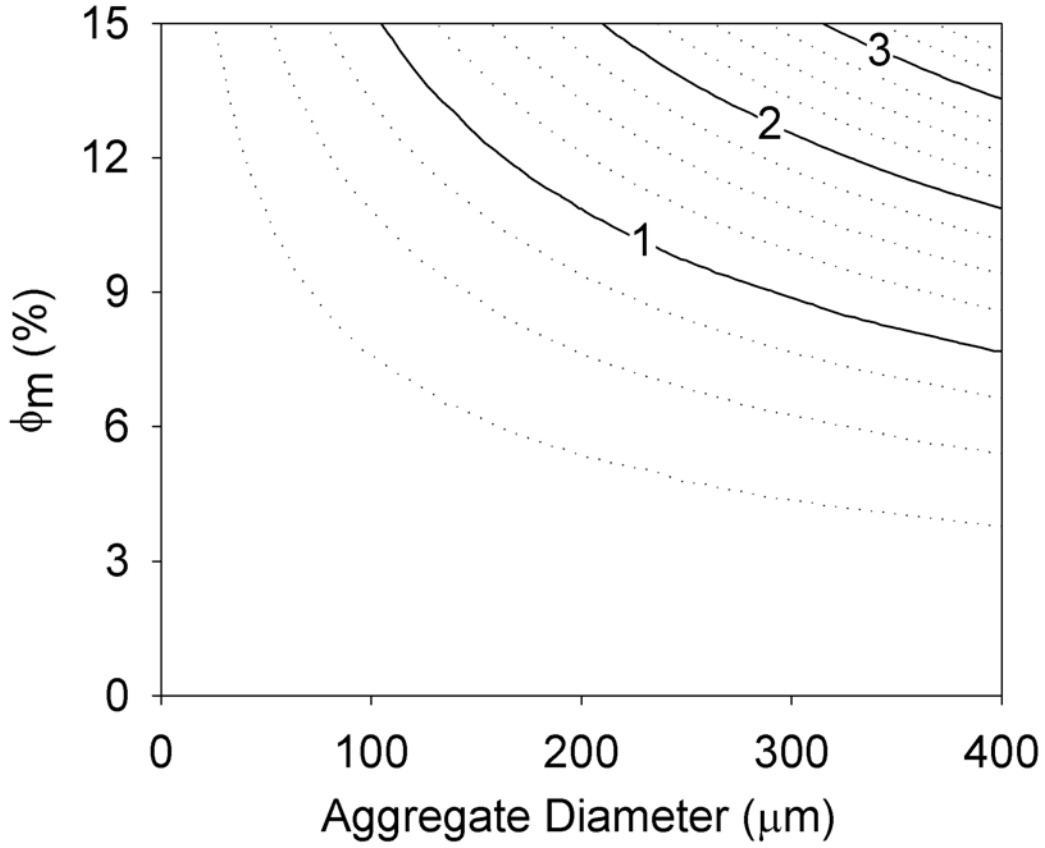

Figure 4. Theoretical nanoparticle aggregate velocity as a function of aggregate diameter and aggregate volume occupied by nanoparticles (ϕ_m). Velocity is calculated based on experimental values in Figure 2 (50 μL volume of 1 mg mL^{-1} 145 nm diameter nanoparticles, CV 0.47), Figure 5. (0.3 T magnetic field, 45 T m^{-1}), manufacturer supplied values (χ = 0.2104), and Anton Paar contract testing ($\eta = 1x10^6$ cP). Solid contours indicate 1 mm hr^{-1} increments; dashed lines correspond to 0.25 mm hr^{-1} increments. Percent occupied volume limited by fractal aggregate packing efficiency values from Tseng et al. (14.6%) (29).

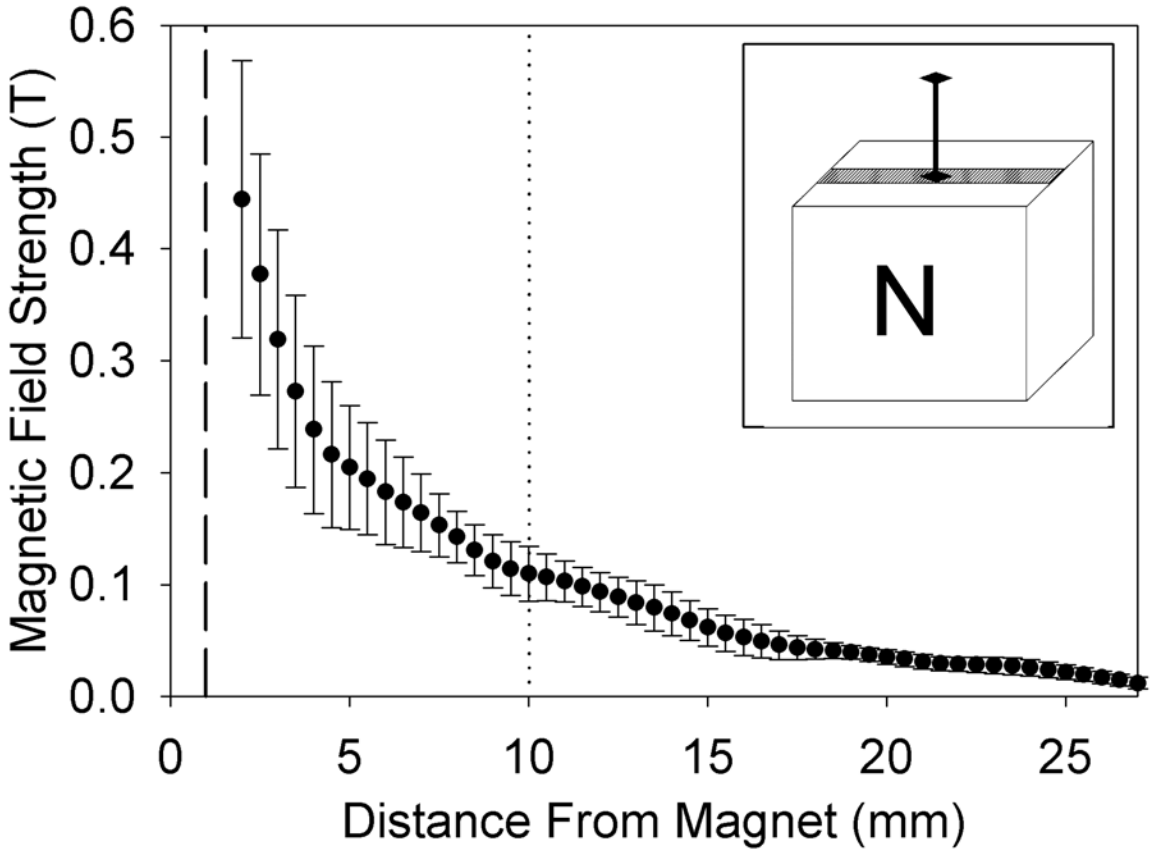

Figure 5. Magnetic field strength in the Z direction (inset, barbell) of a XY plane (inset, hashed region) corresponding to the experimental region. Dashed line (left) corresponds to the interior bottom of the glass vials utilized in this study. Dotted line (right) corresponds to the maximum ECM gel height. Data below 2 mm was unavailable due to gauss meter probe design.

Discussion

The greatly reduced ECM adhesion of the 145 nm PEG surface-coated NPs demonstrates the utility of this system for characterizing NP interactions in a biological environment. The inability of the larger, 400 nm radius, PEG surface-coated NPs of equivalent per NP magnetic susceptibility to enter the ECM gel suggests a balance between passive resistive forces in the ECM matrix and the induced magnetic force. Further analysis of the balance between magnetic and passive forces can set the limits for maximum NP size as a function of NP magnetic susceptibility.

Minimizing surface interactions between nanoparticles and the surrounding environment has become an essential element in development of advanced therapeutics and other nanoscale structures for *in vivo* applications. Advanced surface coatings such as ethylene oxide-propylene oxide block copolymers (*e.g.* Pluronic®) and PEG coatings pose a means to minimize nanoparticle aggregation and adhesion to the extracellular matrix (30). The silica-dextran surface of the 270 nm nanoparticles appears to induce aggregation and/or nonspecific binding to components in the extracellular matrix. These binding events are mediated by hydrophobic/hydrophilic interactions and charge-charge interactions. Modulation of SPM NP mobility mediated by surface characteristics suggests this system as a sensitive method to assess nanoscale surface phenomena in biological systems.

Our quantitative *in vitro* system allowed measurement of superparamagnetic nanoparticle velocity at a distance of 1 to 10 mm from the magnet. Superparamagnetic nanoparticles traversing this distance experience a continuously varying magnetic field strength from 500 mT to 100 mT. The mathematical representations in equations 1 and 3

accommodate the changing magnetic field strength with position in estimating the SPM transport characteristics through the model extracellular matrix.

We expect that the range of magnetic field strengths used in this work will be the upper bound of values appropriate for clinical applications. FeRx, a company that conducted extensive *in vivo* trials with doxorubicin coated magnetic microparticles (MTC-DOX), utilized a 5 T magnetic field source. Based on the known decay of the magnetic field with distance, the FeRx clinical apparatus has a field strength of approximately 200 mT and a magnetic field gradient of 15 T m^{-1} at a the mean therapeutic depth of 11 cm *(31)*. These values correspond well with the values studied in this work.

The theory-driven estimation of NP velocity supports magnetically induced motion within gel and fluid filled cavities. The predicted velocity of the aggregate suggests a low-density structure. Tseng and Kulkarni have separately characterized nanoparticle and microparticle aggregates at maximum densities of 14.6% and 13% (29, 32) in fractal packing systems. Magnetic particles in an external field have been shown to form low-density fractal aggregates due to their anisotropic interactions (33). The data presented in this study were consistent with literature reports that fractal aggregate density increases as a function of colloid concentration (33). Smaller, less dense aggregates had substantially lower velocity (Figure 3), as predicted by our system of equations (Figure 4).

The permeability of fractal aggregates to fluid flow is not fully understood. Kim et al. have proposed that fractal aggregates perform as a sphere with quadratically increasing permeability from the aggregate center (34). In contrast, Li et al. have

characterized macroscale pore diameter to be on the order of 1/9 the fractal aggregate diameter (35). The system explored in this work allows the study of particle dynamics in a gel system that differs from the aqueous systems utilized by Kim and Li. We hypothesize that the components of the ECM are too large to pass through the pores in the growing aggregate without interacting with and binding in the tortuous pores of the aggregate. The primary components of the ECM gel are near the size of the individual SPM NPs utilized in this system: collagen (fiber, 280 nm), laminin (cruciform, 77 nm x 42 nm), and proteoglycans (fiber, 100 - 170 nm) (36-38) . These features combine to cause the SPM NP aggregate to behave as a solid object when interacting with the ECM gel.

Although aggregation is a potential barrier to application of nanoparticles interstitially, the mobility of magnetic nanoparticles in gel and fluid filled cavities is not compromised by aggregation. Cavity mobility of NPs can be enhanced by NP surface coatings that further diminish gel adhesion and by linkage of enzymes to NPs to degrade the protein networks that restrict motion. Theoretical estimation of nanoparticle and aggregate mobility will assist in identification of the optimal NP properties for magnetically induced motion in cavities.

Magnetically driven dispersion of NP therapeutic carriers holds promise for varied applications such as treatment of abdominal cancer metastasis, spinal lesions, and sputum thinning in cystic fibrosis patients. We have demonstrated the ability of SPM NPs to migrate through the gel and fluid barriers that are common in these applications. Optimization of NP mobility in a biological cavity can be achieved by selection of NPs informed by the theoretical equation set and tested in the *in vitro* ECM gel system

described in this work. This work seeks to model *in vivo* conditions and examines SPM NP mobility in undiluted purified ECM as a surrogate for the rheological characteristics of ECM. The calculational methods described in this work are suitable for prediction of SPM NP mobility in less viscous materials. This experimental system is especially useful for determining the impact of surface coating, size and magnetic response on NP mobility in a biological context.

Acknowledgements

The authors would like to acknowledge the technical assistance of R. Chen Chun-Cheng, Jordan Bush, Edwin Donnelly, Ling Geng, and Allie Fu. This study was supported by U.S. Army Medical Research and Materiel Command BCRP-CDMRP: BC023387, Vanderbilt Institute for Nanoscale Science and Engineering (VINSE), NIH grants CA58508, CA70937, CA88076, CA89674, CA89888, P50-CA90949, and Vanderbilt-Ingram Cancer Center, CCSG P30-CA68485.

References

1. Flessner, M.F., R.L. Dedrick, and J.C. Reynolds, *Bidirectional peritoneal transport of immunoglobulin in rats: tissue concentration profiles.* Am J Physiol, 1992. **263**(1 Pt 2): p. F15-23.

2. Olmsted, S.S., et al., *Diffusion of macromolecules and virus-like particles in human cervical mucus.* Biophys J, 2001. **81**(4): p. 1930-7.

3. Sanders, N.N., et al., *Cystic fibrosis sputum: a barrier to the transport of nanospheres.* Am J Respir Crit Care Med, 2000. **162**(5): p. 1905-11.

4. McGuire, S. and F. Yuan, *Quantitative analysis of intratumoral infusion of color molecules.* American Journal of Physiology - Heart & Circulatory Physiology, 2001. **281**(2): p. H715-21.

5. Seisenberger, G., et al., *Real-time single-molecule imaging of the infection pathway of an adeno-associated virus.* Science, 2001. **294**(5548): p. 1929-32.

6. Bledsoe, A.W., G.Y. Gillespie, and C.D. Morrow, *Targeted foreign gene expression in spinal cord neurons using poliovirus replicons.* J Neurovirol, 2000. **6**(2): p. 95-105.

7. Loth, F., M.A. Yardimci, and N. Alperin, *Hydrodynamic modeling of cerebrospinal fluid motion within the spinal cavity.* J Biomech Eng, 2001. **123**(1): p. 71-9.

8. Zhang, X.Y., et al., *Interstitial hydraulic conductivity in a fibrosarcoma.* American Journal of Physiology - Heart & Circulatory Physiology, 2000. **279**(6): p. H2726-34.

9. Boucher, Y., et al., *Intratumoral infusion of fluid: estimation of hydraulic conductivity and implications for the delivery of therapeutic agents.* British Journal of Cancer, 1998. **78**(11): p. 1442-8.

10. Banerjee, R.K., et al., *Finite element model of antibody penetration in a prevascular tumor nodule embedded in normal tissue.* Journal of Controlled Release, 2001. **74**(1-3): p. 193-202.

11. Netti, P.A., et al., *Role of extracellular matrix assembly in interstitial transport in solid tumors.* Cancer Research, 2000. **60**(9): p. 2497-503.

12. Pluen, A., et al., *Role of tumor-host interactions in interstitial diffusion of macromolecules: cranial vs. subcutaneous tumors.* Proceedings of the National Academy of Sciences of the United States of America, 2001. **98**(8): p. 4628-33.

13. Leunig, M., et al., *Angiogenesis, microvascular architecture, microhemodynamics, and interstitial fluid pressure during early growth of human adenocarcinoma LS174T in SCID mice.* Cancer Research, 1992. **52**(23): p. 6553-60.

14. Yuan, F., et al., *Microvascular permeability of albumin, vascular surface area, and vascular volume measured in human adenocarcinoma LS174T using dorsal chamber in SCID mice.* Microvascular Research, 1993. **45**(3): p. 269-89.

15. Yuan, F., et al., *Vascular permeability and microcirculation of gliomas and mammary carcinomas transplanted in rat and mouse cranial windows.* Cancer Research, 1994. **54**(17): p. 4564-8.

16. Lichtenbeld, H.C., et al., *Perfusion of single tumor microvessels: application to vascular permeability measurement.* Microcirculation, 1996. **3**(4): p. 349-57.

17. Monsky, W.L., et al., *Regulation of transport pathways in tumor vessels: role of tumor type and microenvironment.* Proceedings of the National Academy of Sciences of the United States of America, 1998. **95**(8): p. 4607-12.

18. Monsky, W.L., et al., *Augmentation of transvascular transport of macromolecules and nanoparticles in tumors using vascular endothelial growth factor.* Cancer Research, 1999. **59**(16): p. 4129-35.

19. Yuan, F., A. Krol, and S. Tong, *Available space and extracellular transport of macromolecules: effects of pore size and connectedness.* Annals of Biomedical Engineering, 2001. **29**(12): p. 1150-8.

20. Lubbe, A.S., et al., *Clinical experiences with magnetic drug targeting: a phase I study with 4'-epidoxorubicin in 14 patients with advanced solid tumors.* Cancer Research, 1996. **56**(20): p. 4686-93.

21. Gutsmann, T., et al., *Force spectroscopy of collagen fibers to investigate their mechanical properties and structural organization.* Biophysical Journal, 2004. **86**(5): p. 3186-3193.

22. Holligan, D.L., G.T. Gillies, and J.P. Dailey, *Magnetic guidance of ferrofluidic nanoparticles in an in vitro model of intraocular retinal repair.* Nanotechnology, 2003. **14**(6): p. 661-666.

23. Ramanujan, S., et al., *Diffusion and convection in collagen gels: implications for transport in the tumor interstitium.* Biophys J, 2002. **83**(3): p. 1650-60.

24. Torchia, M.G., et al., *Interstitial MR lymphangiography for the detection of sentinel lymph nodes.* Journal of Surgical Oncology, 2001. **78**(3): p. 151-6; discussion 157.

25. Peira, E., et al., *In vitro and in vivo study of solid lipid nanoparticles loaded with superparamagnetic iron oxide.* Journal of Drug Targeting, 2003. **11**(1): p. 19-24.

26. Jaeger, H.M. and S.R. Nagel, *Physics of the Granular State.* Science, 1992. **255**(5051): p. 1523-1531.

27. Zborowski, M., et al., *Analytical magnetapheresis of ferritin-labeled lymphocytes.* Anal Chem, 1995. **67**(20): p. 3702-12.

28. Allen, T., *Particle size measurement*. 4th ed. 1990: Chapman and Hall. xxi, 806 p.

29. Tseng, W.J. and K.C. Lin, *Rheology and colloidal structure of aqueous TiO2 nanoparticle suspensions.* Materials Science and Engineering a-Structural Materials Properties Microstructure and Processing, 2003. **355**(1-2): p. 186-192.

30. Jain, T.K., et al., *Iron oxide nanoparticles for sustained delivery of anticancer agents.* Mol Pharm, 2005. **2**(3): p. 194-205.

31. Leakakos, T., et al., *Intravesical administration of doxorubicin to swine bladder using magnetically targeted carriers.* Cancer Chemother Pharmacol, 2003. **51**(6): p. 445-50.

32. Kulkarni, P. and P. Biswas, *A Brownian dynamics simulation to predict morphology of nanoparticle deposits in the presence of interparticle interactions.* Aerosol Science and Technology, 2004. **38**(6): p. 541-554.

33. Puertas, A.M., et al., *Colloidal aggregation induced by long range attractions.* Langmuir, 2004. **20**(22): p. 9861-9867.

34. Kim, A.S. and R. Yuan, *Hydrodynamic radius of an ideal aggregate with quadratically increasing permeabilityapproach.* Journal of Colloid and Interface Science, 2005. **In Press**.

35. Li, X.Y. and B.E. Logan, *Collision frequencies of fractal aggregates with small particles by differential sedimentation.* Environmental Science & Technology, 1997. **31**(4): p. 1229-1236.

36. Paige, M.F., J.K. Rainey, and M.C. Goh, *Fibrous long spacing collagen ultrastructure elucidated by atomic force microscopy.* Biophys J, 1998. **74**(6): p. 3211-6.

37. Ohno, M., N. Ohno, and N.A. Kefalides, *Studies on human laminin and laminin-collagen complexes.* Connect Tissue Res, 1991. **25**(3-4): p. 251-63.

38. Paulsson, M., et al., *Structure of low density heparan sulfate proteoglycan isolated from a mouse tumor basement membrane.* J Mol Biol, 1987. **197**(2): p. 297-313.

CHAPTER III

MANUSCRIPT 2: PROTEOLYTIC SURFACE FUNCTIONALIZATION ENHANCES *IN VITRO* MAGNETIC NANOPARTICLE MOBILITY THROUGH EXTRACELLULAR MATRIX

Sam J Kuhn[1]

Stephanie K Finch[1]

Dennis E Hallahan[1,2,3]

Todd D Giorgio[1]

[1]Department of Biomedical Engineering

Vanderbilt University

Nashville, TN

[2]Department of Radiation Oncology

Vanderbilt University School of Medicine

Nashville, TN

[3]Department of Cancer Biology

Vanderbilt-Ingram Cancer Center

Vanderbilt University School of Medicine

Nashville, TN

(This manuscript was prepared for submission to *Nano Letters*)

Abstract

Steric barriers such as collagen I sharply limit interstitial delivery of macromolecular and nanoparticles based therapeutic agents. Collagenase-linked superparamagnetic NPs overcame these barriers and moved through *in vitro* extracellular matrix (ECM) at 90 μm hr^{-1}, a rate similar to invasive cells, under the influence of a magnetic field. NP migration in ECM diminished linearly over five days. The collagenase-NP construct overcame two of the most significant barriers to nano- and microscale therapeutics deployment: proteolytic enzyme stability was maintained during a clinically useful time frame by immobilization on the nanoparticle surface and degradation of interstitial barriers to tissue biodistribution was enabled by the conjugated microbial protease.

Introduction

Nanoscale and microscale therapeutic structures have poor mobility when administrated to tissue interstitium. Clinical application of gene therapy, bioactive proteins and other large molecular therapeutics are often limited by geometric effects such as steric barriers, negligible diffusion, and poor interstitial convective mobility (1, 2). Viscous nonspecific molecular and physical interactions with tissue components also restricts transport and further limits the efficacy of these novel therapeutic structures (3, 4).

We propose to overcome these limits to nanoscale and microscale therapeutic tissue distribution by development of a protease-functionalized superparamagnetic nanoparticle (SPM NP) vehicle. The magnetic character of the SPM NP provides spatial

and temporal control of NP localization in the interstitial space using an external magnetic field to facilitate intratissue mobility (5, 6). A surface-linked protease enables degradation of adhesive and steric barriers in the interstitial space (7, 8).

Protease degradation of biological barriers is a common strategy employed by motile and invasive cells. Involvement of a broad spectrum of matrix metalloproteinases in metastasis has been documented, including various collagenases (9, 10). Migrating neural crest cells in embryos utilize matrix metalloproteinase-type 2, tissue plasminogen activator, and urokinase plasminogen activator to migrate to the developing neural crest (11, 12). Embryo implantation following fertilization is marked by dramatic increase in protease secretion (13). Pathogenic microorganisms and viruses, including *S. pyogenes*, Human papillomavirus, *P. insidiosum*, and *P. aeruginosa* secrete proteases or induce the release of endogenous proteases as an invasive mechanism in host tissues (14-17). Reported literature values for *in vitro c*ell migration rates through purified extracellular matrix substrates average 104 ± 44 μm h^{-1} (4 to 434 μm h^{-1}) (18-20), a rate that is consistent with a significant increase in tissue biodistribution of large molecules and nanoparticles.

While collagenase is an approved salve by the United States Food And Drug Administration for tissue debridement, exploration of proteases for enhanced interstitial mobility is still an emerging area of study. Netti et al., for example, documented a two fold increase in diffusion rates of antibodies following *in situ* collagenase treatment of rigid human glioblastoma (U87) and human soft tissue sarcoma (HSTS 26T) tumors (7).

Nanoparticle platforms enable development of multifunctional therapeutic vehicles. Intrinsic material properties such as superparamagnetism or x-ray opacity can

be combined with surface modifications that minimize nonspecific interactions with biological structures (21, 22). The NP surface can be further modified with therapeutic structures ranging from small drug molecules to large gene therapy constructs (23, 24).

The mobility of polyethylene glycol (PEG)-coated SPM NPs with surface-attached collagenase was studied in a quantifiable *in vitro* interstitial model that consisted of purified extracellular matrix and collagen I. Collagenase-linked NPs had enhanced mobility through purified extracellular matrix/collagen I alloy gels. The covalent collagenase-NP construct allowed temporal and spatial localization of the enzymatic function by an external magnetic field. This quantitative system of construction and analysis of protease-nanoparticle mobility in purified extracellular matrix components may provide a useful tool to discretely characterize and model many invasive biological processes. Protease-functionalized NPs may enhance the distribution and delivery of macromolecular therapeutics within targeted tissues such as neoplastic disease that are transport limited.

Methodology

NP Characteristics

SPM NPs were obtained from micromod Partikeltechnologie GmbH (Germany) with 300 Da PEG surface molecules (145 nm radius). The manufacturer reported a diameter CV of 0.47. The NPs had a smooth surface as observed by transmission electron microscopy. The NP was a Fe_3O_4-dextran-silica composite of an inner continuous phase dextran containing Fe_3O_4 crystals and a dextran-silica composite shell.

The PEG terminus was a primary amine group or carboxylic acid group. Percentage Fe_3O_4 mass composition was 75%. The NP volumetric magnetic susceptibility (χ_V) was 0.2105 for under saturating conditions ($H > 7.96 \times 10^5$ A m^{-1}).

Conjugation of bovine serum albumin (BSA) to NP

SPM NPs with a PEG-carboxylic acid surface were conjugated to bovine serum albumin (BSA) by 1-ethyl-3-(3-dimethylaminopropyl)-carbodiimide hydrochloride (EDAC) / N-hydroxysuccinimide (NHS) reaction (Pierce) (25). 5 mg of SPM NP were incubated at 25 ºC for one hour in 0.5 mol L^{-1} 2-(N-morpholino)ethanesulphonic acid (MES) buffer adjusted to pH 6.3 by Na_2CO_3 containing 600 µg EDAC and 1.2 mg NHS. The activated SPM NPs were magnetically washed into 0.1 mol L^{-1} MES buffer containing 50 µg BSA and incubated for three hours. Remaining activated groups were blocked by addition of 50 µL 25 mmol L^{-1} glycine with continued incubation for 30 minutes. The NP-BSA conjugates were magnetically washed three-fold into 1.0 mL of 0.1 mol L^{-1} sodium phosphate, 0.15 mol L^{-1} NaCl pH 7.2 buffer (PBS). Purity of the NP-BSA conjugates was measured by sodium dodecyl sulfate (SDS) polyacrylamide gel electrophoresis. Protein quantity in each lane was calculated based on a standard curve generated from total band intensity in lanes containing known amounts of BSA ($r^2 > 0.89$). Total conjugated BSA per NP was calculated by subtraction of BSA in the two terminal washes and subtraction of protein that was removed by incubation of the conjugate with 10% weight per volume SDS in water, pH 9.0 for 30 minutes from the known starting quantity of BSA.

Sulfhydryl modification of collagenase

Sulfhydryl groups were introduced to the surface of collagenase using *N*-succinimidyl-S-acetylthiopropionate (SATP, Pierce) based on the method described by Duncan *et al.* (26). Collagenase (4 mg) purified from *C. histolyticum* (CLSPA, Worthington Biochemical) was dissolved in 1.0 mL of PBS buffer. SATP (2.9 mg) were dissolved in 20 μL DMSO and incubated with the collagenase solution at 25 °C for 30 minutes. SATP labeled protein was purified by four-fold centrifugal separation with 50 kDa cutoff filters (Amicon). Acetyl protective groups were removed by incubating the labeled protein in a solution containing 0.5 mol L^{-1} hydroxylamine, 25 mmol L^{-1} EDTA in PBS, pH 7.2 for two hours at 25 °C. Sulfhydryl-modified protein was purified from hydroxylamine by four-fold centrifugal separation with 50 kDa cutoff filters (Amicon). Collagenase concentration was analyzed by absorbance at 280 nm.

Quantification of SH labeling efficiency

Sulfhydryl groups on the surface of the protein were quantified by Ellman's Method (27). Samples of collagenase were prepared in 0.1 mol L^{-1} sodium phosphate, 1 mmol L^{-1} EDTA buffer, pH 8.0. Four milligrams of 5,5'-Dithio-*bis*-(2-nitrobenzoic acid)(DTNB, Pierce) were dissolved per milliliter of buffer. The DTNB solution was diluted 1:50 into a 1:10 sample dilution and reacted for 15 minutes at 25 ºC. Absorbance at 412 nm was measured and concentration of colored reactant was quantified based on a 14150 M^{-1} cm^{-1} molar extinction coefficient. Collagenase concentration was analyzed by absorbance at 280 nm.

Heterobifunctional linker modification of SPM NP surface

Primary amines on the surface PEG groups of the SPM NPs were modified to form a maleimide reactive group. The heterobifunctional crosslinker, sulfosuccinimidyl 4-[*N*-maleimidomethyl]cyclohexane-1-carboxylate (sulfo-SMCC, Pierce) was utilized to bind the sulfhydryl modified collagenase to the PEG groups on the SPM NP in a variation of the method described by Duncan et al. (26). SPM NPs (400 mg) in 0.1 mol L^{-1} sodium phosphate, 2.5 mmol L^{-1} EDTA buffer, pH 7.4 were mixed with 2 mg Sulfo-SMCC in an inverting mixer at 37 ºC for 30 minutes. Sulfo-SMCC modified NPs were magnetically washed four times (1 x 10^6 dilution of reactant) into 0.1 mol L^{-1} sodium phosphate, 10 mmol L^{-1} EDTA buffer, pH 7.4.

Collagenase-nanoparticle conjugation

Sulfhydryl labeled collagenase was mixed with 2 mg sulfo-SMCC modified NPs by inversion in 0.1 mol L^{-1} sodium phosphate, 10 mmol L^{-1} EDTA buffer, pH 7.4 at 4º C for 12 hours at a 10,000:1 molar ratio. Unconjugated collagenase was removed by magnetically washing the nanoparticles four times (1 x 10^6 dilution of reactant) into 0.1 mol L^{-1} sodium phosphate, 10 mmol L^{-1} EDTA buffer, pH 7.4.

Enzymatic activity assay

Collagenase activity was assayed by fluorescence production from a dye-quenched gelatin substrate (Invitrogen) at 25 ºC. The assay was linear over an enzyme activity range from at least 0.01 U mL^{-1} to 0.1 U mL^{-1} when conducted using dilutions from a collagenase standard of manufacturer-characterized activity (Worthington

Biochemical). One unit released one micromole of L-leucine equivalents from collagen I in five hours at 37 °C, pH 7.5. NP attenuation of fluorescence from the fluorogenic substrate was corrected with an attenuation standard curve of fluorescence signal intensity of 0.5 U/mL collagenase with concentrations of SPM NPs from 10 μg mL^{-1} to 1000 μg mL^{-1}. Experimental values for functional collagenase molecules per NP were calculated based on a standard curve of collagenase concentrations of known activity and NP optical attenuation.

Three Dimensional Mapping Of The Magnetic Field

An equipolar xy plane on a nonpole face of a 2.54 cm cube of grade 40 NdFeB magnet (National Imports) was utilized for *in vitro* measurement of nanoparticle behavior. The magnetic field was measured by a Lakeshore 421 Gaussmeter with a MMA-2502-VH Hall probe as previously described (28). Data within the equipolar region of the magnet surface utilized during *in vitro* experiments were averaged and characterized by field strength as a function of distance from the magnet surface. The magnetic field was uniform over the xy plane of NP mobility analysis. The permanent magnet utilized in this study generated a magnetic field between 100 mT and 500 mT over the height of the alloy gel contained in the glass vial. The magnetic field gradient in this range was 45 T m^{-1}.

In Vitro Visualization System

The *in vitro* visualization system extended previous efforts to include the formation of collagen I-supplemented gels (28-30). Purified ECM was thawed overnight

at 4 °C from –70 °C storage. Collagen I was prepared at 0.36 mg mL^{-1} in Dulbecco's Modified Eagle Medium (DMEM) supplemented with 30 mmol L^{-1} 4-(2-hydroxyethyl)-1-piperazineethanesulfonic acid, 5.4 g mL^{-1} $NaHCO_3$ at pH 7.2. Purified ECM was mixed 1:4 with collagen I solution to form an alloy gel. 80 μL of alloy gel were deposited into a glass vial measuring 3.5 mm inner diameter by 3 cm height at 4 °C. The vial was stored for at least 2 hours at 4 °C in a sealed microfuge tube to allow release of trapped air from the alloy gel, and then incubated for 40 minutes at 37 °C to induce polymerization. Nanoparticle-conjugate solutions were created at 1000 μg mL^{-1}. 50 μL of 37° C NP solution in 50 mmol L^{-1} Tris-HCl, 150 mmol L^{-1} NaCl, 5 mmol L^{-1} $CaCl_2$, 200 μM sodium azide, pH 7.6 was sonicated for 5 s, and then introduced onto the surface of the alloy gel. The vial was sealed with wax film to minimize evaporation. The vial was placed on the surface of the magnet inside a vertical support frame. Mean maximum alloy gel height above the magnet was 8 mm.

Digital images of the NP location were captured using a 3 megapixel digital camera (Canon) equipped with a macro lens at 37 °C as previously described (28). Camera settings, timing, and data capture were remotely controlled via a personal computer and Cam4you software (Hans-David Alkenius). NP behavior was imaged over 24 hours. The digital images had a resolution of 2020 μm^2 per square pixel. White incandescent lighting was used for particle mobility assays.

Computational Data Analysis

NP position in the alloy gel was determined by contrast measurement of leading edge of the NP motion in the gel as previously described (28). Conversion from pixels to

microns was based on measurement of fixed elements within the digital images. NP velocity was calculated in triplicate by linear regression over a two-hour time interval spanning the median position measurement ($d_{½}$)($r^2 \geq 0.89$). This single velocity value comparison was selected to provide uniform magnetic field characteristics for all samples and to minimize the potential influence of end effects on SPM NP mobility.

Results

Enhanced Conjugate Mobility Through ECM

Collagenase-NP conjugates migrated through the alloy gel at a rate of 90 ± 28 μm hr^{-1}. The NP conjugates rapidly accumulated at the aqueous-gel interface under the influence of the external magnetic field. The layer of NP conjugates subsequently condensed over approximately one hour to form a spherical concentrate on the order of 300 μm in diameter before migrating further into the gel. Mobility of the collagenase-NP particles in the gel was positively correlated with the number of collagenase molecules per NP (Figure 1, Figure 2). BSA-NP conjugates, lacking proteolytic activity, remained in a layer at the aqueous-gel interface and did not enter the alloy gels over the course of 24 h.

Stability of Conjugate Enzymatic Function

Collagenase conjugated to SPM NPs demonstrated substantially enhanced functional stability compared with collagenase in solution at 4 ºC (Figure 2, Figure 3). The activity of free solution collagenase decayed in an exponential fashion with a half-

life of 12 hours. Proteolytic function of the collagenase-NP conjugate decayed linearly, losing 50% of the initial enzymatic activity after 48 hours.

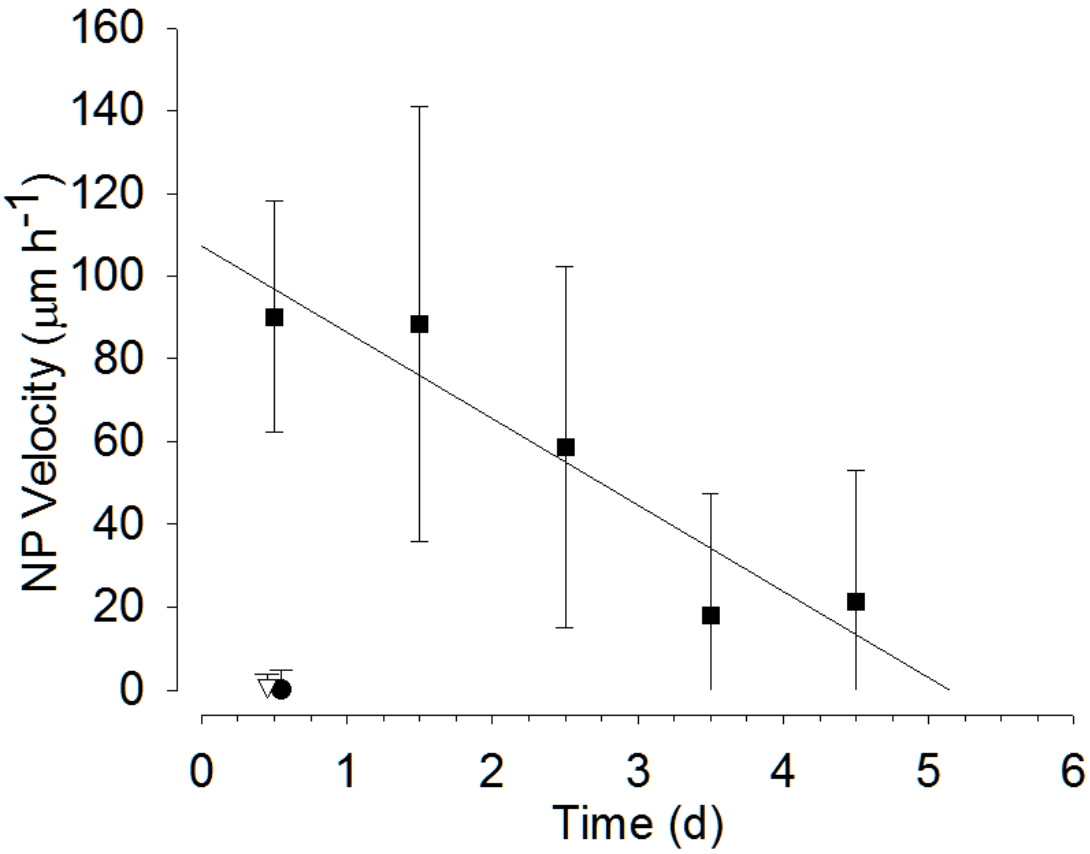

Figure 1. Mean magnetic field induced velocity of proteolytic nanoparticle (■) mobility through alloy gel decreases over the course of five days. BSA conjugate NPs (∇) and native PEG-coated NPs (●) have minimal mobility in the alloy gel. Collagenase-NP conjugates were tested on sequential days for mobility through the alloy gel substrate. Data are mean value ± std.dev. of NP velocity over 8 h; $n \geq 3$. The solid line is a linear regression approximation of the proteolytic nanoparticle velocity as a function of time since conjugation ($r^2 = 0.89$). Error bars < 0 μm h^{-1} are truncated.

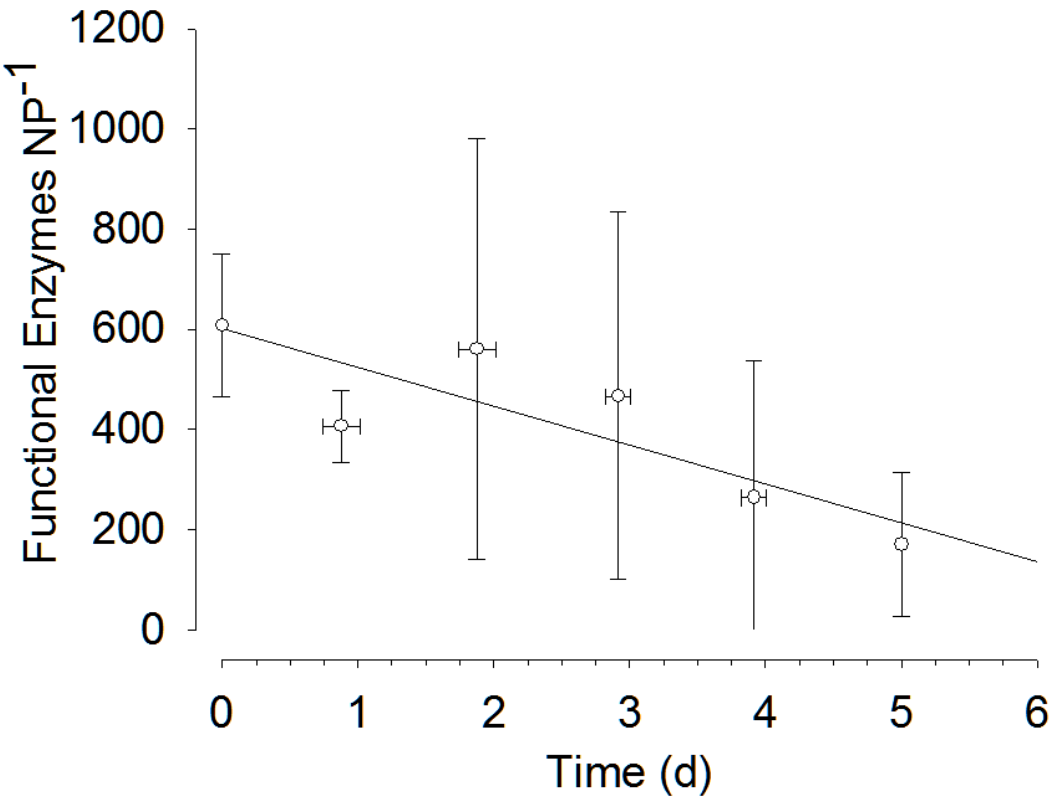

Figure 2. Collagenase bound to the surface of the NPs demonstrated sustained activity over a linear decay pattern during storage at 4 ºC. Data are mean value ± std.dev.; n = 6 (except for t = 5 where n = 3). Vertical error bars are std. dev. of data; horizontal error bars are std. dev. of similar time points. Error bars < 0 functional enzymes NP^{-1} are truncated. The solid line is a linear regression approximation of proteolytic activity as a function of time since conjugation ($r^2 = 0.73$).

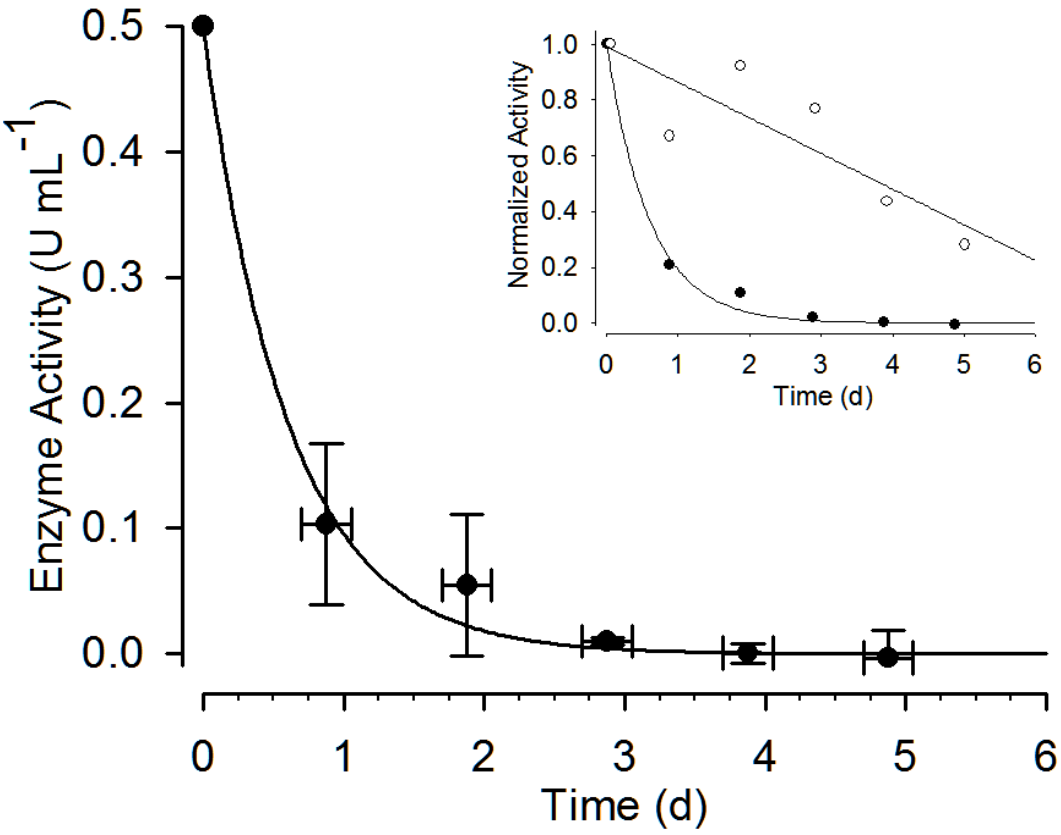

Figure 3. Collagenase free in solution decayed rapidly to less than ten percent of the original activity in 1.5 days. Enzymatic activity of collagenase stored in PBS, pH 7.2 at 4 ºC was measured with a fluorogenic gelatin substrate. Inactivation / degradation occurred following an exponential pattern characterized by: enzymatic activity = $0.498e^{-1.654t}$, $r^2 > 0.99$. Data are mean value ± std.dev. n = 3. Horizontal error bars reflect averaging of data from similar time points. Error bars < 0 U mL^{-1} are truncated. Collagenase conjugated to the NP surface (○) had an enhanced functional lifetime relative to free collagenase in solution (●)(inset); mean values normalized to t = 0 value.

Collagenase-NP Conjugation

Collagenase activity was not significantly affected by sulfhydryl modification up to ten sulfhydryls per collagenase (Figure 4). The number of sulfhydryls applied per collagenase was controllable by reaction stoichiometry and saturated above SATP:collagenase molar ratios of 50:1 at nine sulfhydryl groups per collagenase. NP-collagenase conjugation reached a maximum level of 490 functional enzymes per NP after 1.25 hours of reaction (Figure 5). The number of functional enzymes applied to the NP surface was controllable through selection of the reaction time with half of the maximum surface functionalization occurring at 11 minutes of incubation. Control reactions between SATP modified collagenase/native NP, native collagenase/sulfo-SMCC modified NP, and native collagenase/native NP had negligible collagenase activity after one hour of reaction (Figure 5).

Available Surface Groups For Modification

Each NP had 1550 ± 130 reactive primary amine groups. The number of surface reactive groups was calculated by reaction of native NPs with SATP, deacetylation, then reaction with Ellman's Reagent (27). Spectroscopic analysis of the Ellman's reaction was conducted on the solution phase of the reaction following magnetic separation of the SPM NPs.

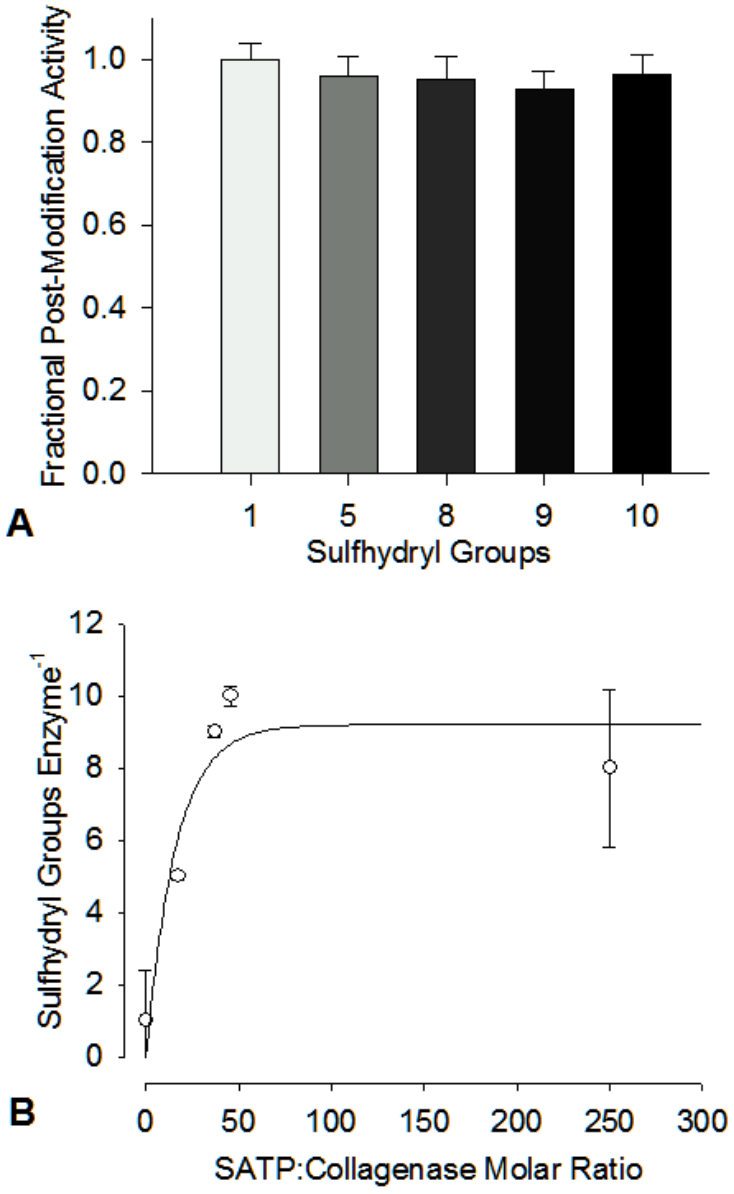

Figure 4. Collagenase function was undisturbed by saturation SATP modification, up to 10 sulfhydryl additions per collagenase (A). Surface-available sulfhydryl groups allowed cross-linking of the active collagenase to the amine SPM NP surface through the maleimide/NHS hetero-bifunctional linker, sulfo-SMCC. The result was active collagenase enzyme conjugated to the SPM NP surface. The number of sulfhydryl groups applied per collagenase molecule is controllable by reaction stoichiometry. (B) SATP addition of sulfhydryl groups to collagenase saturated above a 50:1 molar ratio at 9 sulfhydryl groups per collagenase, SH groups = $9.21(1 - e^{-0.062(\text{Molar Ratio})})$, $r^2 > 0.89$. Native collagenase had 0.9 ± 1.4 sulfhydryl groups per enzyme molecule. Sulfhydryl per collagenase values are rounded up to nearest whole integer value from mean in panel A. Data are ± std.dev of measurements or trials. Panel A: n = 1 except 1 and 8 sulfhydryl groups where n ≥ 3. There were no significant differences in collagenase activity among the various sulfhydryl treatments (P = 0.069 by one-way ANOVA, no significant difference). Panel B: n = 1 except 0:1 and 250:1 SATP:collagenase molar ratios where n ≥ 3.

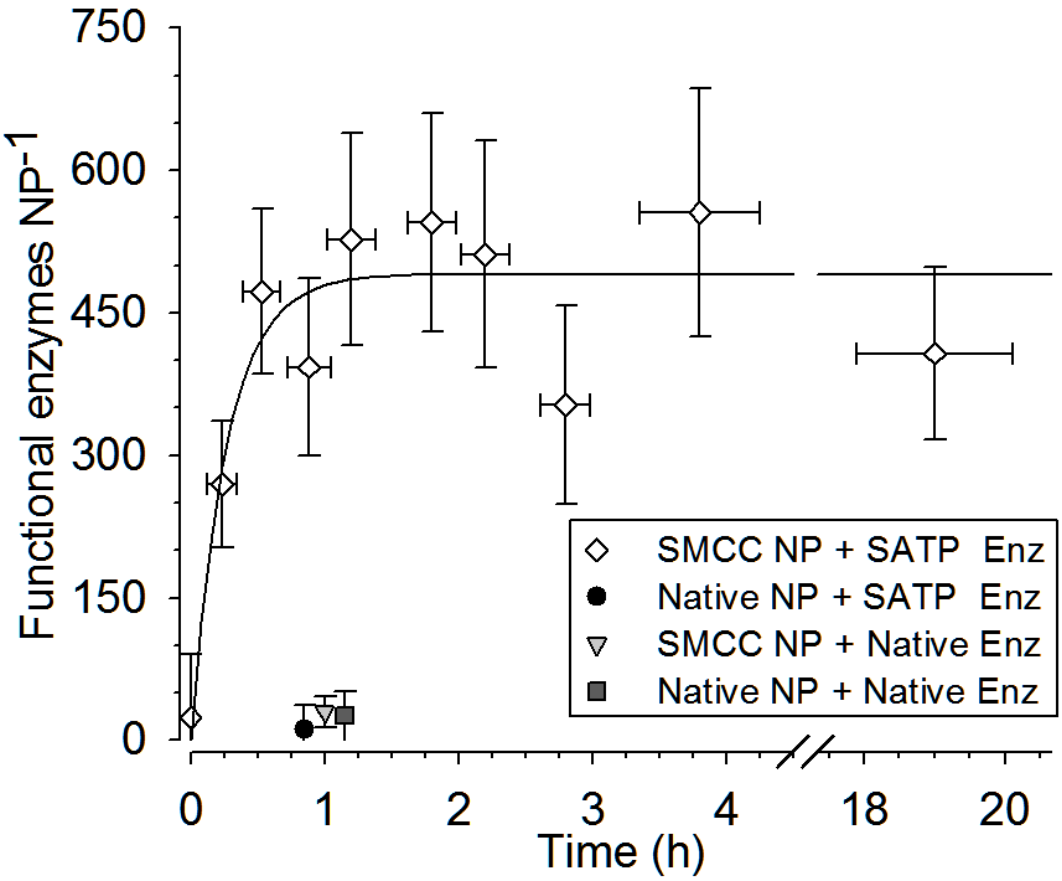

Figure 5. Surface conjugation of collagenase to NPs was modulated by temporal control of binding kinetics. SATP modified collagenase was reacted with Sulfo-SMCC modified NH_2-PEG NPs at a 10000:1 molar ratio (♢). Native NPs reacted with SATP activated collagenase (●), SMCC activated NPs reacted with native collagenase (▼) and native NPs reacted with native collagenase (■) all had minimal functional activity. Collagenase activity of all samples was characterized by cleavage of fluorogenic gelatin. The reaction was essentially complete at t = 1.25 h and was half-maximal at t = 0.2 h. Horizontal axis is broken for 4.5 h < t < 17.5 h to improve clarity. Each data point is mean value ± std.dev.; n = 4 except n = 2 for unreactive controls. Horizontal error bars reflect averaging of data from similar time points. Control populations were evaluated at one hour but are horizontally offset for clarity. Regression plot excludes data t > 10 h where free-solution inactivation / degradation of collagenase is evident (Figure 3). Number of attached enzymes = $491(1-e^{-3.75t})$.

BSA-NP Conjugation

2.6 ± 0.3 μg and 0.8 ± 1.0 μg of BSA were bound per mg NP, for activated and native NPs, respectively. EDC/NHS BSA-NP conjugation yielded 9.2 ± 1.0 μg (mean ± std dev; n=3) of residual free BSA in the sham set (lacking NHS/EDC) and 7.5 ± 0.5 μg (mean ± std dev; n=3) of residual free BSA in the experimental set per mg NP in three separate trials. 10 μg of BSA were available in each reaction.

Discussion

The collagenase-NP construct overcomes two of the most significant barriers to nano- and microscale therapeutics deployment: immobilization on the surface of the nanoparticles increases the stability of the enzyme during a clinically useful time frame and conjugation of microbial proteases allows degradation of interstitial barriers to tissue biodistribution. The combination of reduced tissue resistance, magnetically controllable motion, and extended proteolytic lifetime yield a novel, multifunctional nanoscale construct with potential applications *in vitro* and *in vivo*. Alloy gel mobility of the proteolytic NPs followed a similar temporal trend to the functional activity of the collagenase-NP conjugates, supporting the presumed structure-function relationship (Figure 1, Figure 2).

SPM NPs lacking proteolytic activity, but otherwise identical to the collagenase-functionalized SPM NPs, were unable to enter the alloy gel under the influence of the applied magnetic force. In the absence of surface collagenase, SPM NP *in vitro* mobility through similar ECM gels has been shown to be modulated by NP diameter (28). While it has been previously shown that surface modification of similar NP carriers has a

substantial impact on NP mobility, 300 Da PEG and BSA surface coatings did not allow mobility of NPs through the alloy gels (control sets, Figure 1) (28). The lack of mobility and collagenase activity of control NP populations reinforces the role of conjugate collagenase activity in both systems. This behavior mimics the lack of tissue distribution observed for nanoscale and microscale therapeutics such as gene therapy vehicles (1). The lack of nonproteolytic SPM NP motion through alloy gel is also consistent with previous unsuccessful practical applications of magnetically guided delivery *in vivo* (31). Results here suggest that the quantitative *in vitro* system accurately reflects the *in vivo* environment and that proteolytic surface functionalization sufficiently increases NP mobility to enable magnetically guided delivery *in vivo*.

Therapeutic nanoparticle administration to the tissue interstitium has unique applications for the treatment of cancer, but is currently limited by intratissue transport obstacles. Proteolytic surface functionalization may provide an approach to disbursing viral and nonviral gene therapy constructs or conventional therapeutics within neoplasms. The homogeneity of microscopic dosimetry for radiopharmaceuticals, for example, may be improved by controlled dispersion of radiopharmaceuticals incorporated into proteolytic carriers.

Therapeutics carried by proteolytic SPM NPS and delivered by direct injection have access to 300 percent greater tissue volume than immobile agents. Presuming characteristics compatible with clinical application and an initial 0.52 cm^3 spherical injection volume, NPs migrating unidirectionally toward a magnetic field source would distribute through a tissue volume of 2.35 cm^3 (+350%) over 24 hours. This enhancement

in treatment volume would substantially lower the number of initial seed points necessary for otherwise immobile therapeutics and improve the biodistribution of the agent.

The ability to modulate collagenase activity on the NP surface offers an opportunity to mimic the characteristics of many important complex biological events that depend on proteolysis. Freshly prepared proteolytic SPM NP mobility through the alloy gel averaged 90 ± 28 mm hr^{-1}, comparable with literature values for the velocity of proteolytically-mediated cell invasion (104 ± 44 mm hr^{-1}) (18-20). This velocity reinforces the utility of proteolytic SMP NPs as models for cancer metastasis, neurite outgrowth, bacterial colonization and other invasive processes. Quantitative, decoupled study of matrix metalloproteases directly implicated in metastatic shedding from primary site cancer would be an ideal system to screen pharmaceutical agents that interfere with protease-driven metastatic events. Mobility of the proteolytic SPM NPs can be modulated through multiple, independent mechanisms (*e.g.* NP size, enzyme species), allowing for accurate representation of cell migration in many systems.

The covalent reaction chemistry of surface conjugation produced a construct with robust proteolytic activity that is not easily dissociable from the NP surface under biological conditions. Previous efforts to construct enzyme-nanoparticle conjugates have focused on nonspecific adsorption and enhanced longevity of the enzyme (32, 33). Covalent conjugation restricts undesirable nonspecific release and transport of material to distant locations, an important characteristic for clinical application (34).

Surface conjugation in this nanoscale system alters the enzyme inactivation kinetics from exponential to linear (Figure 2, Figure 3). This transition contributes to the extended functional half-life of collagenase and is presumably related to reduced

collagenase-collagenase access in the surface conjugated arrangement. Quantification of the decay behavior of the enzyme-NP conjugates can be leveraged to attenuate proteolytic activity in a predictable fashion (Figure 2).

The maleimide-sulfhydryl NP conjugation strategy is compatible with most proteins and biomolecules. This flexibility creates the possibility of multifunctional nanoparticles incorporating a variety of lytic enzymes that degrade a wide spectrum of biological barriers, or a construct that has therapeutic moieties in addition to mobility-enhancing components. The NP substrate surface area is also a powerful control element; spherical surface area is proportional to diameter to the second power, enabling a SPM NP with twice the diameter to bind four times the number of surface groups.

The conjugation yield for the BSA- and collagenase-NP conjugates achieved in this work exceeded the manufacturer's specification of 1.75 ± 0.25 μg of protein per mg NP at 2.6 ± 0.3 μg BSA per mg NP and 6.9 ± 1.7 μg of total collagenase per mg NP. However, the number binding sites per NP was experimentally determined to be 1550 ± 130, suggesting a maximum binding capacity of 10.2 ± 0.9 μg protein per mg NP. Activity assays indicated approximately 500 functional collagenase molecules per NP after 1.25 hours of conjugation. Random enzyme orientation during covalent linkage was assumed to result in a maximum of 50 percent active collagenase (3.45 μg) on the NP surface. Differences in protein mass bound per NP between BSA and collagenase may have resulted from greater efficiency of the maleimide-sulfhydryl reaction chemistry than the NHS/EDC reaction chemistry. Nonspecific binding, while present in the BSA NHS/EDC synthesis, did not generate functional collagenase-NP conjugates with partially activated substrates (control sets, Figure 5).

References

1. Favre, D., et al., *Hyaluronidase enhances recombinant adeno-associated virus (rAAV)-mediated gene transfer in the rat skeletal muscle.* Gene Ther, 2000. **7**(16): p. 1417-20.

2. Yuan, F., et al., *Microvascular permeability and interstitial penetration of sterically stabilized (stealth) liposomes in a human tumor xenograft.* Cancer Research, 1994. **54**(13): p. 3352-6.

3. Ruponen, M., S. Yla-Herttuala, and A. Urtti, *Interactions of polymeric and liposomal gene delivery systems with extracellular glycosaminoglycans: physicochemical and transfection studies.* Biochim Biophys Acta, 1999. **1415**(2): p. 331-41.

4. Wiig, H., et al., *Effect of charge on interstitial distribution of albumin in rat dermis in vitro.* J Physiol, 2003. **550**(Pt 2): p. 505-14.

5. Holligan, D.L., G.T. Gillies, and J.P. Dailey, *Magnetic guidance of ferrofluidic nanoparticles in an in vitro model of intraocular retinal repair.* Nanotechnology, 2003. **14**(6): p. 661-666.

6. Jain, T.K., et al., *Iron oxide nanoparticles for sustained delivery of anticancer agents.* Mol Pharm, 2005. **2**(3): p. 194-205.

7. Netti, P.A., et al., *Role of extracellular matrix assembly in interstitial transport in solid tumors.* Cancer Research, 2000. **60**(9): p. 2497-503.

8. Alexandrakis, G., et al., *Two-photon fluorescence correlation microscopy reveals the two-phase nature of transport in tumors.* Nat Med, 2004. **10**(2): p. 203-7.

9. Zinzindohoue, F., et al., *Prognostic significance of MMP-1 and MMP-3 functional promoter polymorphisms in colorectal cancer.* Clin Cancer Res, 2005. **11**(2 Pt 1): p. 594-9.

10. Huntington, J.T., et al., *Overexpression of collagenase 1 (MMP-1) is mediated by the ERK pathway in invasive melanoma cells: role of BRAF mutation and fibroblast growth factor signaling.* J Biol Chem, 2004. **279**(32): p. 33168-76.

11. Erickson, C.A. and R.R. Isseroff, *Plasminogen activator activity is associated with neural crest cell motility in tissue culture.* J Exp Zool, 1989. **251**(2): p. 123-33.

12. Cai, D.H., et al., *MMP-2 expression during early avian cardiac and neural crest morphogenesis.* Anat Rec, 2000. **259**(2): p. 168-79.

13. Paula Reponen, I.L.C.S.S.S.A.I.T.B.R.O.K.T., *92-kDa type IV collagenase and TIMP-3, but not 72-kDa type IV collagenase or TIMP-1 or TIMP-2, are highly expressed during mouse embryo implantation.* American Journal of Anatomy, 1995. **202**(4): p. 388-396.

14. Tamura, F., et al., *Proapoptotic effect of proteolytic activation of matrix metalloproteinases by Streptococcus pyogenes thiol proteinase (Streptococcus pyrogenic exotoxin B).* Infect Immun, 2004. **72**(8): p. 4836-47.

15. Smola-Hess, S., et al., *Expression of membrane type 1 matrix metalloproteinase in papillomavirus-positive cells: role of the human papillomavirus (HPV) 16 and HPV8 E7 gene products.* J Gen Virol, 2005. **86**(Pt 5): p. 1291-6.

16. Avidano, M.A., et al., *Analysis of protease activity in human otitis media.* Otolaryngol Head Neck Surg, 1998. **119**(4): p. 346-51.

17. Ravishankar, J.P., et al., *Mechanics of solid tissue invasion by the mammalian pathogen Pythium insidiosum.* Fungal Genet Biol, 2001. **34**(3): p. 167-75.

18. Young, W.C. and I.M. Herman, *Extracellular matrix modulation of endothelial cell shape and motility following injury in vitro.* J Cell Sci, 1985. **73**: p. 19-32.

19. Friedl, P., K.S. Zanker, and E.B. Brocker, *Cell migration strategies in 3-D extracellular matrix: differences in morphology, cell matrix interactions, and integrin function.* Microsc Res Tech, 1998. **43**(5): p. 369-78.

20. Gunzer, M., et al., *Migration of dendritic cells within 3-D collagen lattices is dependent on tissue origin, state of maturation, and matrix structure and is maintained by proinflammatory cytokines.* J Leukoc Biol, 2000. **67**(5): p. 622-9.

21. Illum, L., et al., *Development of systems for targeting the regional lymph nodes for diagnostic imaging: in vivo behaviour of colloidal PEG-coated magnetite nanospheres in the rat following interstitial administration.* Pharmaceutical Research, 2001. **18**(5): p. 640-5.

22. Weissig, V., J.W. Babich, and V.P. Torchilin, *Long-circulating gadolinium-loaded liposomes: potential use for magnetic resonance imaging of the blood pool.* Colloids and Surfaces B: Biointerfaces, 2000. **18**: p. 293-299.

23. Carlesso, G., et al., *Nanoparticulate system for efficient gene transfer into refractory cell targets.* Biomacromolecules, 2005. **6**(3): p. 1185-92.

24. Prokop, A., et al., *Maximizing the in vivo efficiency of gene transfer by means of nonviral polymeric gene delivery vehicles.* J Pharm Sci, 2002. **91**(1): p. 67-76.

25. Staros, J.V., R.W. Wright, and D.M. Swingle, *Enhancement by N-hydroxysulfosuccinimide of water-soluble carbodiimide-mediated coupling reactions.* Anal Biochem, 1986. **156**(1): p. 220-2.

26. Duncan, R.J., P.D. Weston, and R. Wrigglesworth, *A new reagent which may be used to introduce sulfhydryl groups into proteins, and its use in the preparation of conjugates for immunoassay.* Anal Biochem, 1983. **132**(1): p. 68-73.

27. Ellman, G.L., *Tissue sulfhydryl groups.* Arch Biochem Biophys, 1959. **82**(1): p. 70-7.

28. Kuhn, S.J., D.E. Hallahan, and T.D. Giorgio, *Characterization of Superparamagnetic Nanoparticle Interactions With Extracellular Matrix in an In Vitro System.* Annals of Biomedical Engineering, 2006. **in press.**

29. Faassen, A.E., et al., *A cell surface chondroitin sulfate proteoglycan, immunologically related to CD44, is involved in type I collagen-mediated melanoma cell motility and invasion.* J Cell Biol, 1992. **116**(2): p. 521-31.

30. Demou, Z.N. and L.V. McIntire, *Fully automated three-dimensional tracking of cancer cells in collagen gels: determination of motility phenotypes at the cellular level.* Cancer Res, 2002. **62**(18): p. 5301-7.

31. Leakakos, T., et al., *Intravesical administration of doxorubicin to swine bladder using magnetically targeted carriers.* Cancer Chemother Pharmacol, 2003. **51**(6): p. 445-50.

32. Michaelis, M., et al., *Bovine seminal ribonuclease attached to nanoparticles made of polylactic acid kills leukemia and lymphoma cell lines in vitro.* Anticancer Drugs, 2000. **11**(5): p. 369-76.

33. Gole, A., et al., *On the preparation, characterization, and enzymatic activity of fungal protease-gold colloid bioconjugates.* Bioconjug Chem, 2001. **12**(5): p. 684-90.

34. Wang, Y., et al., *Systemic dissemination of viral vectors during intratumoral injection.* Mol Cancer Ther, 2003. **2**(11): p. 1233-42.

CHAPTER IV

MANUSCRIPT 3: FACILE PRODUCTION OF MULTIVALENT ENZYME-NANOPARTICLE CONJUGATES

Sam J Kuhn

Stephanie K Finch

Todd D Giorgio

Department of Biomedical Engineering

Vanderbilt University

Nashville, TN

Abstract

Nanoparticle (NP) platforms offer the opportunity to develop a unified synthesis method for formation of multifunctional agents. Multifunctional NPs mimic complex invasive biological processes found in metastatic invasion and immune cell interaction. We have demonstrated a facile method of conjugating multiple enzyme species to a NP via sulfhydryl-maleimide reaction chemistry. Horseradish peroxidase, α-glucosidase, and collagenase were conjugated to a superparamagnetic nanoparticle with a functional enzyme:NP ratio of 15:127:103:1, respectively. SATP-mediated addition of sulfhydryl groups to each enzyme was achieved without significant reduction in enzymatic activity. Conjugation of all three enzymes was accomplished using a maleimide reactive group generated from activation of a primary amine associated with a 300 Da polyethylene glycol molecule on the NP surface. Cross reactivity of enzymes between enzyme activity assay systems was negligible.

Introduction

Biological systems utilize cooperative sets of enzymes, ligands and other surface groups to accomplish complex biological tasks ranging from multiligand T-cell interaction with antigen presenting cells to metastatic invasion (1-3). Current physical models can only offer a limited scope of this diversity of function due to the inherent difficulty in developing synergistic effect when the components of these complexes are analyzed independently. Nanoparticle platforms utilizing a uniform synthesis strategy allow creation of multifunctional systems that can generate the biologically relevant synergistic effects.

Multifunctional biomolecules have been generated for analytical and clinical applications, but the construction relies on unique synthetic strategies tailored to linkage of individual elements into a larger construct such as antibodies that have multiple functional ligands attached to their Fc region, or a ligand and a reporter enzyme, such as horseradish peroxidase (4). The necessity of customizing the synthetic assembly of these multifunctional therapeutic structures makes development lengthy and financially burdensome. The ability to translate a protocol for development of a specific multifunctional biomolecular construct to a generalized approach has been further complicated due to substantial variability in the placement of intrinsic reactive groups on the functional protein's surface (*e.g.* an enzyme or antibody) and variability in the impact of modification of those units on protein function (5).

Historically, surface functionalization by enzymes has been achieved primarily by nonspecific adsorption of the enzymes to solid supports (6-8). Nonspecific adsorption relies on poorly characterized elements of the ligands and particle supports such as total surface charge, hydrophobicity or van der Walls interactions, making reproducible and well characterized conjugation problematic (9). Nonspecific interaction binding may also lead to unpredictable and uncontrolled release of ligand when the construct is introduced into a biological environment due to the unique nature of a construct's adsorption binding kinetics (10).

Agricultural and food processing applications have made extensive use of immobilized enzymes, primarily as a means reduce total cost by easing component handling and extending the lifespan of the attached enzymes. Glucose isomerase for conversion of raw glucose syrup to high fructose corn syrup is immobilized to a variety

of supports to extend the functional lifetime and ease handling of the enzyme (11). Immobilized L-aminoacylase is utilized to produce L-amino acids from racemic stock mixtures (12). The lower activity of nonspecifically adsorbed or immobilized enzymes is an acceptable limitation in an industrial process (13).

Facile multifunctional nanoparticle development has only recently become possible due to advances in biocompatible chemical conjugation, nanoparticle surface functionalization and micro scale enzyme function assays. Traditionally, elements in a multifunctional construct were selected for their additive value (*e.g.* increased longevity) and for their ease of conjugation. A standardized synthetic strategy utilizing a nanoparticle platform moves multifunctional constructs to a paradigm where synergy between components, not simple additive features or ease of conjugation, is the focus of synthesis.

Multifunctional nanoparticle platforms hold promise to combine the simple assembly and lifespan of industrial enzyme-adsorbed microparticles with the small dimensions and controlled synthesis of clinically relevant tagged antibodies and enzymes. Introduction of reactive groups (*i.e.* sulfhydryl and maleimide) to the ligand and particle support provide a single thioether binding method that is a stable, well-characterized synthetic route. Introduction of the reactive groups also provides a means to control the absolute and relative number of ligands bound on the particle surface.

Methodology

Sulfhydryl modification of enzymes

Aceylated sulfhydryl groups were introduced to the surface of horseradish peroxidase, α-glucosidase, and collagenase using *N*-succinimidyl-S-acetylthiopropionate (SATP, Pierce) based on the method described by Duncan et al. (*5*). Horseradish peroxidase (1.5 mg) purified from *A. rusticana* root (01-2001, Invitrogen), α-glucosidase (1.5 mg) purified from *S. cerevisiae* (63412, Fluka), and collagenase (1.5 mg) purified from *C. histolyticum* (CLSPA, Worthington Biochemical) were each dissolved in 1 mL of pH 7.5 phosphate buffered saline (PBS). SATP (0.45, 0.58, 0.92 mg, respectively, for horseradish peroxidase, α-glucosidase, and collagenase) was dissolved in 6 μL dimethylsulfoxide (DMSO) and incubated with each enzyme solutions at 25 °C for 30 minutes at a 100:1 SATP:enzyme molar ratio. Acelyated SATP labeled protein was purified by four-fold centrifugal separation with 30 kDa cutoff filters (Amicon). Acetyl protective groups were removed by incubating the labeled protein in a solution containing 0.5 mol L^{-1} hydroxylamine and 25 mmol L^{-1} ethylenediaminetetraacetic acid (EDTA) in PBS, pH 7.2 for two hours at 25 °C. Sulfhydryl-modified protein was purified from hydroxylamine by four-fold centrifugal separation with 30 kDa cutoff filters (Amicon). Protein concentration was analyzed by absorbance at 280 nm.

Quantification of SH labeling efficiency

Enzyme-associated sulfhydryl groups were quantified by Ellman's Method (*14*). Samples of each enzyme were prepared in 0.1 mol L^{-1} sodium phosphate, 1 mmol L^{-1} EDTA buffer, pH 8.0. Four milligrams of 5,5'-Dithio-*bis*-(2-nitrobenzoic acid)(DTNB,

Pierce) were dissolved per milliliter of buffer. The DTNB solution was mixed at a 1:50:0.1 buffer:DNTB solution:enzyme sample ratio, respectively, and reacted for 15 minutes at 25 ºC. Absorbance at 412 nm was measured and the concentration of colored reactant was quantified based on a 14150 M^{-1} cm^{-1} molar extinction coefficient. Protein concentration was analyzed separately by absorbance at 280 nm. Intrinsic horseradish peroxidase absorption at 412 nm was subtracted from values measured from Ellman's Method. Intrinsic α-glucosidase and collagenase absorption at 412 nm was negligible.

NP characteristics

Superparamagnetic (SPM) NPs were obtained from micromod Partikeltechnologie GmbH (Germany) with 300 Da polyethylene glycol (PEG) surface molecules (145 nm radius). The manufacturer reported a diameter CV of 0.47. The NPs had a smooth surface as observed by transmission electron microscopy. The NP was a Fe_3O_4-dextran-silica composite of an inner continuous phase dextran containing Fe_3O_4 crystals and a dextran-silica composite shell. The PEG terminus was a primary amine group. Percentage Fe_3O_4 mass composition was 75%. The NP volumetric magnetic susceptibility (χ_V) was 0.2105 for under saturating conditions ($H > 7.96 \times 10^5$ A m^{-1}).

Heterobifunctional linker modification of SPM NP surface

Primary amines on surface PEG groups of the SPM NPs were modified to form maleimide reactive groups. The heterobifunctional crosslinker, sulfosuccinimidyl 4-[*N*-maleimidomethyl]cyclohexane-1-carboxylate (sulfo-SMCC, Pierce) was utilized to bind the sulfhydryl modified enzymes to the PEG groups on the SPM NP in a variation of the

method described by Duncan et al. (*5*). SPM NPs (400 mg) in 0.1 mol L^{-1} sodium phosphate, 2.5 mmol L^{-1} EDTA buffer, pH 7.4 were mixed with 2 mg Sulfo-SMCC in an inverting mixer at 37 ºC for 30 minutes. Sulfo-SMCC modified NPs were magnetically washed four times (1 x 10^6 dilution of reactant) into 0.1 mol L^{-1} sodium phosphate, 10 mmol L^{-1} EDTA buffer, pH 7.4.

Enzyme-nanoparticle conjugation

Sulfhydryl labeled horseradish peroxidase, α-glucosidase, and collagenase were mixed in an equal molar ratio solution. The equimolar enzyme solution was mixed with 2 mg sulfo-SMCC modified NPs by inversion in 0.1 mol L^{-1} sodium phosphate, 10 mmol L^{-1} EDTA buffer, pH 7.4 at 4º C for 1 hour at a 10,000:1 enzyme:NP molar ratio. Unconjugated enzyme was removed by magnetically washing the nanoparticles four times (1 x 10^6 dilution of reactant) into 0.1 mol L^{-1} sodium phosphate, 10 mmol L^{-1} EDTA buffer, pH 7.4.

Enzymatic activity assay

Horseradish peroxidase was assayed by measurement of the fluorescent product generated from 10-acetyl-3,7-dihydroxyphenoxazine (Amplex Red, Invitrogen)(*15*). One horseradish peroxidase purpurogallin unit catalyzes the oxidation of 1 mg pyrogallol to purpurogallin in 20 seconds at 20 °C and pH 6.0. α-glucosidase was assayed by measurement of the colorimetric *p*-nitrophenol product generated from 4-nitrophenyl-α-D-glucopyranoside (PNPG) as previously described by Baroli *et al.* (16). One unit of α-glucosidase corresponds to the amount of enzyme that hydrolyzes 1 μmol p-nitrophenyl-

α-D-glucopyranoside per minute at pH 6.8 and 37 °C (after 1- 2 hours preincubation in 20 mM borate, pH 9.1, 4°C). Collagenase activity was assayed by fluorescence production from a dye-quenched gelatin substrate (Invitrogen) at 25 ºC. One collagenase unit released one micromole of L-leucine equivalents from collagen I in five hours at 37 °C, pH 7.5. NP attenuation of fluorescence from the fluorogenic substrate was corrected with an attenuation standard of fluorogenic substrate and SPM NPs. NP absorbance at 400 nm was similarly subtracted from values measured in the α-glucosidase assay system. Experimental values for functional enzyme molecules per NP were calculated based on a standard curve of enzyme concentrations of known activity and NP optical attenuation.

Results

Conjugation of three enzyme species to maleimide activated nanoparticle surface.

Three enzyme species, horseradish peroxidase, α-glucosidase, and collagenase were successfully conjugated to the nanoparticle surface in a functional state by a sulfhydryl-maleimide linkage (Figure 1). Sulfhydryl-reactive, PEG-maleimide coated NPs that were mixed with enzymes for covalent conjugation possessed specific function equivalent to 15 ± 3 horseradish peroxidase enzymes, 127 ± 21 α-glucosidase enzymes, and 103 ± 24 collagenase enzymes per NP. PEG-coated NPs lacking the sulfhydryl-reactive maleimide group and treated with the same reactive enzyme mixture had functional activity equivalent to 1 ± 0 horseradish peroxidase enzymes, 11 ± 1 α-glucosidase enzymes, and 4 ± 3 collagenase enzymes per NP.

Minimal cross reactivity of enzymes in corresponding assay systems.

Enzyme cross reactivity between enzyme-specific assay systems was minimal (Figure 2). The enzymatic assay systems were linear over the measured range of 0 to 3 mU mL^{-1}, 0 to 50 mU mL^{-1}, and 0 to 500 mU mL^{-1} for horseradish peroxidase, α-glucosidase, and collagenase, respectively.

50 mU mL^{-1} α-glucosidase activity in the horseradish peroxidase assay system was equivalent to 0.13 mU mL^{-1} horseradish peroxidase activity. 500 mU mL^{-1} collagenase activity in the horseradish peroxidase assay system was equivalent to 0.021 mU mL^{-1} horseradish peroxidase activity.

3 mU mL^{-1} horseradish peroxidase activity in the α-glucosidase assay system was equivalent to 2.5 mU mL^{-1} α-glucosidase activity. 500 mU mL^{-1} collagenase activity in the α-glucosidase assay system was equivalent to 2.4 mU mL^{-1} α-glucosidase activity.

50 mU mL^{-1} α-glucosidase activity in the collagenase assay system was equivalent to 0 mU mL^{-1} collagenase activity. 3 mU mL^{-1} horseradish peroxidase activity in the collagenase assay system was equivalent to 0 mU mL^{-1} collagenase activity.

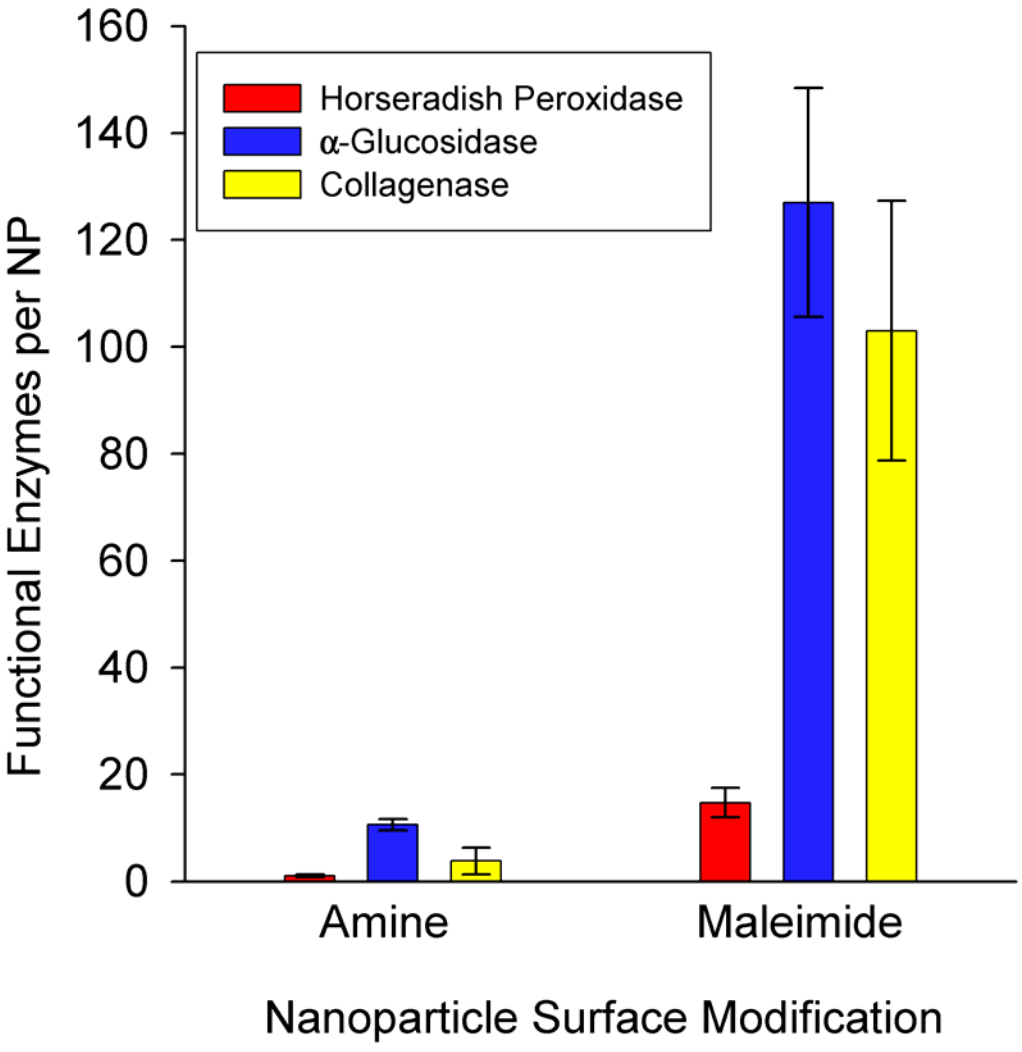

Figure 1. Simultaneous conjugation of three enzyme species was successfully carried out on maleimide-activated nanoparticles. Primary amine-PEG coated NPs were activated with sulfo-SMCC to yield a maleimide-activated NP surface. Each enzyme species was treated with SATP to create surface-available sulfhydryl groups (Table 1). Enzymes were mixed at 3,333:1 enzyme:NP ratio at 4 ºC for one hour (10,000:1 total molar ratio) with amine-PEG (unreactive control) and maleimide-PEG NPs. Unbound enzymes were removed by four-fold magnetic separation of NPs from free enzymes. Enzymes bound per NP were quantified by enzyme-specific fluorometric and colorimetric assays. n = 1, error bars = std. dev. of triplicate measurement.

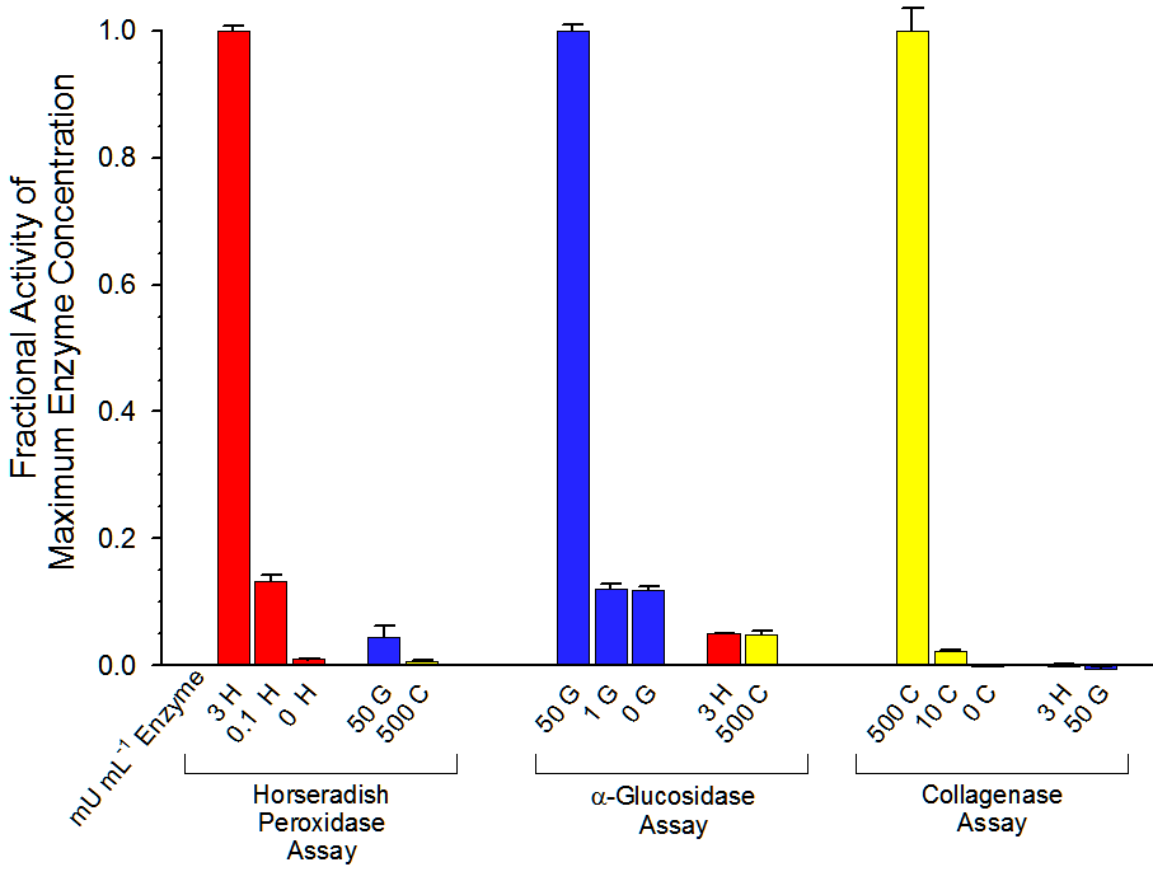

Figure 2. Collagenase (C), horseradish peroxidase (H), and α-glucosidase (G) had minimal cross reactivity in enzyme activity assay systems. For each assay system, the left three bars are the maximum, minimum and background assay values from a linear five-point standard curve to calibrate assay range for a single enzyme (*e.g.* H). The two bars to the right in each assay set represent the enzyme cross reactivity produced by the maximum concentration of other enzymes (*e.g.* G and C) in the absence of the native enzyme (*e.g.* H). Activity values were normalized to the fluorescence or absorbance value of the maximum enzyme concentration utilized in each assay system. Activity values were derived from enzyme specific fluorometric and colorimetric assays. Enzyme units are mU mL^{-1}. n = 3, error bars = std. dev. of triplicate measurement.

SATP modification of each enzyme species does not interfere with enzyme function.

SATP modification of each enzyme species did not interfere with enzyme function (Figure 3). Sulfhydral labeling of the enzyme species at a 100:1 SATP:enzyme molar ratio resulted in 5.7 ± 0.5 SH: horseradish peroxidase, 5.4 ± 1.1 SH: α-glucosidase, and 29 ± 12 SH:collagenase molecule (Table 1). Enzymatic activity in each case was undiminished compared to untreated control samples.

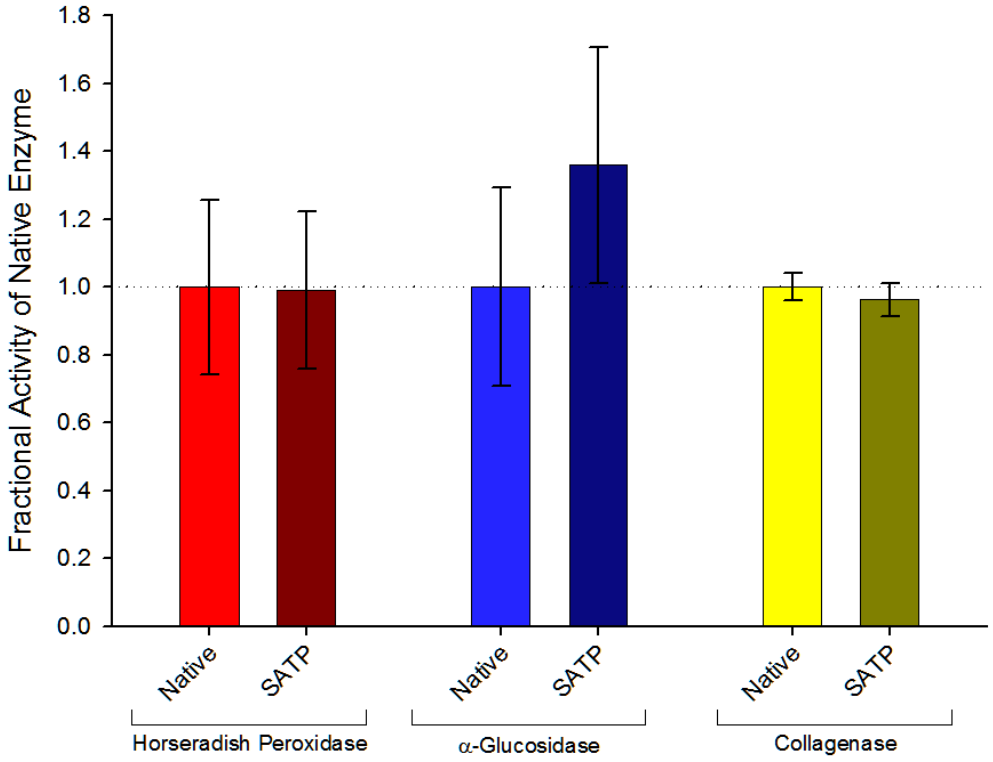

Figure 3. SATP modification of each enzyme species did not interfere with enzyme function. Each enzyme species was modified with a 100:1 SATP:enzyme molar ratio. Enzyme function was quantified by enzyme-specific fluorometric and colorimetric assay. Activity values were normalized to untreated enzyme samples (*i.e.* native) for each species. n = 3, error bars = std. dev. $P > 0.24$ between all native-SATP pairs by paired t-test.

	Horseradish Peroxidase	α-Glucosidase	Collagenase
Native	0.55 ± 0.53	0.44 ± 0.16	0.21 ± 0.23
SATP	5.7 ± 3.3	5.4 ± 1.1	29 ± 12

Table 1. SATP reaction significantly increased the number of reactive sulfhydral groups on each enzyme species. Each enzyme species was treated with a 100:1 SATP:enzyme molar ratio for 30 minutes at 25 ºC. Surface available sulfhydryl groups were quantified by Ellman's Method. Horseradish peroxidase Ellman's values were corrected for intrinsic A_{412} signal. n = 3, error bars = std. dev. $P < 0.001$ between all Native / SATP pairs by Mann-Whitney Rank Sum Test.

Discussion

Sulfhydryl-maleimide mediated covalent binding of three different lytic enzyme species to a NP surface demonstrates the flexibility of this conjugation approach to the formation of complex biomolecule-NP structures. Additional functional groups can be added with the same sulfhydryl-maleimide reactive chemistry in a controlled fashion through regulation of the relative molar ratios of each component during conjugation. We have previously demonstrated that the NP surface has approximately 1550 reactive groups, indicating substantial residual binding capacity (Manuscript 2).

Although our data show limited cross reactivity, other sets of biological ligands may generate levels of interassay cross reactivity. Assessment of enzyme cross-reactivity is a straightforward process that can be performed during the course of purification or enzyme activity measurement. Cross reactivity may be eliminated by choosing an alternate assessment system, or by mathematical compensation.

SATP reaction was a benign modification of the enzymes. For biomolecules that require primary amine availability for function, alternate strategies may be pursued, including incorporation of sulfhydryl groups during ligand synthesis, altered reaction conditions, or the use of other sulfhydryl-additive reactive chemicals such as cystamine that modify carboxylates and phosphates instead of primary amine groups.

The use of NPs as a binding platform has several notable features that enable the development of a multifunctional biological model system. The NP surface provides a uniform binding environment and reaction chemistry for attaching ligands. The small size of the nanoparticle mimics the size scale of protein arrangements in the cell membrane or in cell-cell interactions, providing an accurate spatial arrangement for

mimicry of biological interactions. PEG coating on the surface of the NPs allows further refinement of the platform. PEG chain length can be modulated to provide a small surface stand-off to a long tether, providing either rotational freedom and enhanced surface area, or full solution mobility, respectively.

Multifunctional nanoparticles that mimic particular cellular behaviors such as proteolytic extracellular matrix invasion or immune cell-cell interactions will provide an ideal test structure for screening clinically relevant therapeutic compounds. Controlled, thoroughly characterized, nanoparticles that provide specific and controllable functionality may enable enhanced pharmaceutical development through improved understanding of complex biological mechanisms such antigen presenting cell-T-cell interactions or the proteolytic behavior of metastatic cells (1, 17, 18).

Multifunctional nanoparticles allow a bottom-up approach to studying complex cellular and biological phenomena. Rather than eliminating single, or groups of surface ligands from cell populations, the multifunctional nanoparticles can be constructed to contain only a select set of surface groups. These specifically constructed nanoparticles allow study of complex interactions among a specified set of ligands, allowing direct observation of phenomena, rather than inference of the role of each ligand in complex biological behaviors.

References

1. Grakoui, A., et al., *The immunological synapse: a molecular machine controlling T cell activation.* Science, 1999. **285**(5425): p. 221-7.

2. Zinzindohoue, F., et al., *Prognostic significance of MMP-1 and MMP-3 functional promoter polymorphisms in colorectal cancer.* Clin Cancer Res, 2005. **11**(2 Pt 1): p. 594-9.

3. Huntington, J.T., et al., *Overexpression of collagenase 1 (MMP-1) is mediated by the ERK pathway in invasive melanoma cells: role of BRAF mutation and fibroblast growth factor signaling.* J Biol Chem, 2004. **279**(32): p. 33168-76.

4. Wu, A.M. and P.D. Senter, *Arming antibodies: prospects and challenges for immunoconjugates.* Nat Biotechnol, 2005. **23**(9): p. 1137-46.

5. Duncan, R.J., P.D. Weston, and R. Wrigglesworth, *A new reagent which may be used to introduce sulfhydryl groups into proteins, and its use in the preparation of conjugates for immunoassay.* Anal Biochem, 1983. **132**(1): p. 68-73.

6. Lvov, Y. and F. Caruso, *Biocolloids with ordered urease multilayer shells as enzymatic reactors.* Anal Chem, 2001. **73**(17): p. 4212-7.

7. Qhobosheane, M., et al., *Biochemically functionalized silica nanoparticles.* Analyst, 2001. **126**(8): p. 1274-8.

8. Michaelis, M., et al., *Bovine seminal ribonuclease attached to nanoparticles made of polylactic acid kills leukemia and lymphoma cell lines in vitro.* Anticancer Drugs, 2000. **11**(5): p. 369-76.

9. Kumar, S. and R. Nussinov, *Close-range electrostatic interactions in proteins.* Chembiochem, 2002. **3**(7): p. 604-17.

10. Ko, C., et al., *In vitro slow release profile of endothelial cell growth factor immobilized within calcium alginate microbeads.* Artif Cells Blood Substit Immobil Biotechnol, 1995. **23**(2): p. 143-51.

11. Sharma, B. and R. Messing, *Immobilized Enzymes for Food Processing*, ed. W. Pitcher. 1980, Boca Raton, Florida: CRC Press. 219.

12. Bodalo-Santoyo, A., et al., *Production of optically pure L-valine in fluidized and packed bed reactors with immobilized L-aminoacylase.* Journal of Chemical Technology and Biotechnology, 1999. **74**(5): p. 403-408.

13. Bodalo-Santoyo, A., et al., *Influence of pore size on covalent immobilization of L-aminoacylase on porous glass supports.* Anales De Quimica-International Edition, 1998. **94**(2): p. 78-83.

14. Ellman, G.L., *Tissue sulfhydryl groups.* Arch Biochem Biophys, 1959. **82**(1): p. 70-7.

15. Zhou, M., et al., *A stable nonfluorescent derivative of resorufin for the fluorometric determination of trace hydrogen peroxide: applications in detecting the activity of phagocyte NADPH oxidase and other oxidases.* Anal Biochem, 1997. **253**(2): p. 162-8.

16. Baroli, B., V.P. Shastri, and R. Langer, *A method to protect sensitive molecules from a light-induced polymerizing environment.* J Pharm Sci, 2003. **92**(6): p. 1186-95.

17. Seiki, M., *The cell surface: the stage for matrix metalloproteinase regulation of migration.* Curr Opin Cell Biol, 2002. **14**(5): p. 624-32.

18. Kitagawa, Y., et al., *Expression and tissue localization of membrane-types 1, 2, and 3 matrix metalloproteinases in human urothelial carcinomas.* J Urol, 1998. **160**(4): p. 1540-5.

CHAPTER V

PROTECTION OF RESEARCH SUBJECTS AND SOCIETAL IMPLICATIONS

Protection of Research Subjects

Murine subjects covered under Vanderbilt's IACUC approved protocols M/99/093, M/04/352, M/04/105, and M/03/600 were utilized in these studies. Subjects were given injectable or gas anesthesia as necessary to prevent or minimize pain. Live animal and animal-derived tissue use was minimized in this work. Animal-derived tissue was utilized in a fashion to minimize the total number of animals necessary.

Appropriate training on standard chemical, biological and radiation safety and animal handling, techniques and procedures was provided for personnel involved in this study in compliance with institutional guidelines. The methods utilized in the course of these experiments minimized exposure to potentially infectious material for scientists directly involved in the research as well as other personnel.

Societal Implications

Legal and ethical concerns of this work were minimal, as it extended prior efforts to direct therapeutic intervention into a substantial worldwide cause of mortality and morbidity. Economic results of a successful development of a novel interstitial system of therapy delivery and dispersion may include production of intellectual and physical property of value both to the developing institution and to potential industrial partners.

CHAPTER VI

CONCLUSIONS

Summary of Manuscripts

This dissertation is composed principally of three manuscripts that detail a comprehensive system for the design, synthesis, mathematical description, and *in vitro* testing of multifunctional superparamagnetic nanoparticles (SPM NPs). The three Specific Aims detailed in Chapter I were explored as is described in three manuscripts (Chapters II, III, and IV), each devoted to a single Specific Aim. These manuscripts describe a system of new materials and methods that will allow the clinical development of carriers for macromolecular and nanoscale therapeutic agents with facilitated interstitial mobility. Additionally, these reports detail an experimental system that may find broad application in basic science study of invasive cellular behaviors.

In Chapter II, we developed an *in vitro* system to quantify the suitability of SPM NPs as a site-specific therapeutic vehicle for enhanced transport through fluid and gel based sites. NP diameter and surface coating were found to be predictive characteristics of SPM NP mobility in purified extracellular matrix. The observed velocities are suitable for some clinical applications in macromolecular dispersion. Aggregation played a critical role in determining the behavior of the NPs, consolidating the NP into a central aggregate during gel migration.

Steric barriers such as collagen I fibers sharply limit mobility of macromolecular and NP based therapeutic agents in the interstitial space. To overcome this barrier we

developed and demonstrated *in vitro* activity of a multifunctional collagenase-NP conjugate, detailed in Chapter III. In the course of this effort, we developed a synthetic strategy that provides temporal control of the level of proteolytic enzyme bound on the NP surface. Collagenase-linked, PEG-coated NPs moved through an alloy gel system composed of purified extracellular matrix and collagen I with a velocity suitable for some clinical applications. The observed rate also closely approximates the migration rate of invasive cells and bacteria through tissue. Temporal decay of collagenase activity shifted from an exponential behavior in solution to a linear relationship when NP-attached, producing greater total activity over the course of the collagenase lifetime. The chemical addition of sulfhydryl groups to the collagenase surface did not interfere with enzymatic function at saturation labeling (nine sulfhydryl groups per collagenase enzyme).

The unified strategy of utilizing introduced sulfhydryl groups to bind proteins to the surface of maleimide activated NPs is a simple and versatile synthetic strategy suitable for tethering a vast array of biomolecules to the NP surface. While sulfhydral-maleimide conjugation has been previously utilized to covalently link biomolecules together (*e.g.* fluorescence marker and antibody), the strategy developed in Chapter III and IV employed a constant NP platform, simplifying creation of conjugates that potentially incorporate dozens of unique functional groups.

Multifunctional NPs mimic invasive biological processes found in metastatic invasion and neuronal development. In Chapter IV, we have demonstrated a facile method of conjugating multiple enzyme species to a NP via sulfhydryl-maleimide reaction chemistry. Horseradish peroxidase, α-glucosidase, and collagenase were conjugated to the 300 Da PEG surface of SPM NPs at 15:1, 127:1 and 103:1 functional

enzyme:NP ratio, respectively. Cross reactivity of enzymes between enzyme activity assay systems was negligible.

Basic science study of invasive biological processes can utilize multifunctional NPs as models with specific multifunctional proteolytic capabilities. The greatly enhanced mobility of surface functionalized SPM NP carriers in the interstitial space suggests application for clinical dispersion of large macromolecular therapeutic agents. In both cases, candidate NP conjugates can be developed based on mathematically and analytically characterized behavior derived from the *in vitro* experimental system developed in Chapters II and III that mimics the geometric and chemical properties of the extracellular matrix. Applications for specific surface functionalizations can adapt synthesis and analysis strategies discussed in Chapters III and IV for mono and multivalent enzyme-NP constructs.

Long Term Future Studies

Clinical dispersion of otherwise immobile therapeutics

Advanced therapeutic agents including large proteins, NPs, liposomes and gene therapy vectors are limited in their clinical application, in part, by poor interstitial mobility. These nanoscale therapeutic agents will allow development of treatment strategies for disease states such as genetic disorders that are poorly treated by conventional molecular therapeutic agents. Dispersion of otherwise immobile macromolecular or nanoscale therapeutic structures can presumably be achieved with the proteolytic SPM NP carriers detailed in this work. Enhanced dispersion may also be a

tool to reduce the total number of injection sites utilized to delivery minimally mobile structures such as radiotherapy microdosimetry capsules.

Study of proteolytic cell movement

Basic research into the mechanics of invasive cellular processes has historically relied on genetic modification of organisms and / or the introduction of chemical control agents to the experimental system. Use of genetic modifications or chemical agents retains much of the system complexity that limits interpretation or isolation of particular behaviors. The experimental techniques described in chapters II, III, and IV allow direct study of the contribution of a single protein or a set of surface-bound proteins during invasive cell or cell-group behavior.

In addition to a greater mechanical understanding of cellular behavior, isolated study of sets of enzymes in an invasion experimental system may make an ideal screening tool for blocking pathogenic invasive processes. Invasive cellular processes play a significant role in a variety of pathological processes, including cancer metastasis and necrotizing fasciitis. The ability to control the critical aspects of the model system, including the type and activity of proteolytic enzyme activity, the composition of the barrier material and the magnetic driving force for motion, offers a unique and powerful platform for sophisticated mechanistic study of cell and bacterial invasion.

Short Term Experimental Aims

Optimization of enzyme selection for interstitial invasion

As detailed in Chapter III, collagen I is significant physical barrier to interstitial transport of nanoscale structures. However, other significant barriers exist, including glycoproteins and other structural proteins. An in-depth literature survey may suggest other interstitial degradation targets. The enzymes that degrade these targets may then be incorporated into the existing enzyme-NP construct by using existing methodology detailed in Chapter IV, and tested in alloy gels that contain the target substances in a variation of the methods in Chapter III.

Test enzyme-NP conjugates *in vivo*

Although difficulties were encountered during the *ex vivo* efforts (Appendix A), *in vivo* studies may prove to be a more fruitful method of testing the efficacy of the proteolytic NPs for interstitial dispersion. Due to current IACUC regulations that restrict applications of funds to *in vivo* work, this effort would be best carried out as part of a specific funding proposal at the institutional, or national level.

As evidenced in Appendix B, planar x-ray imaging of the NPs may prove to be a sufficient method for whole-animal detection of mobility. Histological examination can provide the tissue-level documentation of NP mobility in mice. Perls' Method Prussian Blue stain will detect the presence of iron in tissue samples. Whole tissue enzyme blotting or activity-specific staining systems can provide information about the localization of the enzyme activity (1).

Mathematical modeling of current work

A mathematical model system to estimate the role of proteolytic enzymes during invasive cell behavior may be constructed based on the mathematical estimation of NP mobility and *in vitro* system in Chapter II and the synthetic and *in vitro* testing methods in Chapter III. Integrated with the multifunctional NPs described in Chapter IV, the mathematical model would elucidate the interplay between mobility and proteolytic enzymes on the cellular level.

References

1. Eghbali, M., et al., *Enzyme-antibody histochemistry. A method for detection of collagens collectively.* Histochemistry, 1987. **87**(3): p. 257-62.

APPENDIX A

TISSUE-BASED *EX VIVO* ASSAY SYSTEM FOR NANOPARTICLE-ENZYME CONJUGATE EVALUATION

Sam J Kuhn[1]

Jordan R Bush[1]

Dennis E Hallahan[1,2,3]

Todd D Giorgio[1]

[1]Department of Biomedical Engineering

Vanderbilt University

Nashville, TN

[2]Department of Radiation Oncology

Vanderbilt University School of Medicine

Nashville, TN

[3]Department of Cancer Biology

Vanderbilt-Ingram Cancer Center

Vanderbilt University School of Medicine

Nashville, TN

Introduction

Translation of previous *in vitro* testing of nanoparticle conjugates into clinical methods may be accomplished in an *ex vivo* tumor tissue system. Tissue offers sophistication in structure and composition that is not present in purified extracellular matrix. The *in vitro* substrate utilized in previous studies (Manuscripts I, II) did not have structural elements larger than the macromolecular level such as cells, vessels or tissue planes. The purification process for preparation of the extracellular matrix gel likely removes many functional proteins typically found in the interstitium, including enzyme inhibitors such as tissue inhibitors of metalloproteases (TIMPs). The structural and functional elements not present in the *in vitro* system may play a significant role during *in vivo* applications.

Three separate avenues for *ex vivo* tissue work were proposed: an excised whole tumor retained in a plastic frame and visualized with planar x-ray (Figure 1), a modified well migration assay utilizing discs of tumor tissue (Figure 2), and a layered purified extracellular matrix-tumor-extracellular matrix system (Figure 3). Excised whole tumor had the advantage of being the most accurate *ex vivo* model of expected *in vivo* application. Thin tumor sections in a transmigration assay leveraged existing migration assay technology. Layered tumor homogenate systems were a simple extension of the mature *in vitro* system.

While nanoparticles were clearly visible in all systems, by either white-light illumination or x-ray imaging, the tissue substrates proved unstable during the 3 – 24 hour time course required for *ex vivo* studies. The whole tumor system deformed at a rate that would have obscured the expected minute mobility of the nanoparticles in the tissue.

The thin tumor section transmigration assay was compromised by an inability to design a system that would prevent and discrimination nanoparticle migration around, rather than through, the tissue section. Nanoparticles introduced to the tumor homogenate layer system had two discrete behavior patterns: trapping in the homogenate layer or circumvention of the homogenate layer.

There were several weaknesses that prevented successful development and application of an *ex vivo* system. Procedural concerns regarding the stability of *ex vivo* tissue samples, limited ability to control the path of nanoparticles through tissue, and administrative limitations regarding tissue and instrument availability were primary barriers to successful implementation of an *ex vivo* experimental system. Preliminary experiments were completed, including whole tissue stability time course studies, planar x-ray imaging feasibility, and hybrid matrix-tumor-matrix penetration experiments with native nanoparticles. All systems had substantial difficulties that compromised their application and development.

Barriers to *Ex Vivo* System Development

Tissue was unstable over the experimental time course

The tissue underwent macroscopic deformation within three hours (Figure 4) and continued to degrade at longer time intervals. This deformation was much larger than the magnitude of motion we would have expected to observe from nanoparticle conjugate motion in the tissue, thus preventing useful analysis of the data.

Lengthy assay system development

Development of a new assay system may have required construction, troubleshooting, and quality control work unrelated to testing the nanoparticles. Once an assay system was successfully developed, the experimental phase may have generated no useful data. The assay system itself was unlikely to be publishable in the absence of data demonstrating nanoparticle motion. In both cases, assay development required freshly harvested animal tissue rather than store-bought tissue due to the rapid degradation of tissue following sacrifice.

Animal tissue procurement

a. IACUC regulations allowed use of harvested tissue from animals utilized under existing IACUC protocols for other, "off protocol" applications. However, that mechanism only would have provided for sporadic availability of small numbers of tissue samples. The coordination of animal tissue availability, vibratome access, and fresh synthesis of the nanoparticles would have made development of a useful sample size of tissue an exceptionally challenging.

b. Dr. Chris Kao (Neurological Surgery) volunteered use of his vibratome to section live tissue into one millimeter discs. Use of the vibratome with arbitrary tissue samples (*e.g.* tissue from a grocery store) to develop the assay system was prohibited. Dr. Kao had strict rules about sample contamination and cleanliness that prohibited use of anything but freshly harvested tissue on the vibratome. Dr. Anita Mahadevan-Jansen devoted

her thick tissue slicer exclusively to human tissue samples. The inability to utilize mock tissue for assay development further impeded the development course of the *ex vivo* assay system.

In the well-plate based assay limiting nanoparticle migration through, rather than around, the sample was a challenging design element.

Even a small capacity for nanoparticle transport that 'short-circuits' around the tissue sample was hypothesized to significantly complicate quantitation of nanoparticle transport through the tissue. Substances that would have bonded the tissue to the surface of the support or edges of the well may have diffused into the tissue itself, thus compromising the tissue structure. Bonding the tissue to the dish may also have made post-experimental histological analysis difficult.

SPM NPs were unable to penetrate layered ECM-tumor homogenate-ECM except by circumventing the tumor homogenate layer.

A layered system of 50 uL purified ECM, Lewis Lung Carcinoma (LLC) homogenate, 40 uL purified ECM in glass microvials was developed to examine the mobility of the SPM NPs *in vitro (*Figure 3*).* This system built upon previous success of examining SPM NP mobility in purified ECM alone under similar experimental conditions. LLC tumor homogenate was procured from LLC tumors in murine subjects and homogenized to a paste. The vials were assembled as previously described (Manuscript 1) with the addition of an intermediary layer of LLC homogenate. The LLC homogenate layer was designed to provide additional resistance and interaction opportunities with biological material for the SPM NPs over the purified ECM alone.

The SPM NPs were unable to penetrate the homogenized LLC tissue. At low concentrations, the NPs entered the distal face of the ECM layer relative to the magnet and penetrated less than 1 mm overnight. At higher concentrations, NPs migrated around the layer of LLC homogenate along the walls of the glass microvials. Initial assembly difficulties with trapped air in the tumor homogenate were resolved by serial additions of tumor homogenate, followed by a degassing period of 4 ºC for several hours, followed by addition of tumor homogenate, as needed to reach several millimeters of tumor homogenate depth in the glass vial.

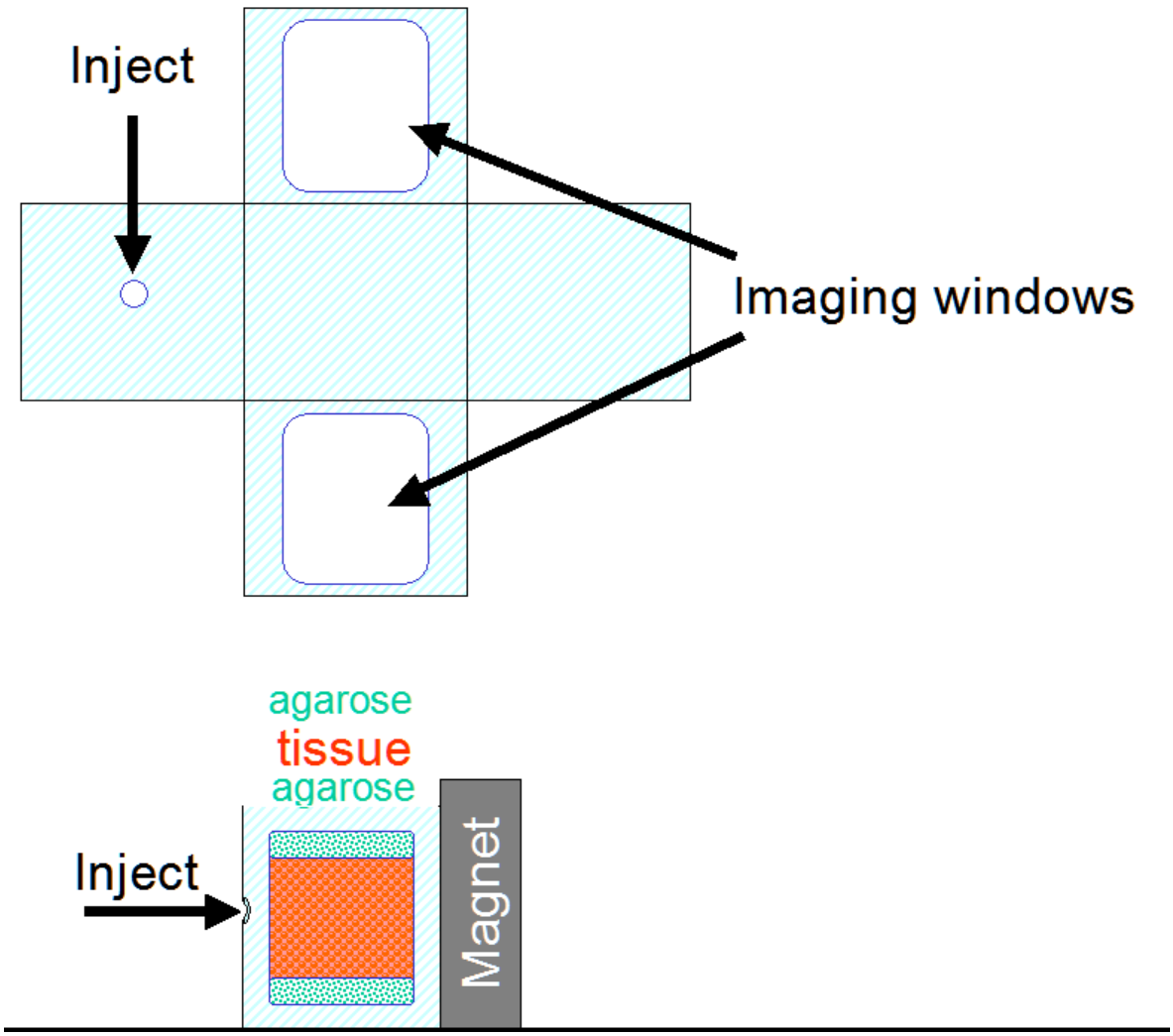

Figure 1. Whole tumor *ex vivo* nanoparticle mobility assay design. Upper image illustrates a flattened schematic of the frame. Notations indicate cutouts in the polycarbonate plastic frame to allow unattenuated planar x-ray imaging. Injection port was available for needle access to tissue.

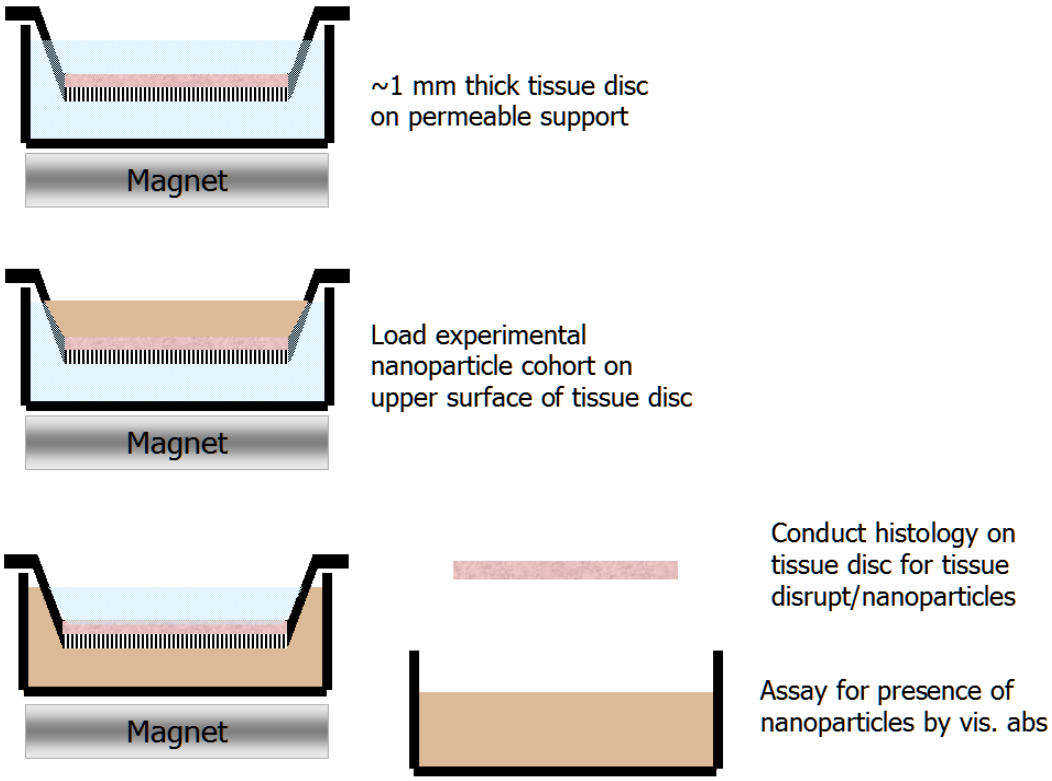

Figure 2. Tumor disc, well plate based nanoparticle mobility assay. Nanoparticle penetration through the tissue was proposed to be assayed by visible absorbance (UV/ Vis spec) and by histology of the tissue disc.

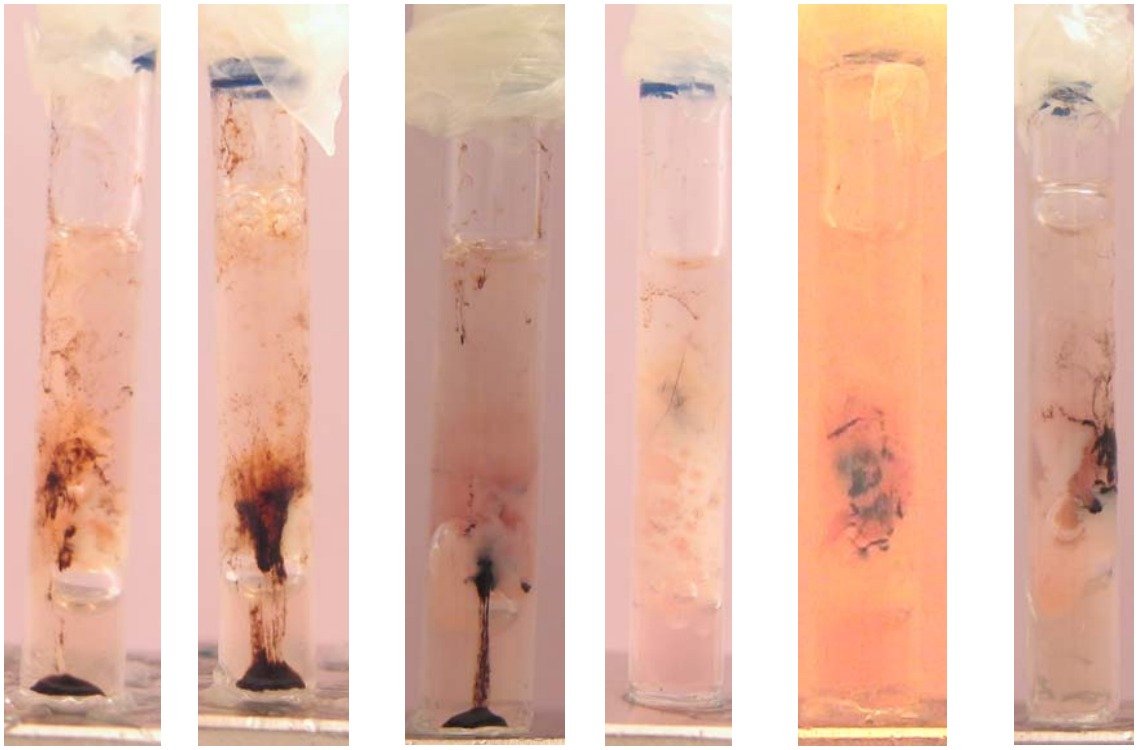

Figure 3. Layered *in vitro* model system of Lewis Lung Carcinoma (LLC) tumor homogenate and purified ECM gel was unsuitable for studying the penetration of tumor tissue by SPM NPs due to NP mobility along the surface of the container. 300Da PEG surface coated SPM NPs were introduced to the surface of the layered construct at various concentrations from 0.2 mg mL^{-1} to 10 mg mL^{-1}. At concentrations above 5 mg mL^{-1} NPs migrated to the bottom of the vial by movement along the glass surface of the vial within 30 minutes. At concentrations below 5 mg mL^{-1}, NPs penetrated into the tumor homogenate approximately 500 μm before becoming immobilized.

A 10 mg mL^{-1}, t = 5 minutes

B 10 mg mL^{-1}, t = 5 minutes

C 5 mg mL^{-1}, t = 30 minutes

D 1 mg mL^{-1}, t = 720 minutes

E 0.2 mg mL^{-1}, t = 720 minutes

F 0.2 mg mL^{-1}, t = 720 minutes

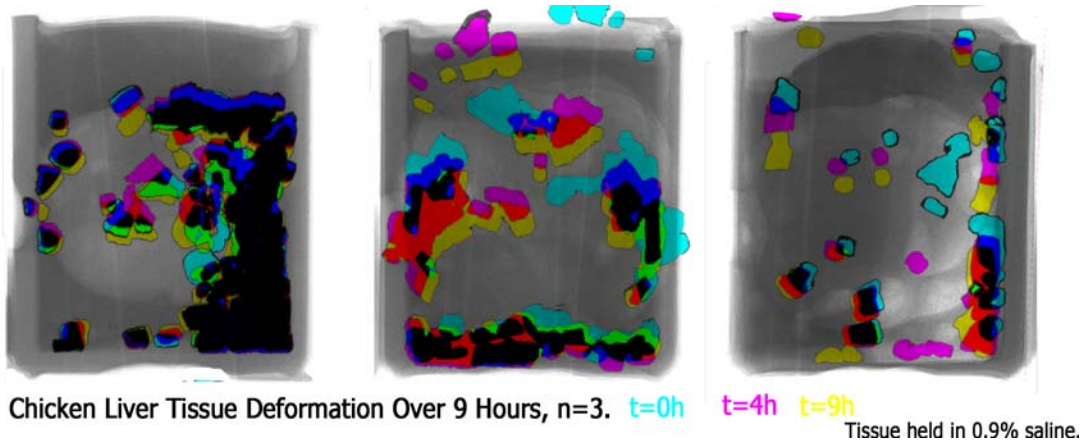

g↓

Figure 4. Fresh tissue exhibited substantial deformation over the course of 9 hours. Tissue deformation is presented as regions of colored material. Tissue deformation utilized the whole tissue imaging system (Figure 1). Fresh chicken liver tissue was coated in iron filings and placed in the ~ 1 cm3 plastic frame. Liquid agarose was utilized to provide support and displace air in the frame. Tissue samples were first washed three-fold and held in isotonic saline with 5mM azide and standard cell culture antibiotic cocktail for nine hours at 37 ºC. Three samples were imaged by planar x-ray at t=0, 4 and 9 hours (cyan, magenta, yellow respectively). The three images were colored and digitally merged. Iron filings are high contrast regions in x-ray imaging and appear colored or black in this image set. Immobile iron filings appear black. Mobile iron filings appear as colored regions.

APPENDIX B

IN VIVO X-RAY IMAGING OF INTERSTITIAL SUPERPARAMAGNETIC NANOPARTICLE MOBILITY IN MURINE SUBJECTS

Sam J Kuhn[1]

Dennis E Hallahan[1,2,3]

Todd D Giorgio[1]

[1]Department of Biomedical Engineering

Vanderbilt University

Nashville, TN

[2]Department of Radiation Oncology

Vanderbilt University School of Medicine

Nashville, TN

[3]Department of Cancer Biology

Vanderbilt-Ingram Cancer Center

Vanderbilt University School of Medicine

Nashville, TN

Hypothesis

We hypothesized that a magnetic force applied to a SPM NP by an external permanent magnet may be used to overcome barriers that limit the transport and uniform distribution of intratumorally delivered antitumor therapies.

Methodology

NP Characteristics

SPM NPs were obtained from micromod Partikeltechnologie GmbH (Rostock-Warnemuende, Germany). The NPs had a narrow size distribution and a smooth surface as observed by transmission electron microscopy. The NP is a Fe_3O_4-dextran-silica composite NP that consists of an inner region of continuous phase dextran containing Fe_3O_4 crystals, with an outer shell of a dextran-silica composite. Total Fe_3O_4 composition by mass is 75%. Two NP cohorts were utilized: one cohort was not functionalized, providing the native characteristics of the dextran-silica shell on the NP surface (270 nm diameter), the other cohort was surface functionalized with 300 Da polyethylene glycol (290 nm diameter).

Lewis Lung Carcinoma Growth in Murine Subjects

Adult, male, 57/BL6 mice obtained from Jackson Labs were utilized as subjects. Both hind limbs of each animal were seeded with 8×10^5 Lewis Lung Carcinoma cells

(LLC1) (ATCC, USA) (1). Tumors were grown over the course of 12 days to a size of 1.5 cm diameter.

Introduction of SPM NPs into Murine Subjects

50 μL of 10 mg mL^{-1} suspension of NPs were injected from the dorsal surface at the distal end of the tumor into the core region of the tumor. The injection volume was introduced under low pressure. Any leakage of fluid from the injection subsequent to needle withdrawal was absorbed and removed from the field of view. A one tesla surface strength permanent NdFeB magnet (Edmund Scientific) was placed against the proximal end of the tumor immediately following the initial injection, and maintained throughout the course of the experiment.

X-ray Imaging of SPM NPs in Murine Subjects

250 μL of a ketamine solution (200 mg kg^{-1}) was subcutaneously injected in the abdomen of each mouse to restrict movement of the subject over the course of imaging. X-ray imaging of the murine subjects was carried out using a GE Senographe 600T mammography unit. The subjects were restrained on the upper surface of the sample platform using laboratory tape to prevent movement of the limbs during imaging. X-ray images were obtained using 26 kV and 5 mAs exposure. Kodak MIN-R 2000 film (CAT 812 6393) was utilized in a Kodak MIN-R cassette, 4 cm below the imaging platform. The imaging system was certified to produce a maximum resolution of 16 line pairs per mm. Images were obtained to document the condition of the tumor prior to treatment,

immediately after injection of SPM NPs, and at several time points following the injection during application of a 1.0 T magnetic field.

NP Coating Impact on Agglomeration Behavior

The solution agglomeration behavior of two cohorts of NPs was measured by light scatter in an aggregometer (Chrono-log corp.). A 5.8 mT permanent magnet (1.2 mT at maximum fluid height) was present on the bottom surface of the 2 mL vials used for analysis. 270 nm silica-dextran NPs (micromod, 13-00-252) and 290 nm NH2-PEG silica-dextran NPs (micromod, 13-55-252) were compared in a variety of solvents at 0.25 mg mL^{-1} concentration (Figure 3).

Results

Silica Dextran NP Interstitial Mobility

Motion of silica-dextran and PEG coated micromod NPs injected into LLC tumors was undetectable from their injection site over the course of 60 minute exposure to a 1.0 T magnetic field (Figure 1Figure 2). The minimum distance observable using X-ray imaging is 7.69×10^{-4} m. The lack of detection of NP motion indicates that the upper limit of NP velocity over the 60 minute experimental course is 2.14×10^{-7} ms^{-1}.

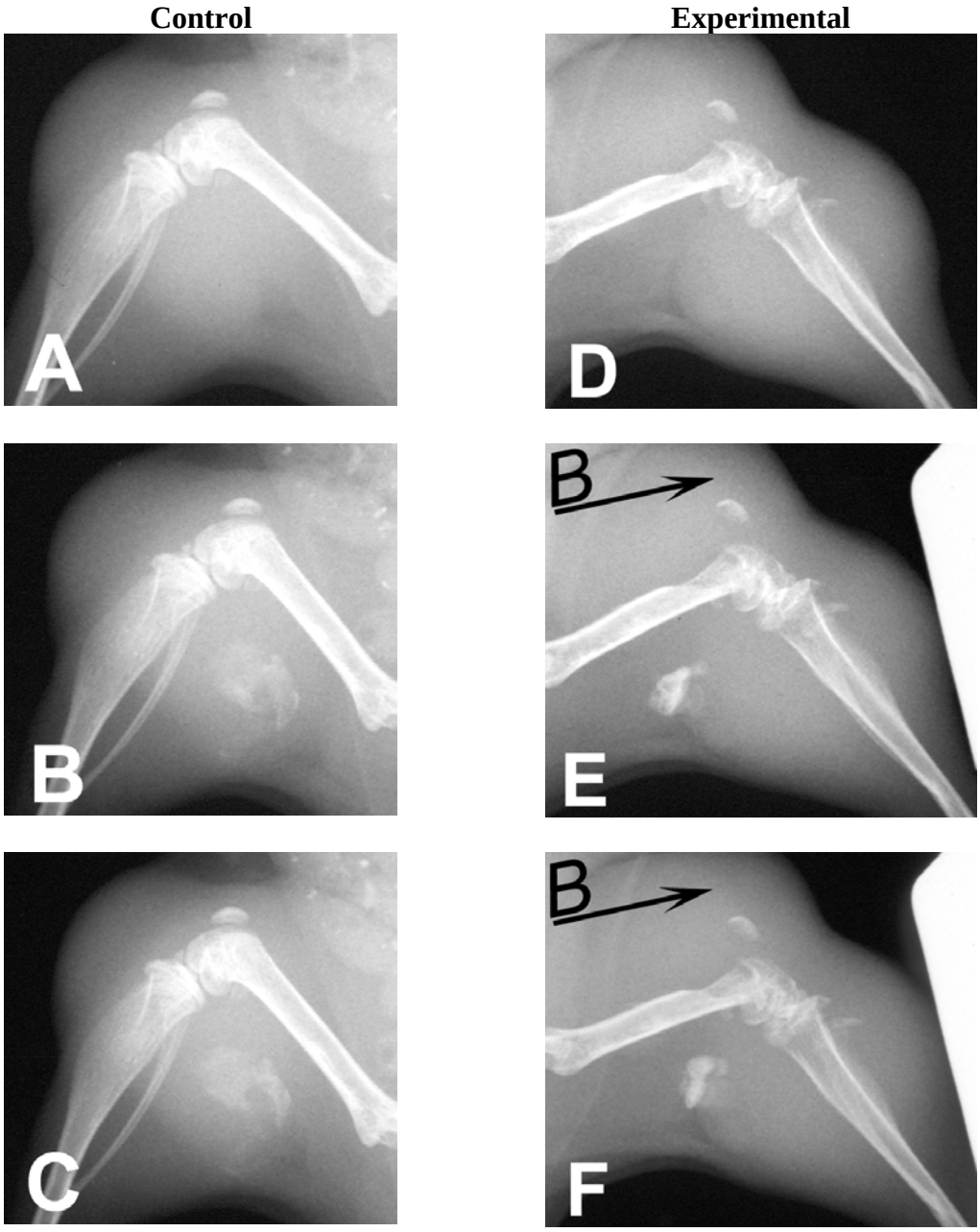

Figure 1. Time based series of micromod SPM NP injection into LLC tumor in murine hind limb. In both limbs, the SPM NPs are visible as a region of high contrast in the interior angle between the upper and lower hind limb. A. Control limb, prior to injection. B. Control limb, 5 minutes post injection. C. Control limb, 60 minutes post injection. D. Experimental limb, prior to injection. E. Experimental limb, 5 minutes post injection. Region of solid contrast (white) illustrates permanent magnet placement. F. Experimental limb, 60 minutes post injection.

Time (min)	Treatment Limb	Control Limb
Prior to injection		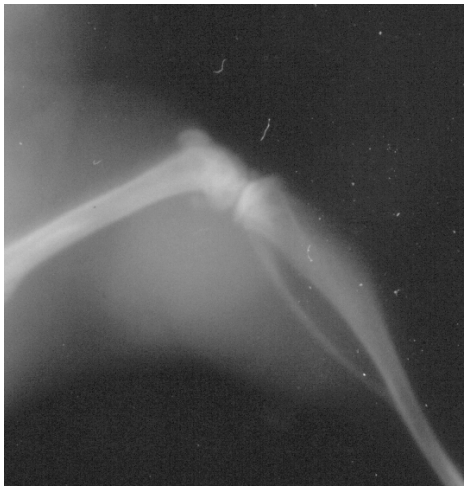
0	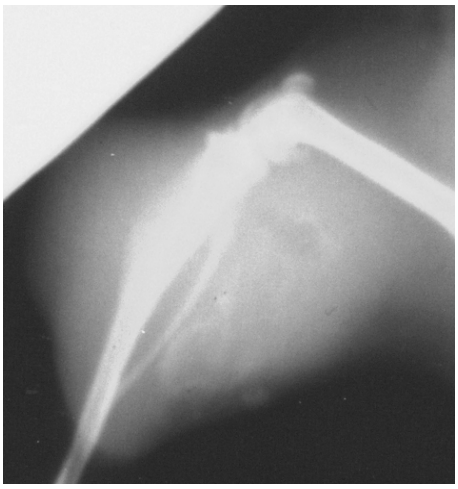	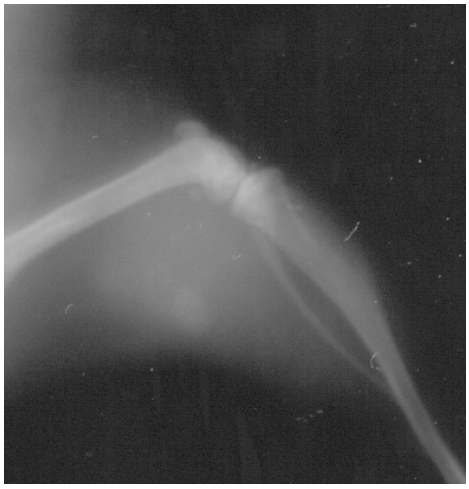

Time (min)	Treatment Limb (cont.)	Control Limb (cont.)
5	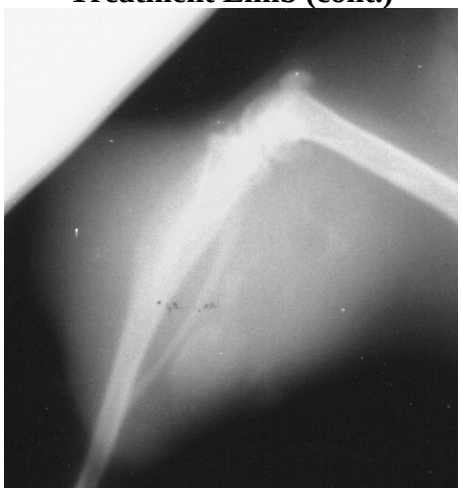	
15	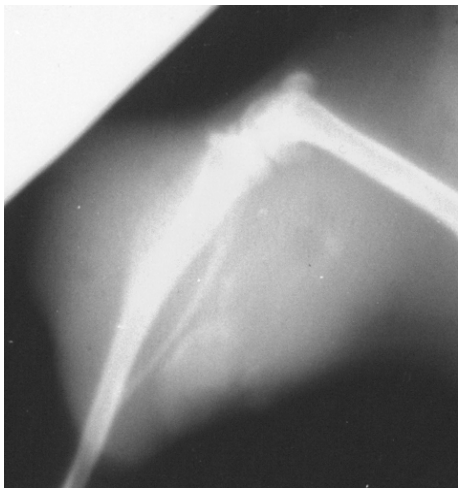	

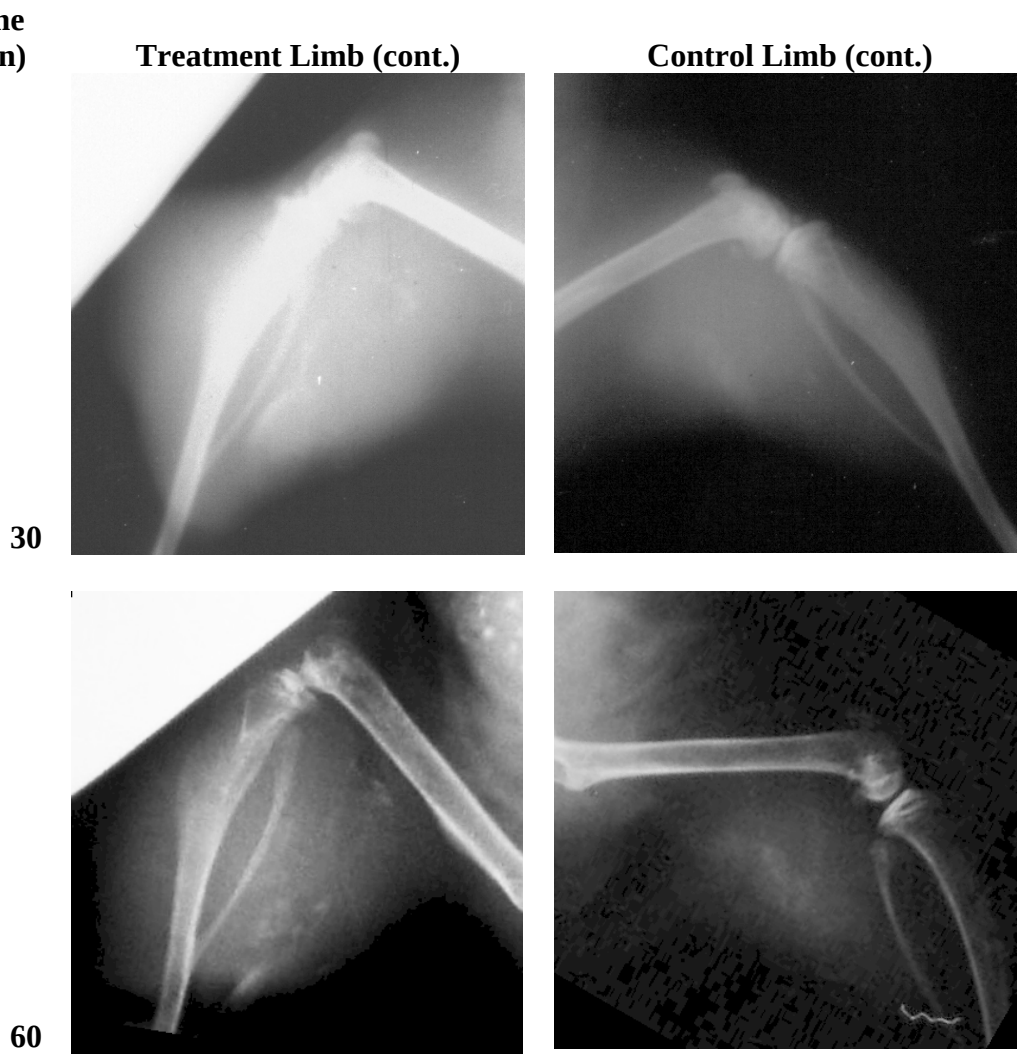

Figure 2. PEG coated nanomag (290 nm diameter) nanoparticle mobility over 60 minutes in LLC tumors in mice was negligable. SPM NPs are visible as regions of high contrast (white). Application of a 1.0 T surface strength magnet to the proximal surface of the hindlimb on one leg (left panels). Control limb (right panels) leg was not exposed to magnetic field. Images at 60-minute time point were computationally gamma and contrast enhanced to enable visualization of nanoparticle contrast.

PEG NP Coating Reduced Agglomeration

In common biological solutions (*i.e.* normal saline, PBS, Dulbecco's Modified Essential Medium + 10% fetal calf serum), the PEG coated particles had significantly reduced agglomeration potential versus the uncoated, silica-dextran surface NPs.

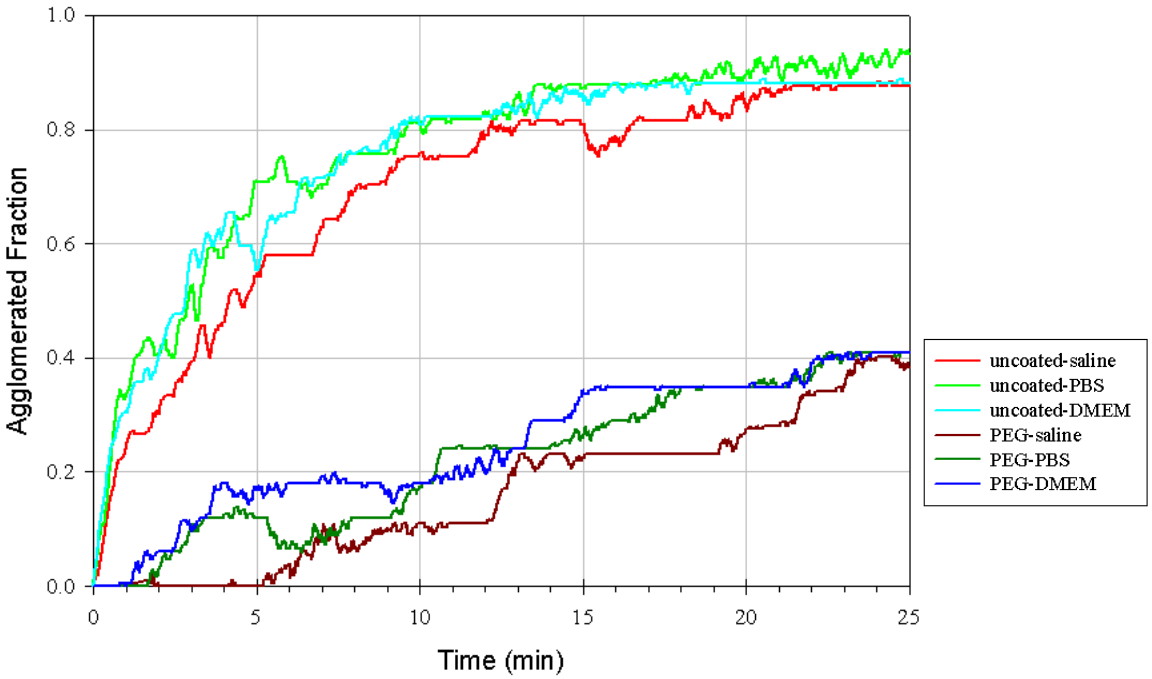

Figure 3. PEG surface coating substantially reduces the agglomeration behavior of SPM NPs in several common biological solutions. Agglomeration fraction was resolved by light scatter measurement of samples. Solvents utilized include: 0.9% saline (*i.e.* normal) (red shades), Phosphate Buffer Saline (green shades), and Dulbecco's Modified Essential Medium (DMEM) with 10% Calf Serum (blue shades). NPs with a silica-dextran composite surface (*i.e.* uncoated)(light shades: red, green, blue, yellow) were compared with NPs with a PEG-functionalized surface (dark shades: red, green, blue, black). n = 1.

Discussion

NP-NP aggregation or adhesion to biological structures is a well characterized limitation to biological applications of NPs (2, 3). The PEG coated NPs were selected to minimize nonspecific binding interactions (4). Free solution aggregation tests supported our hypothesis that PEG surface coating would reduce aggregation of the NPs in a biological environment.

Interstitial magnetic mobility of both NP cohorts was negligible. The lack of mobility of either cohort is suggestive that overcoming NP aggregation is not sufficient to enable interstitial NP motion. Geometric barriers, such as interstitial collagen I fibers, may be the primary barrier to NP mobility in the interstitial space (5, 6).

References

1. Bertram, J.S. and P. Janik, *Establishment of a cloned line of Lewis Lung Carcinoma cells adapted to cell culture.* Cancer Lett, 1980. **11**(1): p. 63-73.

2. Tirado-Miranda, M., et al., *The aggregation behaviour of protein-coated particles: a light scattering study.* Eur Biophys J, 2003. **32**(2): p. 128-36.

3. Tseng, W.J. and K.C. Lin, *Rheology and colloidal structure of aqueous TiO2 nanoparticle suspensions.* Materials Science and Engineering a-Structural Materials Properties Microstructure and Processing, 2003. **355**(1-2): p. 186-192.

4. Illum, L., et al., *Development of systems for targeting the regional lymph nodes for diagnostic imaging: in vivo behaviour of colloidal PEG-coated magnetite nanospheres in the rat following interstitial administration.* Pharmaceutical Research, 2001. **18**(5): p. 640-5.

5. Pluen, A., et al., *Role of tumor-host interactions in interstitial diffusion of macromolecules: cranial vs. subcutaneous tumors.* Proceedings of the National Academy of Sciences of the United States of America, 2001. **98**(8): p. 4628-33.

6. Netti, P.A., et al., *Role of extracellular matrix assembly in interstitial transport in solid tumors.* Cancer Research, 2000. **60**(9): p. 2497-503.